ATOMIC FORCE MICROSCOPY OF BACTERIAL PHOTOSYNTHETIC SYSTEMS:

A NEW MODEL FOR NATIVE MEMBRANE ORGANIZATION

De promotiecommissie:

prof.dr.ir. A. Bliek	Universiteit Twente, voorzitter
prof.dr. V. Subramaniam	Universiteit Twente, promotor
dr. C. Otto	Universiteit Twente
prof. C.N. Hunter	University of Sheffield
prof.dr. C.G. Figdor	Universiteit Twente
prof.dr. G.J. Vancso	Universiteit Twente
prof.dr. B. Poelsema	Universiteit Twente

Acknowledgement
This research was financially supported by the University of Twente to stimulate collaborations in biomedical research with the Vrije Universiteit, Amsterdam.

Cover illustration: a model of the bacterial photosynthetic membrane derived in accordance with the AFM data.
Cover design by Valeri Souchkov

ISBN: 90-365-2154-8

Printed by FEBODRUK BV, Enschede

ATOMIC FORCE MICROSCOPY OF BACTERIAL PHOTOSYNTHETIC SYSTEMS: A NEW MODEL FOR NATIVE MEMBRANE ORGANIZATION

PROEFSCHRIFT

ter verkrijging van
de graad van doctor aan de Universiteit Twente,
op gezag van de rector magnificus,
prof.dr. W.H.M. Zijm,
volgens besluit van het College voor Promoties
in het openbaar te verdedigen
op vrijdag 4 maart 2005 om 16.45 uur

door

Svetlana Bahatyrova
geboren op 9 februari 1978
te Minsk, Wit-Rusland

Dit proefschrift is goedgekeurd door:

prof.dr. V. Subramaniam	promotor
dr. C. Otto	assistent promotor

for my family

The only way to discover the limits of the possible
is to go beyond them into the impossible.
Arthur C. Clarke

Contents

Nature acts without masters.
Hippocrates

Chapter 1

Introduction

Photosynthesis is the process of conversion of sunlight energy to chemical energy which can be used by living organisms. In the photosynthetic membrane of purple bacteria the energy of sunlight is harvested by specialized membrane-bound light-harvesting pigment-protein complexes which transfer energy towards the reaction centers where photochemistry occurs. Despite the fact that the atomic structures of all individual components of the photosynthetic membrane are now available in great detail, the overall supramolecular architecture of a native photosynthetic membrane remained unknown. Several models of the organization of light-harvesting complexes and reaction centers within the photosynthetic unit have been proposed. In this introductory chapter we will first discuss general features of biomembranes and their functional properties. Next we will describe the class of membrane proteins and their functional and structural properties. Common techniques for the detection, purification, and characterization of membrane proteins will be briefly discussed. We will then focus on the photosynthetic membrane in purple bacteria, summarizing all available crystal structures for the individual components of the photosynthetic membrane, and discussing existing models of how these individual components are organized within the native membrane. We will introduce *Rhodobacter sphaeroides* purple bacteria, the species used in this study. Finally, we will give an introduction to the basic principles of atomic force microscopy, the powerful tool for study of biological samples.

1.1 Biomembranes: structure and functions

The dynamic cell, the fundamental unit of life, must possess an outer border in order to maintain cell integrity and to keep the interior of the cell from leaking out into the surrounding environment. A membrane composed of lipids serves this purpose. Most membrane lipids are amphiphilic and have a non-polar (hydrophobic) and a polar (hydrophilic) end. Phospholipids are the main lipid constituents of most biomembranes. A double lipid bilayer is spontaneously formed from lipid molecules, in which hydrophilic regions make contact with aqueous surroundings of the cell and hydrophobic regions are hidden from water. The basic structure of the phospholipid bilayer is identical in every biological membrane. The thickness of the lipid bilayer is ~ 4 nm in most biomembranes.

The membrane proteins determine the unique function of each type of biomembrane (in different cells and cell organelles). There are two main types of membrane proteins: integral proteins, which are fully incorporated into the lipid bilayer and make contact with both the inside and the outside of the cell, and peripheral proteins, which do not make contact with the hydrophobic core of the bilayer. The lipid-to-protein ratio varies in different biomembranes. For example, the inner mitochondrial membrane is 76% protein, while the myelin membrane is only 18%.

Two main structural properties of biomembranes are their motility and asymmetry. Both membrane proteins and lipids are laterally mobile in biomembranes. Phospholipids can rotate around their long axes and diffuse laterally within the membrane (rotational and lateral movements). A typical lipid molecule can diffuse several micrometers distance per second at 37°C. In some membranes the migration of lipids from one leaflet of the membrane to the other occurs (flip-flop movement). Since the hydrophilic regions of phospholipids have to be moved through the hydrophobic core of the lipid bilayer, such flip-flop movement is energetically extremely unfavorable. As for the membrane proteins, it was shown that 30-90% of all integral membrane proteins (depending on the cell type) diffuse quite freely within the plane of a native membrane. According to the modern and commonly accepted fluid mosaic model (Singer and Nicolson, 1972), laterally mobile phospholipids and proteins form a two-dimensional mosaic in the biomembrane (Fig. 1.1).

All integral membrane proteins bind asymmetrically to the lipid bilayer. It means that all molecules of any particular integral membrane protein have a single, specific orientation with respect to the cytoplasmic and periplasmic faces of a membrane. Due to this asymmetry in orientation membrane proteins have different properties on the two opposite membrane faces. Moreover, membrane proteins have never been observed to flip-flop across a membrane. Such

movement is energetically unfavorable as the hydrophilic regions of the proteins have to be transferred through the hydrophobic core of the lipid bilayer.

Biomembranes have several basic functions: *i)* transportation of nutrients into and metabolic waste out of the cell; *ii)* maintenance of a barrier against the unnecessary materials in the extracellular environment; *iii)* preservation of necessary metabolites and maintenance of the proper ionic composition and osmotic pressure of the cytosol.

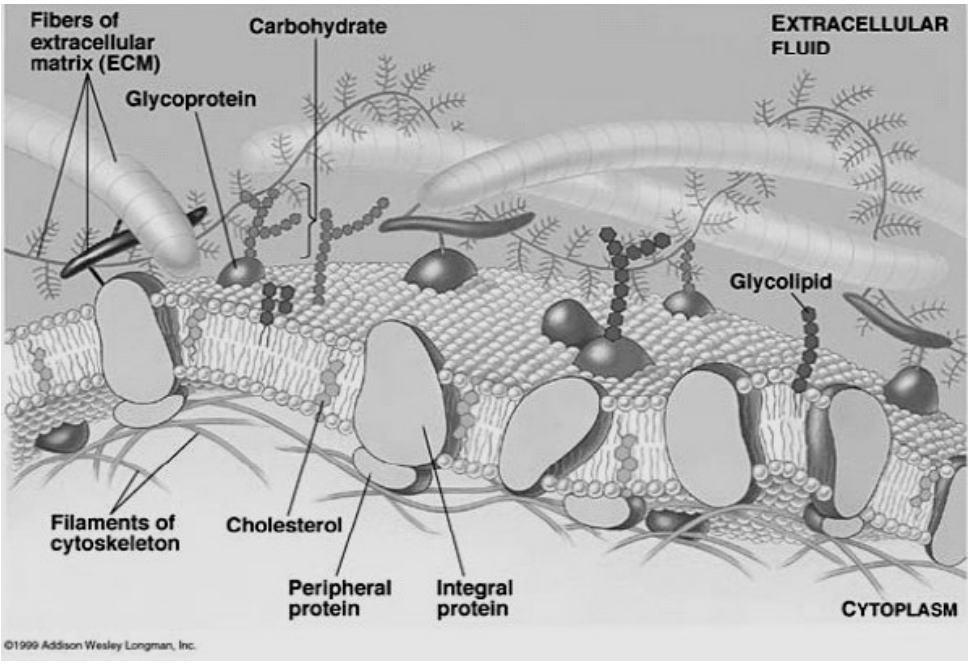

Fig. 1.1. *The fluid mosaic model of a biomembrane (Singer and Nicolson, 1972). Phospholipids and membrane proteins can freely diffuse laterally [From http://fajerpc.magnet.fsu.edu/Education/2010/Lectures/11_Membranes.htm].*

1.2 Membrane proteins

As was mentioned in the previous section of this chapter, there are two types of membrane proteins, integral and peripheral.

Integral membrane proteins usually contain one or more membrane-spanning domains as well as domains which have protrusions on both periplasmic and cytoplasmic sides of the lipid bilayer. The membrane-spanning domains are α-

helices or multiple β-strands. There are many integral membrane proteins which contain multiple transmembrane α-helices (examples: bacteriorhodopsin, bacterial reaction centre, bacterial light-harvesting complexes 1 and 2). Membrane-spanning "barrels" are formed from multiple β-strands (example: porin structure).

Peripheral membrane proteins do not span the hydrophobic core of the phospholipid bilayer. They are bound to the membrane either by interacting indirectly with integral membrane proteins or directly with lipid hydrophilic regions.

Membrane proteins have diverse functions in the biomembranes. Protein domains on the periplasmic membrane surface are often involved in cell-cell signaling and interactions. Proteins that form channels and pores within the membrane move molecules across the membrane. Protein domains on the cytoplasmic face of the membrane are involved in anchoring cytoskeletal proteins to the membrane and triggering intracellular signaling pathways.

1.3 Purification and characterization of cells and their constituents

1.3.1 Purification of cell organelles

Cell organelles can be released out of the cell, when the cells are disrupted by homogenization, sonication and other techniques. Cells can be placed in a hypotonic solution; as a result, cells swell and the cell membrane weakens facilitating its easier rupture. Cell homogenate is further purified by sequential differential-velocity centrifugation, which yields partially purified organelles that differ in mass. Equilibrium density-gradient centrifugation separates cellular organelles according to their density and can further purify cell fractions. Immunological techniques which employ antibodies for various organelle specific membrane proteins can be also very useful in purifying cell organelles.

1.3.2 Purification and characterization of membrane proteins

For many structural studies of membrane proteins it is necessary first to purify these proteins out of the membrane. Purified proteins have exposed hydrophobic regions, which drives proteins to aggregate and precipitate from the solution. Integral membrane proteins are amphiphilic, i.e. they have both hydrophobic and hydrophilic regions, and they can only be solubilized in the presence of detergent molecules, which form "belts" around hydrophobic regions of the proteins preventing them from the aggregation. Detergent molecules disrupt membranes by inserting into the lipid bilayers and solubilizing lipids and proteins. At very low concentrations, detergent molecules do not form micelles but dissolve in

water as isolated molecules. Detergent molecules begin to form micelles when detergent concentration increases. The critical micelle concentration (CMC) is a concentration at which micelles form and is different for each type of the detergent depending on the structures of its hydrophobic and hydrophilic parts. Ionic detergents (examples: sodium deoxycholate, sodium dodecylsulfate (SDS), lauryldimethylamine N-oxide (LDAO)) comprise a charged group. Nonionic detergents (examples: octyl-β-D-glucopyranoside (β-OG), *n*-dodecyl-β-D-maltoside (DDM)) do not have a charged group (Fig. 1.2).

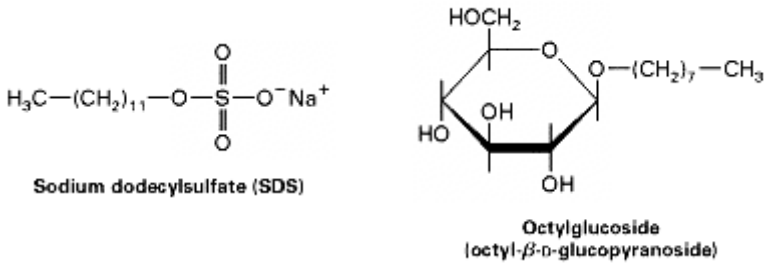

Fig. 1.2. *Chemical structures of two common detergents.*

Because ionic detergents are charged, they can also disrupt ionic and hydrogen bonds and in some cases it can lead to the protein denaturation. Nonionic detergents effect depends on the concentration. Mixed micelles of detergent, phospholipid and integral membrane proteins are formed when detergent concentration is high (above the CMC, Fig. 1.3). At low concentrations (below the CMC), these detergents bind to the hydrophobic regions of membrane proteins, making them soluble in aqueous solution (Fig. 1.3). Although mixed micelles are not formed in this case, the solubilized protein will not aggregate during following purification steps. Careful choice of the detergent, its composition and concentration for solubilization of the particular membrane protein is required.

As for the peripheral membrane proteins, most of them are soluble in watery solutions.

Centrifugation, electrophoresis and chromatography are the most common techniques for purifying and analyzing proteins. Proteins which differ by their mass and shape can be separated by centrifugation based on their rate of sedimentation. Gel electrophoresis separates proteins based on their rate of movement in an applied electric field. Polypeptide chains which differ in molecular weight by 10% or even less can be resolved by SDS-polyacrylamide

gel electrophoresis (SDS-PAGE). In liquid chromatography, a column packed with spherical beads separates proteins based on their rate of movement through the beads. Gel filtration, ion-exchange and affinity columns separate proteins differing in mass, in charge and in ligand-binding properties, respectively. Antibodies are widely used to detect, quantify and isolate proteins. They are used in affinity chromatography and combined with gel electrophoresis in Western blotting, which is a powerful method for separating and detecting a protein in a mixture of various components.

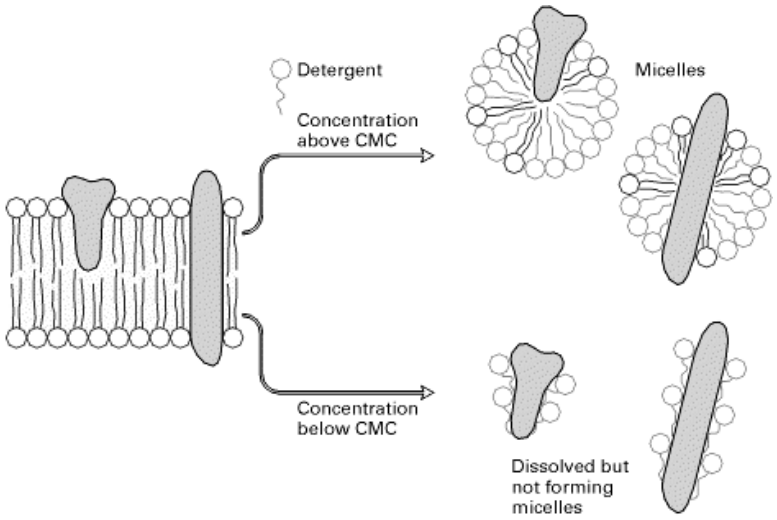

Fig.1.3. *Solubilization of integral membrane proteins by nonionic detergents (Lodish et al 2000).*

1.3.3 Methods used to determine membrane protein conformation

Three-dimensional atomic structures of membrane proteins can be obtained by X-ray crystallography, NMR spectroscopy and theoretical modeling. In the last 30 years more than 27.000 high-resolution three-dimensional protein crystal structures have been deposited into the Protein Data Bank (http://www.rcsb.org). Even though membrane proteins represent 30% of the proteome, relatively little is known about the structure of these proteins. Structures of only about hundred membrane proteins have been resolved up till now. A reason for the slow progress in membrane protein structure determination lies in the amphiphilic nature of these proteins. Membrane proteins have to be solubilized in the presence of a detergent and, as a consequence, they do not readily form well-ordered 3D-

crystals suitable for high-resolution X-ray analysis, due to the limited hydrophilic surfaces available to form crystal contacts and reduced stability. The production of sufficiently large and high quality crystals is a prerequisite to achieve a resolution in the order of couple of angstroms. Unfortunately, a universal recipe for producing high quality crystals does not exist. All optimization procedures for crystallization process are still empirical due to the complexity of theories taking into account many variables that affect the outcome of a crystallization procedure, such as conditions of crystallization and different components involved (temperature, concentrations, lipids and detergents used, proteins themselves). Nevertheless, for a limited amount of membrane proteins the production of highly ordered 3D-crystals was successful. For example, the first X-ray crystal structure of a membrane protein was obtained in 1985 on the bacterial reaction center (RC) from *Rhodopseudomonas viridis* (Deisenhofer et al 1985). This achievement, for which J. Deisenhofer, R. Huber and H. Michel shared the 1988 Nobel Prize in Chemistry, revealed for the first time the locations of the cofactors involved in the earliest steps of photosynthesis and the arrangement of the bacteriochlorophyll special pair.

An alternative to 3D-crystallization is the reconstitution of membrane proteins into 2D-crystals as it is relatively easier and faster to reconstitute membrane proteins into 2D-crystals than into 3D-crystals. Electron microscopy allows the projection maps of membrane proteins to be calculated at atomic resolution (Karrasch et al 1995; Walz et al 1998). However, specimens for electron microscopy generally must be fixed, sectioned and dehydrated, and then stained with electron-dense heavy metals. On the other hand, unfixed and unstained specimens can be viewed in the cryoelectron microscope if they are frozen in hydrated form.

Another, quite recent, alternative to X-ray crystallography and electron microscopy, atomic force microscopy (AFM) has proven to be a powerful tool for structural and functional studies of membrane proteins. AFM has several unique features, such as the ability to image biological samples in their native environment (in buffer solutions, at room temperature and normal pressure), the lack of requirement of special treatment of the biological sample, and the lack of a special need to produce large and highly ordered crystals in order to achieve high-resolution topographs of the protein surfaces. Topographs of several membrane proteins and their protruding termini have been obtained with subnanometer lateral and up to 1 Å vertical resolution (Engel and Müller, 2000; Fotiadis et al 2000; Fotiadis et al 2004; Müller et al 1995a, b; Scheuring et al 1999), while when using cryo-electron microscopy connecting loops and protruding surfaces of integrated membrane proteins are often unresolved (Breyton et al 2002).

1.4 Photosynthesis, the most important process on Earth

One of the fundamental biological processes in nature is the process of photosynthesis in which sunlight energy is converted to chemical energy that can be used by biological systems. All photosynthetic organisms are divided into two groups. When photosynthesis is carried out in the presence of air it is called oxygenic photosynthesis, otherwise it is anoxygenic. Higher plants, algae and cyanobacteria perform oxygenic photosynthesis, while anoxygenic photosynthesis is carried out in some photosynthetic bacteria, such as purple bacteria. Both anoxygenic and oxygenic photosynthesis have the same general principles of energy transduction. Energy for the photosynthesis process is provided by light, which is absorbed by pigments (carotenoids and chlorophylls in plants, bacteriochlorophylls (Bchls) in bacteria). Pigment molecules are non-covalently bound to the protein matrix, forming the membrane-bound pigment-protein complexes. Sunlight energy is harvested by the pigment-protein complexes (often called antenna or light-harvesting (LH) complexes) and transferred to the reaction center (RC), where photochemistry occurs. In most purple bacteria two types of LH complexes are synthesized, B875 (LH1) and B800-850 (LH2) complexes according to their *in vivo* absorption maxima. In some bacteria, such as *Rhodopseudomonas acidophila* and *Rhodospirillum molischianum* there is a third type of LH complex, LH3 (McLuskey et al 2001). The B800-820 LH3 complex is structurally similar to the B800-850 LH2 complex and is synthesized when growing under low intensity illumination and/or low temperature (<30°C) conditions (McLuskey et al 2001).

Very fast and highly efficient energy transfer from LH2 to LH1 and finally to the RC (the lowest energy state in the photosystem) occurs due to the different absorption properties of LH and RC complexes. The energy of the excited LH's reaches the RC on a timescale of less than 100 ps. The overall efficiency of the photosynthesis process is very high (~ 95%) due to the close arrangement and appropriate molecular geometry of light-absorbing pigments with respect to each other (Fleming and van Grondelle, 1997; Pullerits and Sundstrom, 1996).

The photosynthetic apparatus of the anoxygenic purple bacteria is one of the simplest among numerous photosystems and therefore is the most studied and best characterized by biochemical, spectroscopic and imaging techniques during the last several decades (for a vast review on bacterial photosynthesis see Hu et al 2002). In this thesis, we will focus on the photosynthetic processes in the *Rhodobacter sphaeroides* species of anoxygenic purple bacteria.

1.4.1 Photosynthesis in purple bacteria. Function of a photosynthetic membrane in purple bacteria.

In Fig. 1.4 a schematic representation of a photosynthetic membrane of purple bacteria is shown. Generally, photosynthetic apparatus channels, through excitation by sunlight, a cyclic flow of electrons and protons, which leads eventually to synthesis of ATP, an energy-storing compound of the cell.

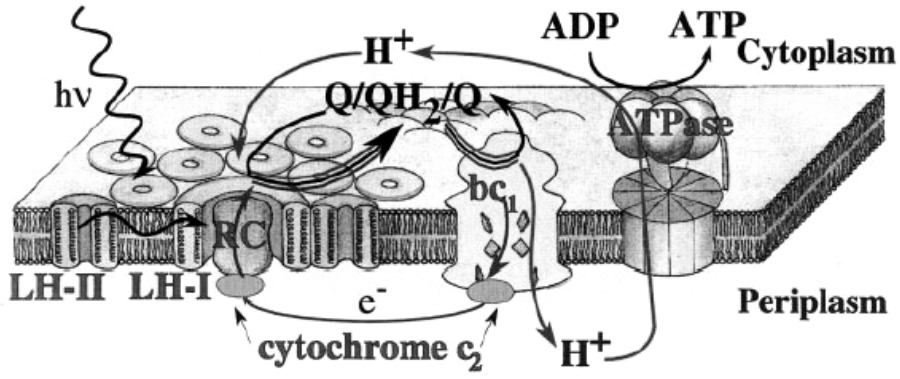

Fig. 1.4. *Schematic representation of a photosynthetic apparatus in a photosynthetic membrane of purple bacteria. The LH1 complex surrounds the RC to form the LHI-RC core complex. LH2 complexes are located in close vicinity to the core complex and form altogether the bacterial photosynthetic unit (PSU). The light energy absorbed by LH complexes reaches the special pair of Bchls in the RC. The special pair looses an electron, which is transferred to quinone molecule (Q). After second photoreaction and uptake of two protons from the cytoplasm the reduced quinone QH_2 is produced and dissociates from the RC and diffuses through the membrane. Reaching cytochrome bc_1 complex QH_2 donates its two electrons to a soluble cytochrome c_2 molecule, which transports them back to the special pair in the RC. The oxidized Q travels back through the membrane to the quinone-binding site (Q_B) on the cytoplasmic face of the RC. Two protons are released to the periplasm generating a proton-motive force, which is used by the ATP-synthase complex to synthesize ATP (Hu et al 2002).*

The organization of photosynthetic RC's and associated peripheral LH complexes into PSU provides collection of light from a broader spectral range and use of energy much more efficiently. LH antennae enlarge the absorption cross-section for capturing sunlight by the RC. The excitation energy is funneled to the RC, maintaining high efficiency of the photosynthesis process.

1.4.2 Individual components of a photosynthetic membrane in purple bacteria

Reaction center

Considerable progress in the understanding of bacterial photosynthesis was initiated by the determination of the structure of the bacterial photosynthetic reaction center from *Rhodopseudomonas viridis* by X-ray crystallography (Deisenhofer et al 1985). It was followed by the discovery of the RC structure from *Rhodobacter sphaeroides* (Allen et al 1987; Chang et al 1986; Ermler et al 1994). The structure of bacterial RC is now known to a resolution better than 2 Å (Fritzsch et al 2002). In Fig. 1.5 the three-dimensional structure of the photosynthetic RC from *Rhodobacter sphaeroides* is shown. It contains three protein subunits, known as L (light), M (medium) and H (heavy), respectively. Multiple pigment molecules (cofactors) are bound to the L- and M-subunits and are arranged in two symmetric branches. Two Bchls form a special pair, two accessory Bchls are located in close proximity to a special pair, and there are also two bacteriopheophytins and a pair of quinone molecules. The L- and M-subunits each form five transmembrane α-helices. The H-subunit is anchored to the membrane only by a single transmembrane α-helix and protrudes considerably above the membrane plane on its cytoplasmic side.

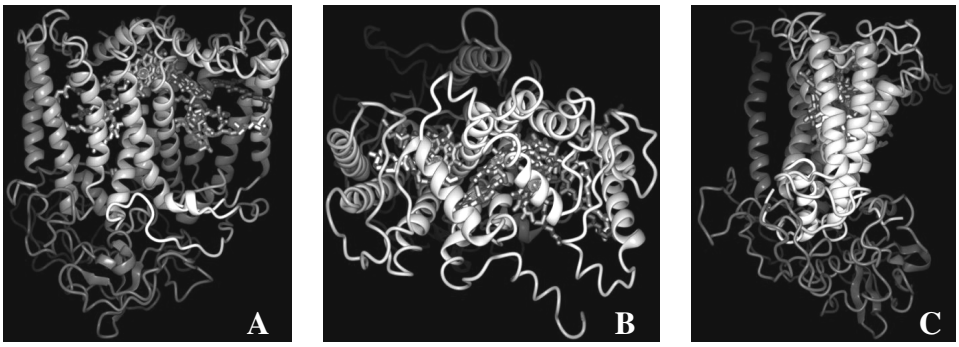

Fig. 1.5. *The three-dimensional structure of the photosynthetic RC from Rhodobacter sphaeroides.* ***A****: Front view;* ***B****: Periplasmic face;* ***C****: Side view [From Prof. Richard Cogdell Internet web site http://www.gla.ac.uk/ibls/BMB/rjc/rcgallery.html].*

LH2 complex

Further X-ray crystallography experiments led to atomically resolved structures of two LH2 complexes from *Rhodopseudomonas acidophila* (McDermott et al 1995; Papiz et al 2003) and *Rhodospirillum molischianum* (Koepke et al 1996). In the former bacterium LH2 appeared to be nonameric, while in the latter LH2 appeared to have an octameric arrangement. Electron crystallography of 2D-crystals of LH2 complexes from *Rhodovulum sulphidophilus* and *Rhodobacter sphaeroides* (Montoya et al 1995; Walz et al 1998) revealed nonameric organization of these LH2 complexes. The overall LH2 structure is an $\alpha_9\beta_9$ nonamer (or $\alpha_8\beta_8$ octamer) and has a ring-like shape (Fig. 1.6). The transmembrane helices of the α-polypeptides are packed side-by-side to form the inner wall of the complex, forming a hollow cylinder of radius 1.4 nm. The nine β-polypeptides are arranged radially around the α-polypeptides helices and form the outer wall of the cylinder of radius 3.4 nm (McDermott et al 1995). The α-polypeptides are parallel to the nine-fold axis of symmetry of the complex, while the β-polypeptides are inclined, at about 15° to the symmetry axis (McDermott et al 1995). All light-absorbing pigments (Bchls and carotenoids) are arranged within this protein scaffold. The Bchl molecules are organized into two concentric rings. Nine well separated Bchls form the B800 ring, and 18 tightly coupled Bchls form a closely interacting B850 ring. Thus, each subunit in the LH2 ring comprises the αβ-polypeptide dimer, three BChls molecules (one from the B800 ring and two from the B850 ring) and two carotenoids.

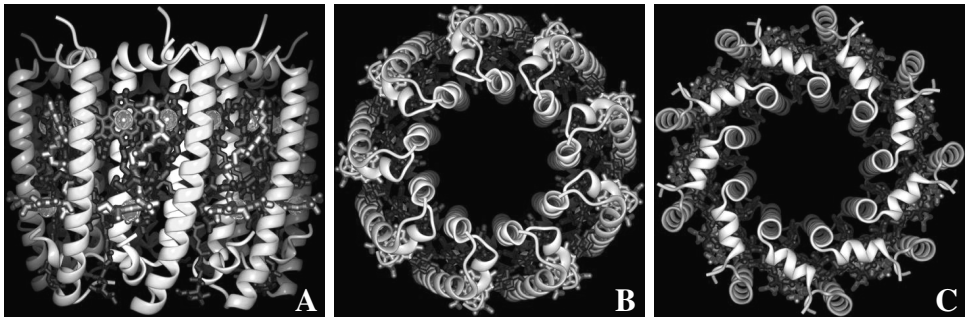

Fig. 1.6. *The three-dimensional structure of the photosynthetic LH2 complex from Rhodopseudomonas acidophila.* ***A****: Side view, periplasm at top;* ***B****: Cytoplasmic face;* ***C****: Periplasmic face. β-polypeptides, α-polypeptides, the 850 nm absorbing Bchls, the 800 nm absorbing Bchls, the carotenoid molecules are shown [From Prof. Richard Cogdell Internet web site http://www.gla.ac.uk/ibls/BMB/rjc/rcgallery.html].*

LH1 complex

For the LH1 complex, only a medium-resolution structure derived from cryo-electron microscopy projection maps is currently available. An 8.5 Å resolution projection map of a reconstituted LH1 complex from *Rhodospirillum rubrum* (Karrasch et al 1995) revealed circular $\alpha_{16}\beta_{16}$ structure with overall architecture similar to LH2 but twice as large in ring diameter, ~12 vs. ~6 nm (Fig. 1.7). The ring hole size (~ 8 nm) was sufficient to accommodate a single RC. Similar projection maps of LH1-RC core complexes from several species of purple bacteria (*Rhodospirillum rubrum, Rhodobacter sphaeroides* and *Rhodopseudomonas acidophila*) have confirmed that the RC is located within the LH1 ring (Jamieson et al 2002; Walz and Ghosh, 1997; Walz et al 1998).

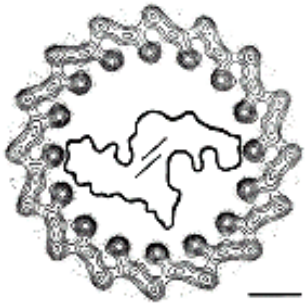

Fig. 1.7. *The 8.5 Å electron microscopy projection map of LH1 from Rhodospirillum rubrum (Karrasch et al 1995; reprinted by permission from EMBO J., copyright 1995 Macmillan Publishers Ltd.). Scale bar 2 nm.*

Further, the LH1 structure was modeled based on homonuclear NMR spectroscopy data (Conroy et al 2000). The LH1 model is shown in Fig. 1.8.

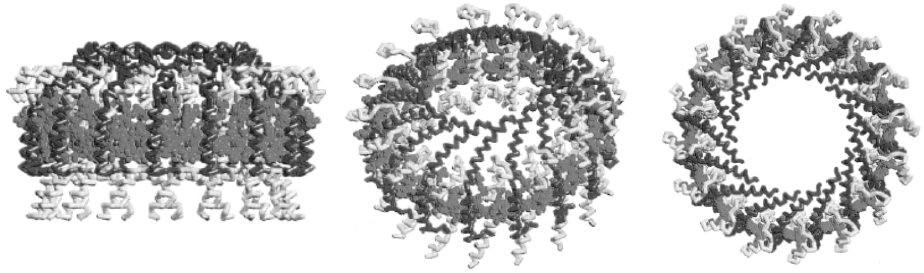

Fig. 1.8. *Conroy's model of LH1 complex from Rhodobacter sphaeroides. The N-terminal helix of LH1 β-polypeptide is directed towards the RC and is predicted to make contact with the RC-H subunit. Three views are shown: side view (cytoplasmic face at top), tilted and top view (facing the cytoplasm), respectively (Conroy et al 2000; reprinted with permission from Elsevier).*

LH1-RC core complex

Very recently the crystal structure of the LH1-RC core complex from *Rhodopseudomonas palustris* at 4.8 Å was published (Roszak et al 2003). The structure shows the RC surrounded by an oval LH1 complex that consists of 15 pairs of αβ-polypeptides and their Bchls (Fig. 1.9). Complete closure of the RC by the LH1 ring is prevented by a single transmembrane helix W.

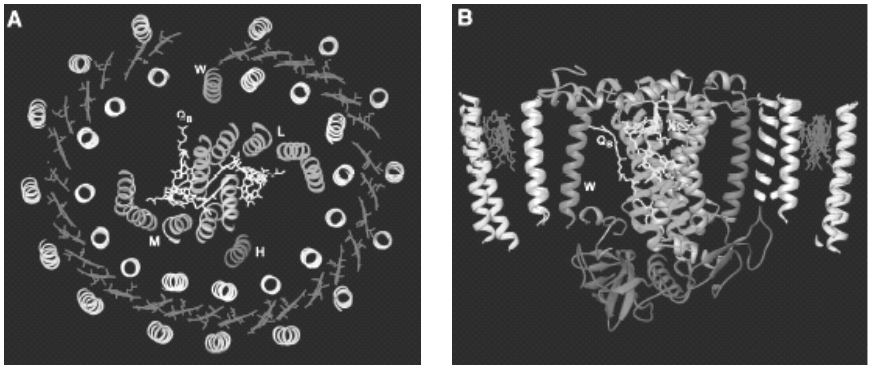

Fig. 1.9. *Schematic model of the LH1-RC core complex from Rhodopseudomonas palustris.* ***A:*** *Top view of the complex (perpendicular to the membrane plane).* ***B:*** *Narrow section of the complex viewed parallel to the membrane plane (Roszak et al 2003).*

Cytochrome bc_1 complex

The very recently published X-ray structure of the bacterial cytochrome bc_1 complex (the simplest form of the cytochrome bc_1 complex) from *Rhodobacter capsulatus* at 3.8 Å resolution (Berry et al 2004) was compared with the available structures of its homologues from mitochondria and chloroplast (Fig. 1.10). The most striking difference between mitochondrial and bacterial bc_1 complexes is that in the latter there is very little surface topology on the cytoplasmic face of the membrane when compared with the mitochondrial bc_1 complex.

ATP-synthase

The crystal structure of the F_1-ATP-synthase (a subunit of a larger enzyme, ATP-synthase) from bovine heart mitochondria was obtained in 1994 (Abrahams et al 1994). In 1997 the rotation of the F_1-ATP-synthase was directly observed by Noji et al. (Fig. 1.11). The F_1-ATP-synthase motor has nine components, five different proteins with the stoichiometry of 3α:3β:1γ:1δ:1ε. The F_1-ATP-synthase is a flattened sphere about 10 nm across by 8 nm high. The membrane-embedded

rotary engine, the F_0 domain, which drives the extra-membranous F_1 domain, consists of subunits a_1b_2 and a cylindrical rotor assembled from 9-14 c-subunits. According to structural analyses, rotors contain 10 c-subunits in yeast and 14 in chloroplast ATP-synthases. AFM and cryoelectron microscopy were successfully employed to show that the 5-7 nm large cylindrical c-oligomer in F_0 consists of 11 c-subunits in the *Ilyobacter tartaricus* bacterium (Stahlberg et al 2001).

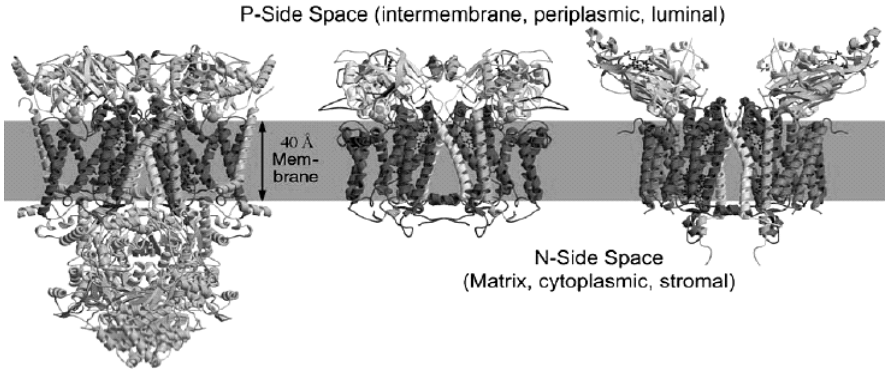

Fig. 1.10. *Structures of mitochondrial, bacterial and chloroplast cytochrome bc_1 complexes. Bovine heart (left), Rhodobacter capsulatus (middle) and C. reinhardthii (right) enzymes are shown (Berry et al 2004).*

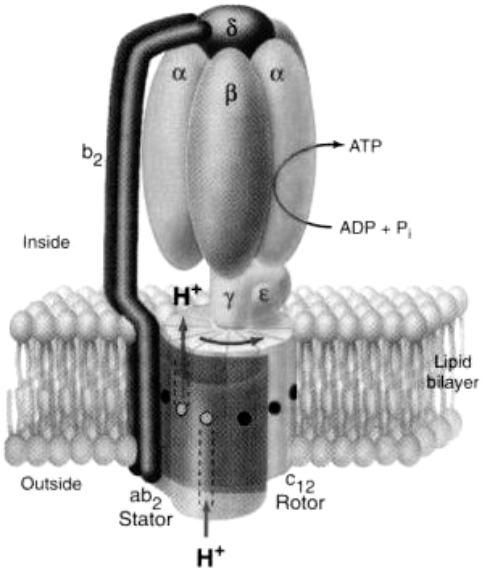

Fig. 1.11. *ATP-synthase motor [From http://www.answersingenesis.org/docs/3799.asp; Noji et al 1997].*

PufX protein

One of the most "mysterious" components of the bacterial photosynthetic membrane is so-called PufX protein. In *Rhodobacter sphaeroides* and *Rhodobacter capsulatus* species, photosynthetic growth requires the presence of this single transmembrane spanning 70-amino acid PufX protein, which is essential to promote an efficient quinone exchange between the RC and cytochrome bc_1 complex (Barz et al 1995a, b; Parkes-Loach et al 2001; Recchia et al 1998; Walz and Ghosh, 1997). Biochemical studies showed that independent of growth conditions one PufX molecule per RC was observed in *Rhodobacter sphaeroides* native membranes as well as in detergent-solubilized LH1-RC complexes (Francia et al 1999). PufX has a strong tendency to interact with the LH1 α-polypeptide (Recchia et al 1998). However, the exact location of PufX protein in the LH1 ring is still unknown. From the functional point of view it is not clear how a reduced quinone molecule is capable of escaping the RC through the surrounding barrier of the LH1 ring if the ring is completely closed. The suggestion was made that in the PufX-containing species of purple bacteria PufX prevents the LH1 ring from complete closure and provides a portal for transient movement of the quinone molecule in and out of the LH1 ring (Cogdell et al 1996). Interestingly, recent electron microscopy data suggest that LH1 complex indeed forms an open ring with a gap of ~ 3 nm width around the RC (Jungas et al 1999; Scheuring et al 2004a). At the same time, the work of Siebert et al. (2004) is contradictory to the open LH1 ring model (Jungas et al 1999; Scheuring et al 2004a), as the electron microscopy projection maps obtained by Siebert et al. showed a continuous ring of LH1 protein round each RC. As for the PufX-lacking species of purple bacteria (*Rhodospirillum rubrum*, *Rhodopseudomonas viridis*, *Rhodospirillum photometricum)*, it was shown using EM and AFM techniques that LH1 completely encircles the RC (Jamieson et al 2002; Scheuring et al 2003b; Scheuring et al 2004b, c). Thus, the question of how the quinone molecule can escape the closed LH1 ring and reach the cytochrome bc_1 complex and what is the role of PufX protein in this process (if any) remains to be answered.

Assembly factors for LH complexes

Little is known about proteins that might interact with LH complex components to facilitate membrane insertion of protein subunits, delivery of Bchls, complex assembly, or stabilization in the membrane. Such a lack of information on assembly is a general problem in all energy transducing systems. Assembly of pigment-protein complexes has been shown to be dependent on factors encoded by open reading frames (ORFs) in the photosynthetic gene cluster (PGC) of *Rhodobacter sphaeroides* and other related photosynthetic bacteria. LhaA is the gene product of one such ORF in *Rhodobacter capsulatus* and has been shown to influence the assembly of LH1 complexes in this organism (Young et al 1998).

The PGC of *Rhodobacter sphaeroides* contains a direct homologue of LhaA, ORF479. There is evidence that the gene product of ORF479 is a functional homologue of LhaA and its disruption leads to obliteration of LH1 assembly in the photosynthetic membrane of *Rhodobacter sphaeroides* (Tucker and Hunter, unpublished). The assembly of the peripheral LH2 complex is mediated by PucC assembly factor (Gibson et al 1992) and PucC and LhaA are related, as are their substrates, LH2 and LH1. However, exact functions of the assembly factors in the biogenesis of PSU components remain to be elucidated.

All components in one plane

The relative positions of individual components in the lipid bilayer of a photosynthetic membrane are shown in Fig. 1.12. LH2 complex, LH1-RC core complex, cytochrome bc_1 complex and quinone molecule are shown positioned next to each other within the plane of a membrane and vertical and lateral dimensions of the complexes as well as the height differences in the protruding termini on both periplasmic and cytoplasmic faces of the membrane can therefore be directly compared. The LH2 ring has a diameter half the diameter of the LH1 ring, ~ 6 nm vs. ~ 12 nm (Fig. 1.6 and 1.7). The size of the RC (~ 8 nm) is small enough to fit in the interior of the LH1 complex (Fig. 1.9). The RC-H subunit protrudes above the LH1 ring on the cytoplasmic face of the membrane, while on the periplasmic face the RC surface is at a lower level than the surrounding LH1 ring (Fig. 1.5 and 1.9B). In contrast to LH1-RC topology, in the cytochrome bc_1 complex the subunits of the complex protrude noticeably above the lipid bilayer on the periplasmic face of the membrane, but there is very little surface protruding above the plane of the membrane on its cytoplasmic side (Fig. 1.10). In turn, the ATP-synthase complex (not shown in Fig. 1.12) protrudes considerably on the cytoplasmic face of the membrane (Fig. 1.11).

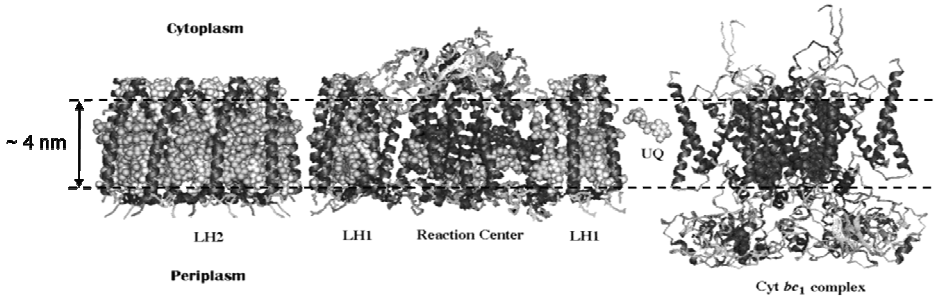

Fig. 1.12. *Individual components of a photosynthetic membrane are shown inserted into the lipid bilayer. Approximate thickness of the lipid bilayer is 4 nm. LH2 complex, LH1-RC core complex, cytochrome bc_1 complex and quinone molecule (UQ) are shown [From A. R. Crofts lab home page http://www.life.uiuc.edu/crofts/ahab/hetchrm.html].*

We note that many components of the bacterial photosynthetic membrane are quite distinct in topography. This, in principle, allows the use of high-resolution AFM as an analytical tool. Probing the shape and size of the membrane proteins and their protruding termini above the reference plane (lipid bilayer) can provide a direct interpretation of the composition of a photosynthetic membrane.

1.4.3 Organization of a bacterial photosynthetic unit

As was shown in the section 1.4.2 of this chapter the 3D crystal structures of all individual components of a photosynthetic membrane in purple bacteria are now available in great detail. At the same time, the question how these individual components are positioned with respect to each other within the native photosynthetic membrane remained extremely topical during the last several decades.

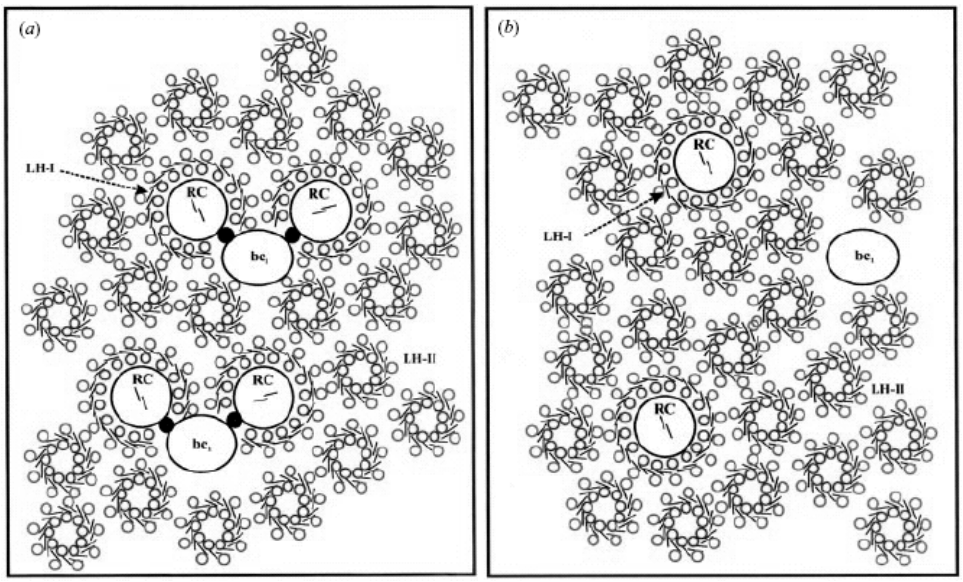

Fig. 1.13. *Proposed models of a bacterial PSU.* ***A:*** *Model A - PSU according to Niederman (Westerhuis et al 1998) and Parson (Monger and Parson, 1977; Nagarajan and Parson, 1997). LH1-RC-PufX-bc_1 supercomplex is formed from a pair of LH1-RC-PufX core complexes. LH1 rings are open. The supercomplex is surrounded by peripheral LH2 complexes. The PufX protein (solid dot) is shown located between the RC and cytochrome bc_1 complex.* ***B:*** *Model B - PSU according to Cogdell and colleagues (Papiz et al 1996). The PSU is formed by the LH1-RC core complex which is surrounded by LH2's. LH1 rings are closed. Cytochrome bc_1 complexes randomly located in the membrane are also shown (Hu et al 2002).*

Fig. 1.13 depicts two proposed models for the bacterial PSU. These models are based on low-resolution electron microscopy projection maps and spectroscopic analyses (Nagarajan and Parson 1997; Papiz et al 1996; Westerhuis et al 1998). The two models of bacterial PSU display significant differences in two major aspects: *i)* the LH1-RC core complex is monomeric in model B, while in model A LH1-RC core complexes are dimeric; *ii)* in model A the LH1 ring is open that allows shuffling of quinone molecule between the RC and cytochrome bc_1 complex, while in model B LH1 forms a closed ring structure. Model A was supported by electron micrographs of purified tubular membranes from *Rhodobacter sphaeroides* (Jungas et al 1999; Vermeglio and Joliot, 1999). It was shown that in the $LH2^{-}PufX^{+}$ tubular membranes LH1-RC core complexes were organized as S-shaped dimers and each LH1 ring encircling the RC was open (Jungas et al 1999). The remaining positive density in the projection maps was tentatively attributed to one cytochrome bc_1 complex, which was placed in between two LH1-RC core complexes forming a dimer (Jungas et al 1999). Model B is based on spectroscopic observations (Deinum et al 1991) and an 8.5 Å resolution electron micrograph of LH1 complex from *Rhodospirillum rubrum* by Karrasch and colleagues (Karrasch et al 1995, see Fig. 1.7). Electron micrographs of LH1-RC complexes from *Rhodopseudomonas viridis* and *Rhodobacter sphaeroides* ($PufX^{-}$ strain) also indicated a single RC inside a closed ring of the LH1 (Ikeda-Yamasaki et al 1998; Walz et al 1998).

The inability to resolve differences between two PSU models shown in Fig. 1.13 originates from the limitation of low-resolution electron microscopic data in resolving atomic level details. Poorly ordered samples (such as multi-component photosynthetic membranes) are not suitable for high-resolution EM imaging. From this point of view, the AFM technique provides a unique possibility to perform structural studies on native membranes since well-ordered arrays of proteins are not necessary for high-resolution AFM imaging. AFM has such a high signal-to noise ratio that single molecules can be observed at a resolution better than 1 nm, as was demonstrated by imaging of membrane proteins imbedded into the 2D-crystals. The next challenge for high-resolution AFM imaging was visualization of the spatial organization of heterogeneous membrane proteins within the native membrane network. Very recently the first direct high-resolution topographs of the intact architecture in native photosynthetic membranes from *Rhodopseudomonas viridis* were acquired by means of AFM (Scheuring et al 2003b). LH1-RC core complexes were found to be packed hexagonally in the membrane. A single RC surrounded by a closed ellipsoid of 16 LH1 subunits was revealed. It was also shown that the LH1 subunits rearranged into a circle after the complete removal of the RC from the core complex by the scanning AFM tip (nanodissection), suggesting a flexible LH1 ring structure (Scheuring et al 2003b). It is important to note that photosynthetic membranes from *Rhodopseudomonas viridis* species lack the LH2 complex as well as PufX

protein *in vivo* and thus represent relatively simple supramolecular architecture of a photosynthetic membrane. The same authors (Scheuring et al 2004b, c) performed AFM imaging of a multi-component native photosynthetic membrane from *Rhodospirillum photometricum*. Several proteins (LH1, LH2, RC and cytochrome c_2) could be seen and identified. The analysis and modeling of the lateral organization of multiple components of the photosynthetic apparatus showed that their arrangement is far from random, with significant clustering both of LH2 complexes and LH1-RC core complexes. Note that *Rhodospirillum photometricum* is also a PufX-lacking species. The lateral organization of the proteins in the *Rhodospirillum photometricum* native membranes found by Scheuring and colleagues (Scheuring et al 2004b, c) is similar to the model B shown in Fig. 1.13B, where single LH1-RC core complex is surrounded by several peripheral LH2 complexes.

The role of PufX in the photosynthetic membrane organization

The role of PufX protein in the supramolecular organization of the pigment-protein complexes in the PufX-containing photosynthetic membranes (*Rhodobacter sphaeroides* and *Rhodobacter capsulatus* species) has been extensively studied over the last decade. Gel filtration chromatography and electron microscopy of photosynthetic proteins from *Rhodobacter sphaeroides* revealed dimeric LH1-RC complexes and it was concluded that PufX plays a central structural role in forming dimeric LH1-RC complexes (Francia et al 1999). Recent AFM and EM experiments (Scheuring et al 2003b; Scheuring et al 2004b, c; Siebert et al 2004) showed that in the native membranes extracted from PufX-lacking species (or $PufX^-$ *Rhodobacter sphaeroides* mutant cells used by Siebert et al 2004) LH1-RC core complexes did not form dimers but stayed monomeric, which confirmed the role of PufX in dimerization of core complexes.

Furthermore, from polarized absorption spectra on oriented $LH2^-$ native membranes from *Rhodobacter sphaeroides* (in the presence or absence of the PufX protein) it was concluded that PufX induces a specific orientation of the RC in the LH1 ring, as well as the formation of long-range regular arrays of LH1-RC core dimers in the photosynthetic membrane (Frese et al 2000). A model of how the RC is positioned within the LH1 ring relative to the long orientation axis of the membrane was constructed (Frese et al 2000).

Currently there are two models for the organization of LH1-RC-PufX dimeric supercomplexes. In the EM work of Siebert and colleagues (Siebert et al 2004) on tubular native membranes ($LH2^-$ mutant cells) from $PufX^+$ and $PufX^-$ strains of *Rhodobacter sphaeroides* the model of LH1-RC-PufX supercomplex was derived. In dimeric LH1-RC-PufX complexes LH1 formed a continuous ring of a protein around each RC and PufX was located at the heavily stained region created by the

absence of LH1 β-polypeptide. This arrangement, coupled with a flexible ring, would give the RC Q_B site transient access to the openings in the LH1 ring, which might be of functional importance (Siebert et al 2004). In the model of Scheuring and colleagues (Scheuring et al 2004a) derived from the cryo-EM experiments on *Rhodobacter sphaeroides* LH1-RC-PufX 2D-crystals, LH1-RC-PufX core complexes were assembled in a S-shaped dimeric complex, where each core complex was composed of one RC, twelve LH1 αβ-heterodimers and one PufX protein. The LH1 assemblies were open with a gap of density of ~ 3 nm width and surrounded oriented RC's. A maximum density was found at the dimer junction. In contrast to Siebert's model (Siebert et al 2004), two PufX proteins were positioned at the dimer junction. This implied that PufX is a structural key for the dimer complex formation rather than a channel-forming protein for the exchange of quinone molecules between the RC and cytochrome bc_1 complex (Scheuring et al 2004a).

Interestingly, in the crystal structure of LH1-RC core complex from *Rhodopseudomonas palustris* (described in section 1.4.2.3) a single transmembrane protein, W, was found (Roszak et al 2003). W protein prevented the LH1 ring from a complete closure. This break, located next to the Q_B site in the RC for the quinone molecule, may provide a portal through which quinone can transfer electrons to cytochrome bc_1 complex. It is possible that this W protein is a functional analogue to the PufX protein in *Rhodobacter sphaeroides* and *Rhodobacter capsulatus* species; however this remains to be proven.

To summarize, the supramolecular organization of individual components of a photosynthetic membrane in purple bacteria was shown to be dependent on: *i)* species (PufX or LH2 presence/absence) and *ii)* growth conditions. In the PufX-containing species, the supramolecular organization of the wild type native membranes, containing both LH1-RC-PufX core complexes and peripheral LH2 complexes, remained unknown. It was, however, known that $LH2^-$ mutant cells start producing highly-ordered tubular membranes composed of ordered arrays of LH1-RC-PufX core complexes. This allowed Jungas et al. (1999) and Siebert et al. (2004) to obtain high-resolution EM data on these tubular membranes. In contrast, photosynthetic membranes from wild type cells are spherical (due to the presence of peripheral LH2 complexes). In these spherical membranes a highly ordered crystalline arrangement of the proteins is not longer expected due to the possible perturbation of the long-range order of LH1-RC-PufX core complexes by LH2 complexes. Thus, for EM technique, achievement of high-resolution data on wild type native membranes is a very difficult (if not impossible) task due to the poorly developed diffraction pattern. In turn, direct imaging of single individual proteins by means of AFM does not require large and highly-ordered arrays of protein aggregates. On the other hand, the main difficulties in imaging of this kind of sample (non-crystalline native membranes) by means of AFM are the curved

surface and waviness of the membranes, which still makes the achievement of high-resolution topographs of membrane proteins in their native environment extremely challenging.

1.4.4 *Rhodobacter sphaeroides* purple bacteria

Rhodobacter sphaeroides is a Gram-negative[1], purple, non-sulfur, facultative anaerobe[2], capable of anoxygenic photosynthesis[3] (Naylor et al 1999). Under low aeration, a morphological change occurs within the bacterial cell cytoplasmic membrane resulting in the formation of highly-invaginated intracytoplasmic membrane (ICM) (Fig. 1.14, Niederman et al 1976). The ICM invaginations house the photosynthetic apparatus (LH complexes and RC's). The average size of ICM chromatophores is ~ 50-100 nm in diameter. The proliferation of this membrane provides an increased surface area for the absorption and utilization of light by the photosynthetic apparatus.

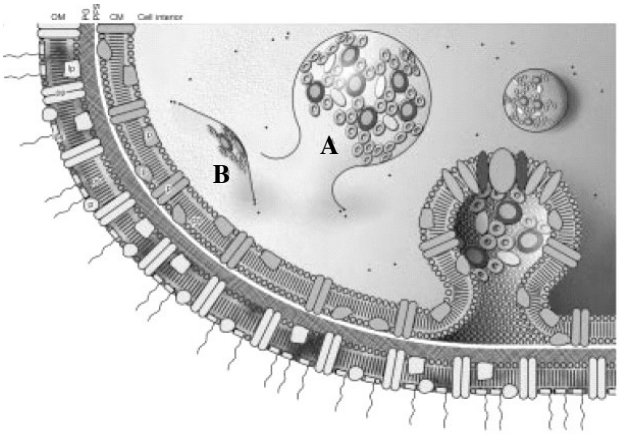

Figure 1.14. *Representation of the ICM system formed in Rhodobacter sphaeroides as a result of a reduction in the oxygen tension. A = fully formed invagination; B = site of initiation of ICM growth. Adapted from Naylor et al 1999.*

[1]**Gram-negative:** to describe a prokaryotic cell whose cell wall stains pink (negative) in Gram stain.
[2]**Facultative anaerobe:** an organism which is normally aerobic but can also grow without oxygen.
[3]**Anoxygenic photosynthesis:** a type of photosynthesis in green and purple bacteria in which oxygen is not produced.

The PSU of purple bacteria needs to achieve a high enough efficiency to provide sufficient energy for the bacteria to survive, while at the same time the PSU needs to be protected against photodamage. This balance is maintained for a large range of environmental conditions. Bacteria adapt to changes in environment by rebuilding the complete photosynthetic apparatus on a timescale of minutes to at most a few hours (Hu et al 2002). Two environmental factors, oxygen tension and light intensity regulate the synthesis of photosynthetic proteins. Oxygen at atmospheric levels (21%) represses ICM formation almost completely (Hu et al 2002). In contrast, under anaerobic conditions (<1% oxygen) ICM invaginations containing photosynthetic apparatus are formed. Light intensity, in its turn, regulates synthesis of peripheral LH2 complexes, which content in ICM increases when sunlight intensity decreases (Sturgis and Niederman, 1996).

Mutagenesis of Rhodobacter sphaeroides (deletion/complementation system for bacterial photosynthetic genes)

One way to investigate structural features of a photosynthetic membrane is to use the technique of site-directed mutagenesis to construct mutant complexes (Jones et al 1992). A system for the analysis of protein function by site-directed mutagenesis requires three major components: a sequenced target gene cloned into vectors suitable for the introduction of site-directed changes, a deletion/insertion strain to provide a null genetic background and mobilizable vectors which facilitate complementation of the deletion strain with altered genes (Jones et al 1992). Within the context of photosynthetic bacteria the most notable application of this technique has been done in the study of *Rhodobacter sphaeroides* and *Rhodobacter capsulatus*.

In order to express mutant complexes in a suitable genetic background Jones and colleagues (Jones et al 1992) constructed deletion/insertion mutants of *Rhodobacter sphaeroides,* in which the genes of either the *puf* operon (coding for the LH1 α- and β-, RC L- and M-subunit polypeptides and the X protein (PufX)) and/or the *pucBA* genes (coding for the LH2 α- and β-polypeptides) have been deleted and replaced by an antibiotic-resistance cassette. The absence of the genomic copies of both the *puc* and *puf* operons ensures that the properties of the plasmid-borne LH complex can not be influenced by the presence of polypeptides of the second LH complex (Jones et al 1992).

Strain DD13 was constructed, in which *pufBALMX* and *pucBA* have been replaced by kanamycin and streptomycin cassettes, respectively (Jones et al 1992). DD13 strain therefore is devoid of all three pigment-protein complexes and can be used to express LH1, LH2 or RC as the sole complex. Three *Rhodobacter sphaeroides* mutant strains (described previously in Jones et al 1992) were used in our study for growing bacterial cells, isolation of ICM's, purification and 2D-crystallization

of membrane proteins for further AFM imaging of photosynthetic 2D-crystals and native membranes: *i)* DD13, $LH2^{-}$ $LH1^{-}$ RC^{-}; *ii)* DPF2, LH2-only (for production of LH2-only native membranes and 2D-crystals); *iii)* pRKEK1, LH1-only (for production of LH1-only native membranes and 2D-crystals).

The role of individual photosynthetic membrane components in the morphology and organization of the membrane could be studied using mutant strains of purple bacteria cells (Hunter et al 1988). Genetic manipulation of the wild type cells resulted in a modified cell morphology. It was for example shown for the first time that in the $LH2^{-}$ mutant strain of *Rhodobacter sphaeroides* tubular ICM were formed rather than vesicular (Hunter et al 1988), as shown in Fig. 1.15C. In contrast, in the $LH1^{-}RC^{-}$ mutant strain vesicular, not tubular, internal membranes were observed (Fig. 1.15B). The authors concluded that in the absence of LH2, morphogenesis of internal membranes is incomplete and is arrested at a tubular stage (Hunter et al 1988). As we discussed earlier in section 1.4.3 of this chapter, $LH2^{-}$ highly-ordered tubular membranes isolated from mutant *Rhodobacter sphaeroides* cells were studied using EM technique (Jungas et al 1999; Siebert et al 2004). However, vesicular wild type, LH1-only and LH2-only native membranes have never been investigated before using high-resolution imaging techniques.

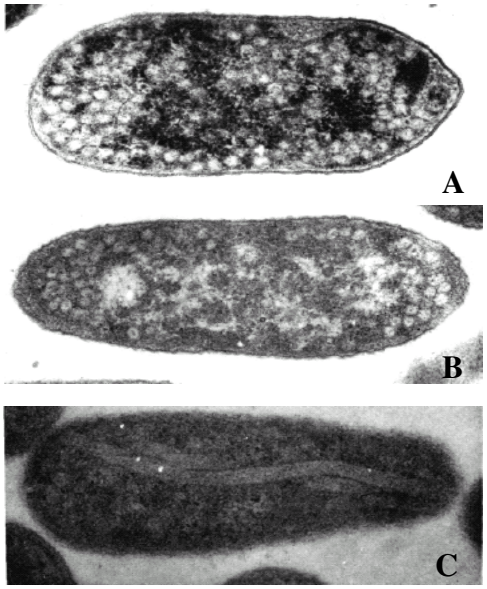

Fig. 1.15. *Electron micrographs of a thin section of Rhodobacter sphaeroides cells. A – wild type cells; B –* $LH1^{-}RC^{-}$ *mutant strain; C –* $LH2^{-}$ *mutant strain (Hunter et al 1988).*

1.5 Principles of atomic force microscopy and its applications in biology

In our laboratory a compact stand-alone AFM set-up was developed (van der Werf et al 1993) which was used for the AFM experiments described in this thesis. Very recently, a combined AFM/confocal fluorescence setup was constructed in our group (Kassies et al 2004), which allows simultaneous topographic and fluorescent imaging of photosynthetic pigment-protein complexes and has a tremendous potential for future experiments on biological systems.

Generally, in AFM the sample is scanned with a sharp probe (tip) which is mounted to the free end of the cantilever. Forces between the tip and the surface cause the cantilever to deflect. Deflections of the cantilever are recorded and stored in a computer. There are two possibilities to scan the surface: when the cantilever with the tip is at rest and the sample is scanned with a piezo (x-y-z)-translator and an alternative approach is that the tip is scanned and the sample is at rest. In our laboratory the latter approach is used. The sample is imaged by scanning the tip across the surface with the help of a (x, y, z)-piezo tube, which is connected to the cantilever (Fig. 1.16).

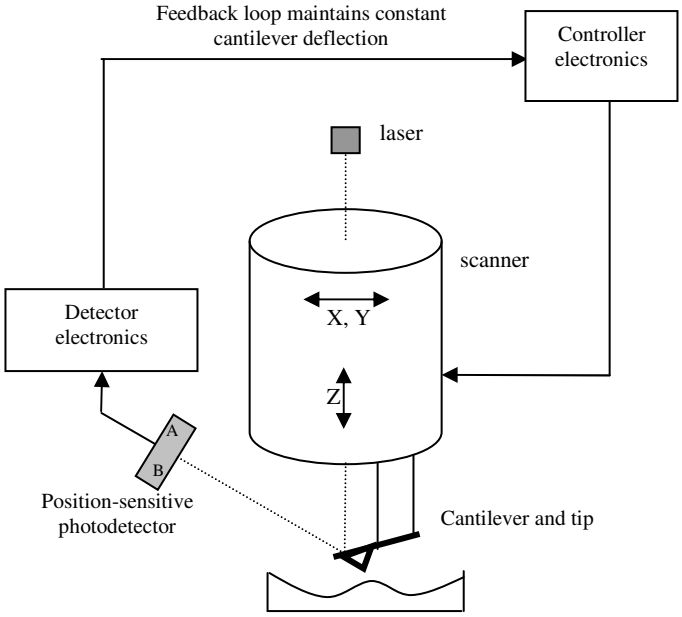

Fig. 1.16. *Principle of the AFM work. AFM operates by scanning a tip attached to the end of a cantilever across the sample surface while monitoring the change in cantilever deflection with a photodiode detector.*

A diode laser is positioned in the piezo tube and the laser beam is focused on the back side of the cantilever. The reflection of the laser light is projected through a mirror onto a quadrant photodiode. Cantilever deflections cause change in the position of the laser beam on the detector. The difference in the intensity between the left and the right half of the detector is proportional to the cantilever deflection and is thus a measure for the tip position. The deflection of the cantilever resulting from the tip-sample interaction can be detected with an optical detector at a resolution of 0.1 nm, allowing forces of 10-50 pN to be measured.

Once the AFM has detected the cantilever deflection, it can generate the topographic data set by operating in one of two modes: *constant-height* or *constant-force* mode. In constant-height mode, the deflections of the cantilever can be used directly to generate the topographic data because the height of the cantilever is fixed as it scans. This mode of scanning is not applicable for samples with large height variations.

In constant-force mode the scanner moves up and down in Z, responding to the topography by keeping the cantilever deflection constant. In this case, the image is generated from the scanner's motion. With the cantilever deflection held constant, the total force applied to the sample is constant. In constant-force mode, the speed of scanning is limited by the response time of the feedback loop, but the total force exerted on the sample by the tip is well controlled. Constant-force mode is generally preferred for most applications.

For imaging, the tip is raster scanned over the sample, and at each position the cantilever deflection is measured, with which a topography map can be constructed. The topographic data are the height of the scanner in Z for constant-force mode or cantilever deflection for constant- height mode.

Several forces contribute to the deflection of the AFM cantilever. The force most commonly associated with AFM is an interatomic van der Waals force. The dependence of the van der Waals force on the distance between the tip and the sample is shown in Fig. 1.17. In Fig. 1.17 it can seen that there are three distance regimes (modes): 1) contact regime, 2) non-contact regime and 3) tapping regime. In the contact regime, the cantilever is brought from the surface less than a few angstroms, and the interatomic force between the tip and the sample is repulsive. In the non-contact regime, the cantilever is held about tens or hundreds angstroms from the surface and the interatomic force between tip and surface is attractive. In the intermittent (or tapping) regime the vibrating tip touches the surface at the bottom of its oscillation motion.

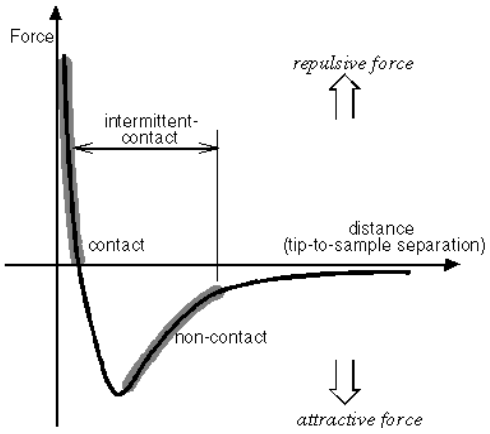

Fig. 1.17. *Interatomic force vs. distance curve.*

All experiments performed and described in this thesis were done using tapping mode AFM imaging, as it has proved to be a powerful method for achievement of high-resolution topographs of soft biological samples (Möller et al 1999).

Another, not so widespread, scanning mode is the so-called jumping mode, which allows the simultaneous measurement of the topography and of some other physical properties (adhesion, electrostatic interaction) of the sample (Pablo et al 1998). In phase imaging the phase lag of the cantilever oscillation relative to the driving signal is recorded. This signal is sensitive to variations in the material properties such as viscoelasticity and adhesion. In adhesion force imaging AFM takes a force curve at each pixel by ramping a piezoactuator, moving the tip up and down towards the sample (van der Werf et al 1994). Force curve provides information on repulsion, attraction and adhesion between the tip and sample surface.

There are several important parameters, which should be adjusted while scanning. Though lateral forces strongly reduced in tapping mode in comparison with contact mode, normal forces can have a great impact on the sample stability and image quality. In general, the smaller the amplitude, the less energy is available for damaging work during the impact on the sample. Keeping the tapping amplitude small is advantageous for keeping the sample stable for a second reason. The *setpoint* parameter tells the feedback loop what amplitude (tapping mode) or deflection (contact mode) to maintain at a constant value during scanning. It is also desirable to keep the difference between the free tapping amplitude and the setpoint amplitude (damping value) as small as possible, in the

order of 5-20%, as the amount of damping determines the amount of the force applied by the oscillating tip onto the sample surface.

The *gain* controls the amount of the integrated error signal used in the feedback loop. The higher this parameter is set, the better the tip will track the sample topography. However, if the gain is set too high, noise due to the feedback oscillation will be introduced into the scan. Setting the gain too low may result in the tip not tracking the surface properly.

The *scan rate* is the number of trace and retrace scan lines performed per second (Hz). The scan rate should be set so that the feedback loop has time to respond to changes in the sample topography. Setting the scan rate too high will result in poor tracking of the surface. The actual tip speed depends on two parameters: scan rate and scan size. The scan rate greatly depends on the scan size and the height of the features being imaged. The taller the features and/or larger the scan size, the slower the scan rate. Typically, line frequencies of 2÷7 Hz were used for the measurements presented in this thesis.

Number of points per line: determines the number of pixels in X and Y. The spacing between data points is called the *step size*. The step size is determined by the full scan size and the number of data points per line. For example, in the scan area of 2500x2500 nm^2 the step size will be ~ 10 nm at 256 pixels, which is larger than the size of some membrane proteins. Zooming-in to the smaller scan areas reduces the step size and allows the specimen to be sampled more accurately.

Cantilevers and their tips are critical components of AFM because they determine the force applied to the sample and the lateral resolution of the system. Tip and cantilever assemblies can be fabricated from silicon or silicon nitride. Atomic force microscopes require not only sharp tips, but also cantilevers with optimized spring constants. The spring constants of commercially available cantilevers range from 0.01 N/m to 70 N/m. Resonant frequency ranges from a few kilohertz to hundreds of kilohertz. The desirable properties for a cantilever depend on the imaging mode and the application. In contact mode, soft cantilevers (0.01÷0.1 N/m) are preferable because they deflect without deforming the surface of the sample. In tapping mode, stiffer (0.5 N/m and higher) cantilevers with high resonant frequencies give optimal results.

The resolution of AFM images can be presented in terms of *lateral (X, Y)* resolution and *vertical (Z)* resolution. The smaller the radius of curvature, the smaller the feature that can be resolved. A sharper tip will be able to resolve smaller features than a dull tip with a larger radius of curvature. The typical radius of curvature of AFM tip is 20-50 nm. However, at the very end of the pyramidal tip small protrusions can provide a probe to contour the surface at a resolution

better than 1 nm, as was demonstrated, for example, by imaging of membrane proteins surface (Fotiadis et al 2004; Möller et al 1999; Scheuring et al 2001; Scheuring et al 2003a). The sharpness of the AFM tip is one of the most important components of the successful high-resolution imaging and at the same time is the most uncontrollable. The shape of the tip can constantly vary during imaging, especially when imaging soft biological samples in liquid environment. Tip gets contaminated very fast and fine details in the surface topology can no longer be resolved. The tip shape does not determine the vertical resolution; it is determined by the resolution of the vertical scanner movement which is ~ 1Å.

Glass, mica and gold surfaces are the most common substrates for immobilization of biological samples for AFM imaging. For our experiments on photosynthetic membrane proteins we chose mica as a support. Mica is chemically inert, atomically flat over the area of several hundreds of square micrometers and therefore is ideally suitable for adsorption of membrane proteins onto the solid substrate and further high-resolution mapping of their surfaces.

When imaging in air, the thin water film at the sample surface forms a capillary meniscus at the AFM tip. Capillary forces exceed all other attractive forces by orders of magnitude, leading to sample deformation, thereby limiting the resolution. Although experimentally more difficult than scanning in air, biological samples should be imaged in aqueous solutions because this provides the best preservation of the biological structure and allows the tip-sample interactions to be controlled more precisely. A major improvement to our stand-alone AFM was the design of a liquid cell, which made possible performing AFM experiments in liquid environment (van Noort et al 1998). Results presented in this thesis were obtained using tapping mode imaging in liquid.

Over the last decade AFM was extensively used for diverse biological applications. The ability of AFM to monitor conformational changes of biological assemblies directly and under native conditions was demonstrated (Müller et al 1995a; Müller et al 1996). Imaging and manipulation of double-layered 2D-crystals and native membranes of membrane proteins has allowed the acquisition of valuable functional and structural information (Fotiadis et al 2004; Müller et al 1999a; Scheuring et al 2001; Scheuring et al 2003a, b; Scheuring et al 2004a, b, c). Mechanical disruption of the upper layers of stacked crystalline sheets and double-layered native membranes has enabled the investigation of otherwise hidden surfaces (Fotiadis et al 2000; Schabert and Engel 1994; Schabert et al 1995; Scheuring et al 2004b).

1.6 Thesis overview

This thesis takes a detailed look at diverse bacterial photosynthetic systems. In order to visualize photosynthetic membrane pigment-protein complexes in their native environment high-resolution AFM imaging in liquid was employed.

In Chapter 2 the structural and physical properties of the peripheral ring-like LH2 complex in both reconstituted 2D-crystals and in the native membranes are investigated by AFM. The possible mechanisms of the influence of the detergent and the mica substrate on the spatial organization of the LH2 complexes in the native membranes are discussed.

In Chapter 3 AFM is used to compare 2D-crystals of LH2 and of LH1 complexes. The structural basis for variations in size and shape of the LH1 complex and for the invariable LH2 ring architecture is derived.

In Chapter 4 the organization of a multi-component bacterial native photosynthetic membrane from *Rhodobacter sphaeroides* is directly visualized for the first time by AFM. The relative positions and associations of the individual components of a membrane are shown and a new model for native membrane organization is presented.

In Chapter 5 the role of the PufX protein in the supramolecular architecture of a photosynthetic membrane from *Rhodobacter sphaeroides* is directly demonstrated. The difference in the spatial organization of the photosynthetic complexes in the PufX-containing and PufX-lacking membranes is shown.

In Chapter 6 future experiments on bacterial photosynthetic systems and recommendations on high-resolution AFM imaging are suggested.

Absence of proof
is not proof of absence.
Michael Crichton

Chapter 2

AFM imaging of the photosynthetic peripheral light-harvesting complex LH2

It is believed that in order to obtain a fully functional photosynthetic membrane the various components have to form a network of interacting proteins within the membrane. In order to be able to image an intact photosynthetic native membrane and to be able to unambiguously recognize and characterize each type of its constituent individual proteins, it is necessary first to analyze each individual component separately. To investigate various possibilities of protein-protein interactions we have acquired AFM images of the peripheral LH2 complex both reconstituted into the 2D-crystals and in the native membranes. Aspects of 2D-crystallization and spatial organization of the LH2 complexes within the 2D-crystals and native membranes are discussed. We have shown that regardless of the type of crystalline packing and environment (fully native or within the 2D-crystal), the LH2 complex behaved as an essentially rigid structure which conserved its circular shape and invariable ring size. The influence of the detergent and the substrate on the organization of the LH2 complexes in the LH2-only native membranes is discussed.

2.1 Introduction

In the photosynthetic membrane of purple bacteria sunlight energy is first collected by the peripheral LH2 antennae and then transferred from the LH2 complexes to the LH1 complexes and finally to the RC, where charge separation takes place. The atomic structures of the LH2 complexes from different species of purple bacteria are available. The crystal structure of the nonameric ring-like LH2 complex from *Rhodopseudomonas acidophila* strain 10500 was discovered by X-ray crystallography in 1995 (McDermott et al 1995, Fig. 1.6 in Chapter 1). The LH2 complex from *Rhodospirillum molischianum* was shown to be octameric (Koepke et al 1996). Based on the cryo-EM data at 6 Å resolution the LH2 complex from *Rhodobacter sphaeroides* is nonameric, comprising 9 subunits of αβ-heterodimers (Walz et al 1998). The LH2 of *Rhodobacter sulphidophilus* (Montoya et al 1995) is also nonameric as demonstrated by high resolution cryo-EM. The low light peripheral complex of *Rhodopseudomonas palustris* has been crystallized and a 7.5 Å structure produced that indicates that this complex has an octameric structure in which half of the pigments are arranged radially so that they do not form an overlapping ring as in all other purple bacterial LH complexes (Hartigan et al 2002).

Recently, the LH2 complexes from *Rubrivivax gelatinosus* (Scheuring et al 2001), *Rhodobacter sphaeroides* (Scheuring et al 2003a) and *Rhodopseudomonas acidophila* (Gonçalves et al 2004; Stamouli et al 2003) reconstituted into the 2D-crystals have been successfully imaged using AFM. Circular nonameric rings were resolved in a 2D-crystal plane. The LH2 rings were observed in two opposite orientations with a slight tilt of the rings with respect to the lipid bilayer plane (Scheuring et al 2003a), both with a tilt or without depending on the type of crystal packing (Gonçalves et al 2004), and a small ellipticity (Scheuring et al 2001).

Using a deletion complementation system (Jones et al 1992) 2D-crystals reconstituted from *Rhodobacter sphaeroides* LH2 complexes have been produced that did not contain any other LH complexes providing an opportunity to study physical parameters and aggregation states of only the LH2 complex in its lipid bilayer environment. In contrast, the methodology used for 2D-crystallizaion of the LH2 complexes from *Rubrivivax gelatinosus* (Scheuring et al 2001) resulted in the production of LH2 crystals which also contained minor contaminants with larger rings, ~ 12 nm in diameter, which were attributed to the LH1 complexes. No such contamination with LH1 rings was found in our LH2 2D-crystals.

Direct visualisation of the reconstituted LH2 proteins using tapping mode AFM in liquid allowed us to demonstrate variability in 2D-crystal morphology. Various types of crystals could be distinguished and analysed. We found that LH2 crystals

had three different packing forms and despite the different packing forces the LH2 complexes were always circular and of identical size. In order to study spatial organization and physical properties of the LH2 complexes in their native environment, LH2-only native membranes directly isolated from *Rhodobacter sphaeroides* cells have also been imaged by AFM and their topographs were compared with the images of the LH2-only 2D-crystals.

We expected to observe differences in the AFM topographs of LH2 2D-crystals and LH2 native membranes due to the following reasoning. Generally, 2D-crystals are produced from the mixture of purified proteins, detergents and lipids, when at certain conditions and certain stages of the 2D-crystallization process, membrane proteins get incorporated into the lipid bilayer in a specific way and well-ordered 2D-crystals can be formed. In the previous cryo-EM and AFM studies on photosynthetic membrane proteins it was shown that in the 2D-crystals the LH2 proteins were found to be inserted into the reconstituted lipid bilayer in two opposite orientations, so that both periplasmic and cytoplasmic sides of the proteins were exposed on the same side of the crystal (Scheuring et al 2001; Scheuring et al 2003a; Walz et al 1998). The orientation of the native LH complexes in the photosynthetic membrane had been determined by protease treatment of chromatophores and spheroplasts which demonstrated that the N-termini of LH1, LH2 and the RC subunits L- and M- were all exposed on the cytoplasmic face (Tadros et al 1987). This arrangement aligns the rings of bound Bchls vertically within the membrane so that efficient light energy transfer can take place. In the naturally crystalline native membranes such as purple membrane of bacteriorhodopsin (Müller et al 1995a, b) or the ICM of the bacterium *Rhodopseudomonas viridis* (Scheuring et al 2003b) all the protein complexes are inserted in the same orientation. Reconstituted 2D-crystals impose order upon the constituent proteins (Fotiadis et al 2004; Scheuring et al 2001; Scheuring et al 2003a) as they are packed into the artificial bilayer but in the absence of the associated assembly factors that assist membrane insertion *in vivo* the proteins are free to insert in either orientation. The “up-down” arrangement of the LH2 complexes in the 2D-crystals is most likely an artifact of the packing of the slightly conical complexes, driven by purely physical forces. The packing arrangement of membrane proteins in the majority of native biomembranes is expected to be quite disordered in contrast to the highly ordered 2D- or 3D-crystals of purified proteins. Just such a disordered system has recently been demonstrated in the PSU’s of *Rhodobacter sphaeroides* (Bahatyrova et al 2004b) and *Rhodospirillum photometricum* (Scheuring et al 2004b, c). Therefore, we could expect different spatial organization of the individual membrane proteins in the reconstituted 2D-crystals and native membranes. In addition different packing forces existing in the well-ordered 2D-crystals and less ordered native membranes might possibly influence the protein shape and conformation within the different packing environments.

Our AFM topographs of LH2-only native membranes indicated similar (crystalline-like) spatial organization of the LH2 complexes in the 2D-crystals and detergent treated native membranes. The influence of the detergent molecules and sample deposition onto the mica substrate on the arrangement of the LH2 complexes in the native membranes observed by us is discussed.

We have observed that in both systems the LH2 complexes displayed identical ring architecture, in terms of both shape and size, which confirmed that our AFM images of LH2 proteins (both reconstituted into the 2D-crystals and in their native membranes) reflected intrinsic structural and physical properties of this LH complex.

2.2 Materials and methods

Biological samples were prepared in the laboratory of Prof. Dr. C. N. Hunter (University of Sheffield, UK).

Strains and plasmids

The *Rhodobacter sphaeroides* strain DPF2 ($LH2^+$, $LH1^-$, RC^-, X^-) has been described previously (Jones et al 1992).

Bacterial growth

The LH2-only strain DPF2 was grown semiaerobically and the chromatophores prepared according to the methods in Olsen et al. (1994).

LH2 purification and 2D-crystallization

LH2 complexes were purified and crystallized as described in Walz et al. (1998).

Detergent treatment of chromatophores to produce membrane fragments for AFM

Chromatophores that had been prepared as described above were diluted to approximately 20 ODunits/ml with 50 mM HEPES pH8 buffer and 400 µl of this suspension were made up to 600 µl with 1% DDM, 50 mM HEPES pH8 such that the final concentration of DDM was either 0.005% or 0.01%. This was incubated at RT for 10 minutes prior to layering onto a 20/25/30/35/40/50% sucrose, 0.005% DDM, 50 mM HEPES pH8 or 0.01% DDM, 50 mM HEPES pH8 step gradient as appropriate. The gradients were centrifuged in a Beckman SW41 rotor at 40 krpm for 10 hours. The resultant bands were harvested using a syringe and wide bore needle and frozen at –20^{o}C until use.

Atomic force microscopy and image processing

Muscovite mica purchased from Ted Pella (Redding, CA, USA) was chosen as a support for the samples. For AFM measurements the sample of LH2 crystals was prepared by adsorbing 1 µl of sample solution onto the surface of freshly cleaved mica for ~ 30 sec, followed by immersion into distilled and filtered water for 1 min in order to remove weakly bound crystal patches. The sample was immediately placed onto the AFM stage and 300 µl of recording buffer (10 mM Tris-HCl pH7.5, 150 mM KCl) was added to the liquid cell. For firm attachment of LH2-only native membranes the adsorption buffer (10 mM Tris-HCl pH7.5, 150 mM KCl, 25 mM $MgCl_2$) was applied and the adsorption time was increased to 1-1.5 hour. The imaging buffer used was the same as for the LH2 crystals.

For the experiments a custom-built stand-alone AFM was employed (van der Werf et al 1993). Standard silicon nitride cantilevers with a length of 85 µm, force constant 0.5 N/m and operating frequencies 25 – 35 kHz (in liquid) purchased from Veeco (Veeco NanoProbe Tips, USA) were used. High-resolution AFM images were obtained using tapping mode in liquid with a free amplitude of 2-5 nm and amplitude setpoint adjusted to minimal forces (damping of the free amplitude was 10-20%). Images contain 256x256 pixels and were recorded at a line frequency of 2-4 Hz. The calibration of the setup was made with UltraSharp Calibration Gratings from NT-MDT (NT-MDT Co., Moscow, Russia). Topographical images were quantitatively analysed by means of Scanning Probe Image Processor program (Image Metrology ApS, Lyngby, Denmark).

2.3 Results

2.3.1 General description of LH2 2D-crystal morphology

2D-crystals of LH2 complexes were not too heterogeneous. Two distinct classes could be recognized, tubular and vesicular crystals. Fig. 2.1 illustrates typical examples of observed LH2 2D-crystals. It is important first to note that the image shown in Fig. 2.1A was acquired under ambient conditions (in air), while Fig. 2.1B, C show images obtained in liquid environment. For imaging in air the sample adsorbed to the mica surface is gently dried with the stream of nitrogen and no buffer solution is applied during scanning. The buffer, in which 2D-crystals were suspended and stored before conducting AFM experiments, contained 50 mM NaCl. The drying of the sample caused formation of salt crystals on the mica surface, which could be recognized as numerous objects of different shapes and sizes randomly distributed on the mica and also on the crystals themselves (Fig. 2.1A, circles). Further zooming-in into the 2D-crystals and high-resolution imaging of LH2 proteins in ambient environment could not be

achieved due to the following: *i)* imaging in air requires much larger tapping amplitudes in order to overcome the capillary forces always present in ambient environment, and as a consequence, high tapping amplitudes can cause the deformation of the soft biological samples leading to a loss of high resolution information; *ii)* artifacts due to the biological sample handling in air (washing and drying) can emerge, such as the contamination of the sample with salt crystals that we observed. Therefore, only imaging under physiological conditions (applying appropriate buffer solutions) was further employed by us in order to achieve high-resolution topographs of photosynthetic membrane proteins.

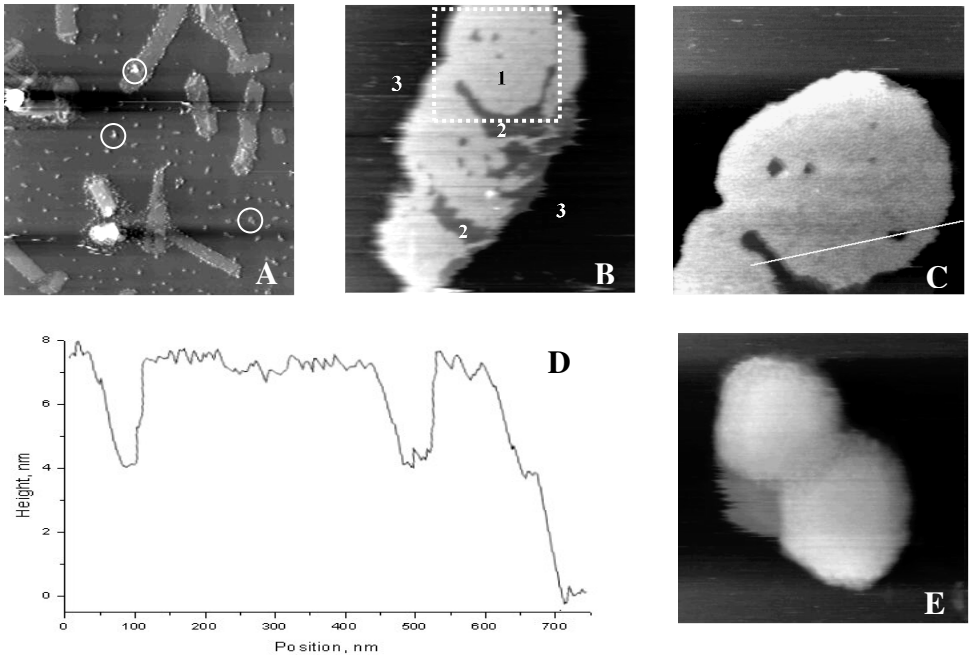

Fig. 2.1. *Examples of LH2-only 2D-crystals.* ***A****: Tubular LH2 crystals, frame size 11x11 μm^2, full grey scale 13 nm. The salt crystals contaminating the mica and LH2 crystals surfaces are marked with the circles;* ***B****: In the single-layered LH2 crystal (broken tube) three different surface types are evident, 1 – crystal surface, 2 – empty lipid bilayer areas, 3 – mica surface, frame size 1700x1700 nm^2, full grey scale 15 nm;* ***C:*** *Zoom-in of the area in the dashed box in* ***B****, frame size 1000x1000 nm^2, full grey scale 11 nm;* ***D:*** *Section analysis along the white line in* ***C****, lipid areas (dark spots in* ***C****) can be distinguished clearly from single-layered crystals by their height. The central region of a crystal shows repetitive topographic features corresponding to the LH2 complexes imbedded into the lipid bilayer.* ***E****: Vesicular LH2 crystals, frame size 500x500 nm^2, full grey scale 25 nm.*

The tubular LH2 crystals (Fig. 2.1A) formed the majority of the two LH2 crystals forms. Nearly half of the tubes adsorbed onto the mica surface were broken, forming planar single-layered sheets (n = 32 and 30 respectively). An example of a broken tube is shown in Fig. 2.1B. The tubular crystals showed considerable variation in length, from 2 to 6 µm, while the width had a more constant value 646 ± 64 nm (n = 32). Single-layered sheets varied significantly both in length and width and displayed a variety of shapes. We observed whole tubes ruptured into up to 1 µm wide sheets, as well as small patches possibly representing the fragments of the broken tubes. Intact tubes could be distinguished from the single-layered sheets (open tubes) also by analyzing their average height above the mica surface. The height histogram of the accumulated data showed two peaks in the height distribution: 7.2 ± 3.2 nm and 16 ± 2.4 nm (n = 62). One peak corresponded to the fraction of single-layered sheets and the second to the double-layered intact tubular crystals. In some crystals (mostly in broken tubes) areas of empty lipid bilayer without incorporated LH2 complexes were found (dark areas in the crystal patch in Fig. 2.1B marked with the number 2 and zoom-in of this crystal area in Fig. 2.1C). The average height of these lipid regions above the mica surface was 4.1 ± 0.1 nm (n = 16) and they could be easily recognized in single-layered crystals (Fig. 2.1D).

The vesicular LH2 crystals formed only a small fraction of the two types of LH2 2D-crystals, ~ 15% (n = 11) of the whole. The vesicular LH2 crystals had much smaller lateral dimensions than the tubular crystals. The average diameter of the vesicular crystals was ~ 200 nm (Fig. 2.1E). The average height above the mica surface was 15.9 ± 0.8 nm (n = 11) indicating that the vesicles were also double-layered.

2.3.2 Variations in crystalline packing in the LH2 2D-crystals

Crystalline packing of LH2 complexes in the 2D-crystals was clearly resolved and AFM images indicated that more than one type of packing could occur within one crystal. Three different patterns of crystalline arrangement of the LH2 complexes could be observed. We have termed these *i)* Type A, a "zigzag" pattern, *ii*) Type B, a rectangular pattern, and *iii)* Type C, disordered (Fig. 2.2). The ring-like structure of the LH2 complexes was clearly resolved in all three types of periodicities.

We found that tubular LH2 2D-crystals (Fig. 2.1A) in most cases displayed a high level of crystallinity and two types of LH2 packing, Types A and B (Fig. 2.2A, B). Usually, in an individual tube only one type of periodicity could be observed, either Type A or Type B. Remarkably, LH2 complexes wound around the tube plane in a helical fashion, i.e. not changing their direction of periodicity over the whole length of the tube.

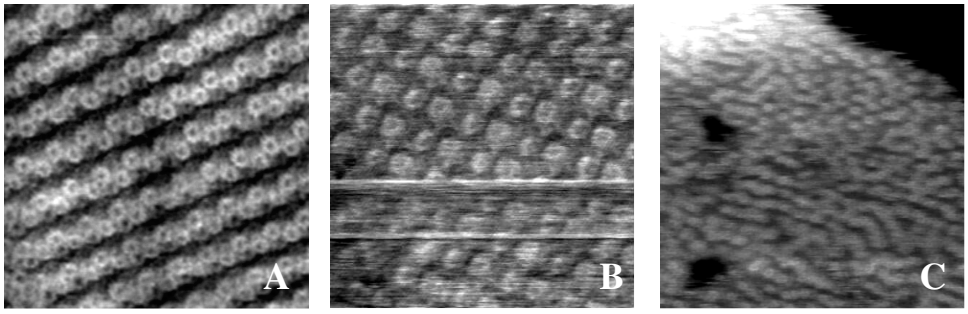

Fig. 2.2. *Variations in crystalline packing for LH2 complexes in the 2D-crystals.* ***A****: Type A (zigzag), frame size 150x150 nm^2, full grey scale 3 nm;* ***B****: Type B (rectangular), frame size 100x100 nm^2, full grey scale 3 nm;* ***C****: Type C (disordered), frame size 250x250 nm^2, full grey scale 6 nm.*

In the broken tubes (single-layered sheets, Fig. 2.1B, C) all three or combinations of all three types of crystalline packing of LH2 complexes could be found. An example of a single-layered sheet in which all three patterns could be simultaneously recognized is shown in Fig. 2.3. It is not quite clear what exactly happens along the dislocation from one type of periodicity to another. In some crystal areas the change in LH2 packing arrangement caused the alteration of the crystalline lattice. Smooth transitions from the ordered arrangements (Type A and B) to the disordered packing (Type C) could occur within an area as small as 500 by 500 nm^2 (Fig. 2.3). In the central region of the crystal shown in Fig. 2.3 the area which seems not to contain any strongly protruding LH2 rings (for a detailed analysis of the strongly and weakly protruding LH2 complexes see below in this section) is marked with an arrow. This could be a defect in the crystalline lattice where no LH2 proteins were inserted at all and therefore the empty lipid bilayer surface was exposed. On the other hand, it could as well be that in this particular area of the crystal only weakly protruding LH2 complexes were present but their protruding termini above the lipid surface could not be resolved by the AFM tip.

In the broken tubes (Fig. 2.1B, C) the disordered pattern, Type C (Fig. 2.2C), could be observed mostly in the distorted areas in the close vicinity of the regions of empty lipid bilayer. In contrast to the tubular crystals, in the single-layered sheets the direction of periodicity (both for Type A and B) could change all over the plane of the sheets. In the vesicular crystals (Fig. 2.1E), the long-range ordering of the LH2 complexes was mostly absent and the packing arrangement was disordered, Type C (Fig. 2.2C).

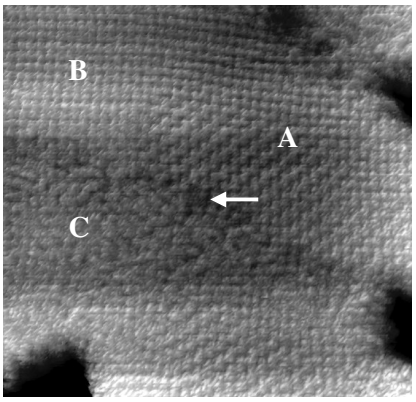

Fig. 2.3. *LH2 crystal displaying all 3 types of periodicity, frame size 500x500 nm^2, full grey scale 10 nm. Three areas in the crystal with different types of crystalline lattice (A, B or C) are marked with the corresponding letters. The arrow points to the area where the strongly protruding LH2 complexes are absent and the weakly protruding complexes are not resolved.*

In all three crystal forms the Type C packing did not show any distinct periodical pattern (Fig. 2.2C and 2.3), as the LH2 complexes were incorporated into the lipid bilayer in a random way.

2.3.3. Physical parameters and disposition of the LH2 complexes

The well ordered Type A and B crystal forms allowed the direct measurement of the dimensions of the LH2 rings and also the height of the two extrinsic regions above the lipid bilayer to be measured. Fig. 2.4 shows two examples of high magnification images of LH2 rings embedded into the 2D-crystals.

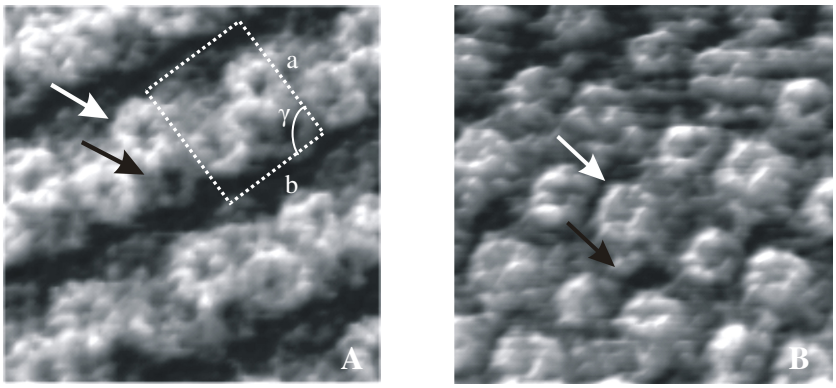

Fig. 2.4. *High-resolution AFM topographs of LH2 complexes incorporated into the 2D-crystals.* ***A****: Type A (zigzag), frame size 50x50 nm^2, full grey scale 2 nm. Unit cell housing four LH2 complexes is shown. White arrow points to the strongly protruding LH2 complex and black arrow points to the weakly protruding LH2 complex;* ***B****: Type B (rectangular), frame size 50x50 nm^2, full grey scale 2 nm. White and black arrows point to the strongly and weakly protruding LH2 complexes, respectively.*

LH2 complexes are presented in two types of periodical patterns, Type A and B (Fig. 2.4 A and B, respectively). The strongly protruding LH2 rings alternate with the weakly protruding complexes. For clarity, representative strongly and weakly protruding LH2 rings are marked with white and black arrows respectively (Fig. 2.4). Regardless of the protein packing arrangement, both in the well-ordered crystals (periodicities of Type A and B) and in the disordered crystal areas (Type C) all LH2 rings were found to be circular. The outer and inner diameters of the strongly protruding LH2 rings were 7.5x7.3±0.3 nm (measured for two orthogonal directions) and 3.2x3.1±0.2 nm, respectively, for Type A; 7.3x7.2±0.3 nm and 3.3x3.3±0.3 nm for Type B; 7.1x7.0±0.3 nm and 3.0x3.0±0.2 nm for Type C. The weakly protruding LH2 rings were not fully accessible to the AFM tip, and their lateral dimensions could not be measured accurately.

The angle between three neighboring strongly protruding LH2 rings in the crystals with crystal packing of Type A was measured to be 93.8 ± 5.4° (n = 32). An example of such an angle is shown in Fig. 2.5. In order to measure the angle, the geometric centers of the LH2 rings were determined by finding the minimal height value inside the LH2 rings (thus the deepest points in the rings which could be accessed by the scanning AFM tip).

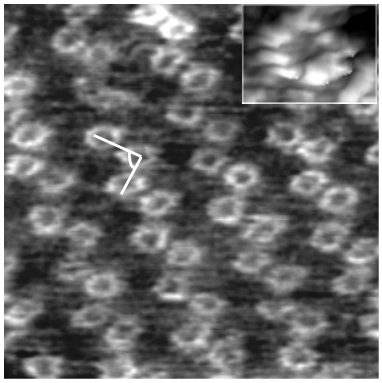

Fig. 2.5. *High-resolution image of the LH2 complexes in the 2D-crystal (periodicity Type A), frame size 85x85 nm^2, full grey scale 2 nm . The angle between adjacent up LH2 rings is shown. Inset: individual LH2 complex, in which 9 subunits could be resolved.*

Well-ordered LH2 2D-crystals with the periodicity of Type A (Fig. 2.2A and 2.4A) allowed us to perform a Fourier-analysis of the images and to define a unit cell. The crystalline lattice had a unit cell with the parameters a = 19.9 nm, b = 15.9 nm, γ = 87°. The unit cell encompassed four LH2 rings. Two of the complexes housed in the unit cell protruded above the lipid bilayer more than the other two complexes, with the height 1 ± 0.1 nm (n = 105) and 0.5 ± 0.1 nm (n = 96), respectively. Similar observations of two different heights of the reconstituted proteins above the lipid plane within the unit cell was reported before in recent AFM studies on *Rubrivivax gelatinosus* and *Rhodobacter sphaeroides* LH2 2D-crystals (Scheuring et al 2001; Scheuring et al 2003a). This

phenomenon was explained by the insertion of the LH2 complexes into the lipid bilayer in two opposite orientations, when half of the complexes were inserted in the membrane with an upside-down orientation. Using thermolysin treated and untreated LH2 complexes from *Rubrivivax gelatinosus*, Scheuring and co-workers established that the strongly protruding side of the complex was the periplasmic face (Scheuring et al 2001). As there is a strong homology between the polypeptide sequences of *Rubrivivax gelatinosus* and *Rhodobacter sphaeroides* (Fig. 2.6) we propose that the strongly protruding face in our data also represents the periplasmic face of the LH2 complex.

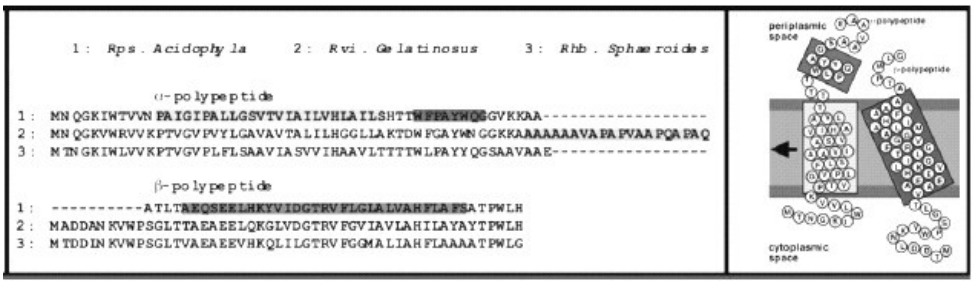

Fig. 2.6. *Rhodobacter sphaeroides LH2 topology. On the left: sequence alignment of the LH2 α- and the β-polypeptide of (1) Rhodopseudomonas acidophila, (2) Rubrivivax gelatinosus and (3) Rhodobacter sphaeroides. On the right: Rhodobacter sphaeroides topology model derived from the sequence alignment with Rhodopseudomonas acidophila. [From Scheuring et al 2003a].*

In some of the LH2 rings the resolution was high enough to permit us to count the number of monomers per LH2 ring (Fig. 2.5, inset), confirming the nonameric nature of the complex.

2.3.4 Imaging of LH2-only native membranes

We performed high-resolution AFM imaging of LH2-only native membranes in order to compare the spatial organization and conformation of the LH2 complexes in the native system and in the 2D-crystals (as discussed in sections 2.3.1, 2.3.2 and 2.3.3 of this chapter). The LH2 membranes directly isolated from *Rhodobacter sphaeroides* cells were fractionated in the presence of two different concentrations of β-dodecyl-maltoside detergent (DDM), 0.01% and 0.005%, and the resultant membrane fragments fractionated on sucrose gradients for each DDM concentration. Each gradient isolated two bands which can be seen in Fig. 2.7 and the four different membrane fractions were examined by AFM.

Fig. 2.7. *Solubilization of LH2-only membranes with DDM with subsequent fractionation by ultracentrifugation on sucrose density gradients. On the left: membranes solubilized with 0.005% DDM, on the right: membranes solubilized with 0.01% DDM [Image courtesy of John Olsen, University of Sheffield].*

Large-scale overview images of the membranes from each band are shown in Fig. 2.8.

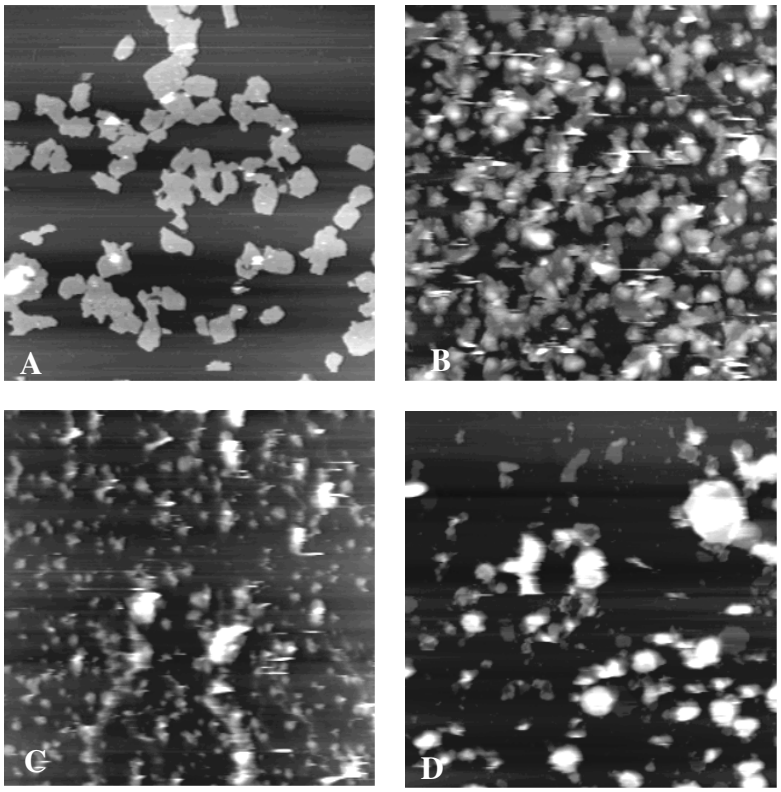

Fig. 2.8. *AFM images of LH2-only membranes.* ***A****: Membranes treated with 0.01% DDM, band 2, frame size 2500x2500 nm^2, full grey scale 21 nm;* ***B****: 0.01% DDM, band 1, frame size 2500x2500 nm^2, full grey scale 24 nm;* ***C****: 0.005% DDM, band 2, frame size 2500x2500 nm^2, full grey scale 27 nm;* ***D****: 0.005% DDM, band 1, frame size 2500x2500 nm^2, full grey scale 28 nm.*

As can be seen in Fig. 2.8, the membranes fragments from both bands in the same DDM concentrations had different morphology. At 0.01% DDM, band 2, LH2-only membranes were quite big and on this scale appeared to be rather flat resembling fragments of the LH2 2D-crystals (Fig. 2.8A). Band 1 from the same DDM concentration produced somewhat smaller and rather curved patches (Fig. 2.8B). In contrast, at 0.005% DDM, band 2, the majority of membrane fragments were very small in size (less than 50 nm), and at the same time some very high chromatophore-like fragments were also present (Fig. 2.8C). Band 1 from the same DDM concentration contained mainly highly curved chromatophore-like membranes with the height above the mica surface more than 20 nm (Fig. 2.8D). Thus, it appeared that only in band 2 at 0.01% DDM full fractionation of IC membranes occured resulting in the production of relatively flat fragments, while the other three bands contained substantial populations of curved and chromatophore-like fragments. It is likely that our AFM images captured the consequences of using different detergent concentration during the membrane fractionation process, from the full fractionation (band 2, 0.01%) to a very subtle effect of the detergent (band 1, 0.005%).

High-resolution AFM imaging of all available bands of LH2-only native membranes was conducted. Band 2, 0.005% DDM, produced very small membrane patches which were not suitable for high-resolution AFM imaging. Rare curved vesicles, also found in this band, were extremely difficult to measure at a high resolution due to their high curvature and flexibility. Thus no high-resolution data could be obtained when imaging this band. AFM scans of the chromatophore-like membranes from band 1, 0.005% DDM produced marginally clearer images (Fig. 2.9A, B), but no substructure in the membranes could be resolved. The curvature and flexibility of these membrane fragments suggests that only the periphery of the fragments are in firm contact with the mica surface, thus these membranes most resemble the curved membranes *in vivo*. Furthermore, we suggest that, due to the minimal influence of the detergent on the overall morphology of the membranes from this band, all LH2 complexes protrude above the lipid bilayer with an equal height.

The resolution in the images of LH2 membranes from band 1, 0.01% DDM was not high enough due to the difficulties in imaging of small curved membrane patches. Therefore, a clear picture of protein distribution in the membranes from this band could not be achieved (Fig. 2.9C, D). Nevertheless, a strong suggestion of the periodical packing of the LH2 rings exists in this band (Fig. 2.9C, D, arrows).

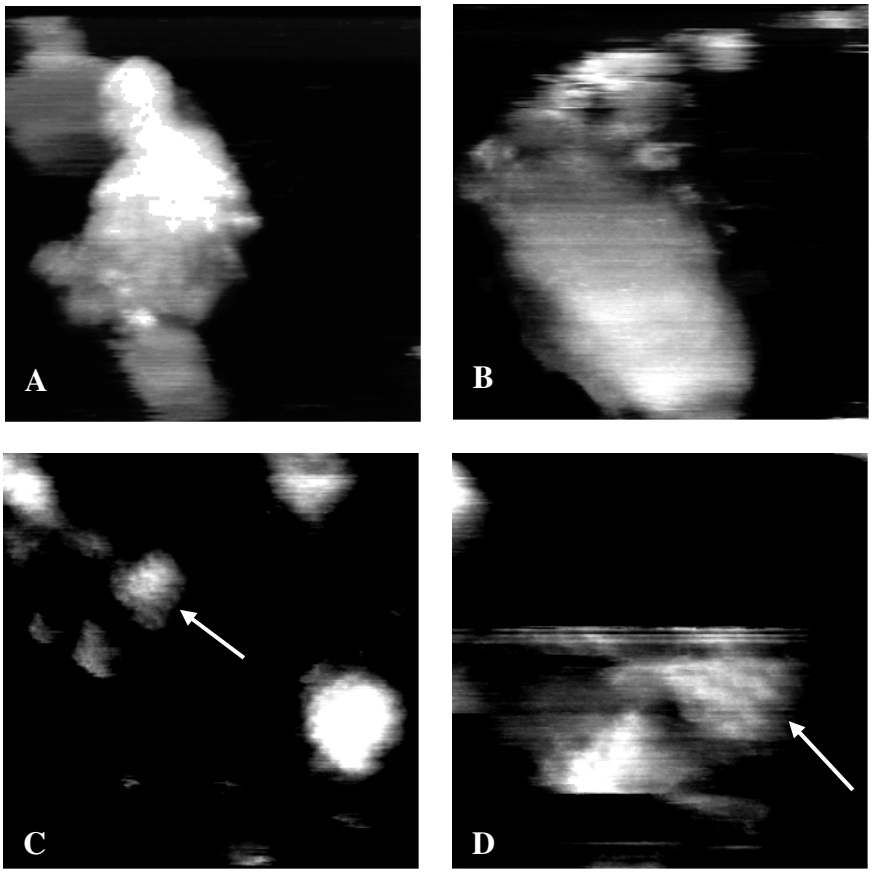

Fig. 2.9. *LH2-only membranes.* ***A, B****: 0.005% DDM, band 1, frame sizes 500x500 nm^2 and 250x250 nm^2 (****A*** *and* ***B****, respectively), full grey scale 6 nm;* ***C, D****: 0.01% DDM, band 1, frame sizes 500x500 nm^2 and 250x250 nm^2 (****C*** *and* ***D****, respectively), full grey scale 6 nm. Arrows point to the areas with tentative periodical packing of the LH2 complexes (as Type A periodicity in the LH2 2D-crystals).*

High magnification images of LH2 membranes from band 2, 0.01% DDM (Fig. 2.8A) are presented in Fig. 2.10. The membrane patches had diverse shapes with a lateral size ranging from 100 to 500 nm. The height above the mica surface was ~ 7 nm. The membrane patches consisted of a single lipid bilayer with LH2 complexes embedded into it. Unlike the 2D-crystals, the membranes did not lie completely flat on the mica substrate, as can be seen in the representative images of LH2-only membranes from this band (Fig. 2.10).

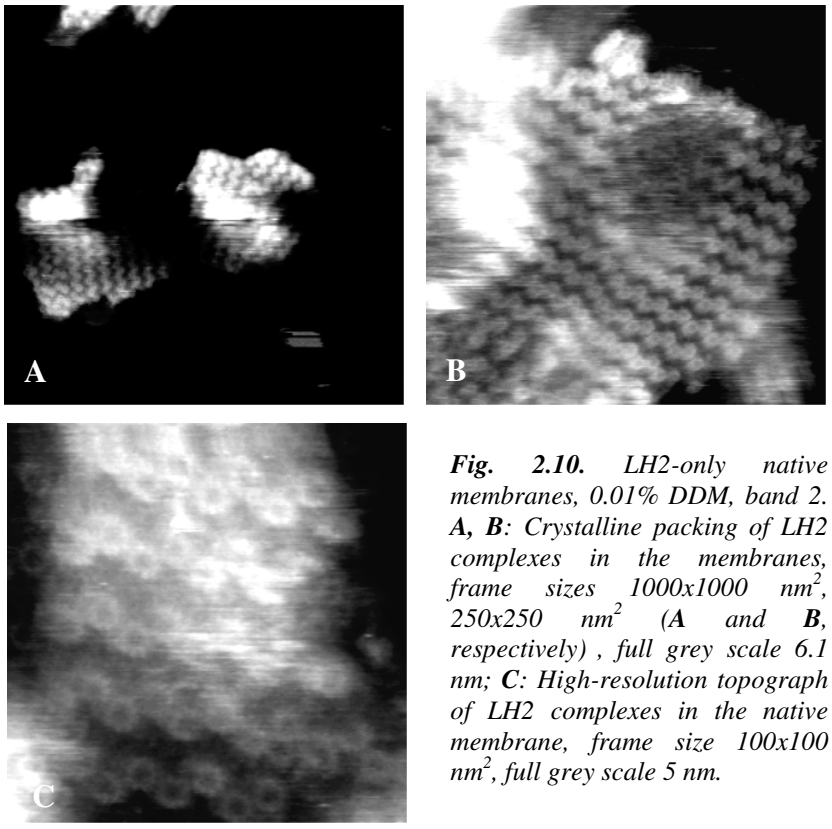

Fig. 2.10. *LH2-only native membranes, 0.01% DDM, band 2.* ***A, B****: Crystalline packing of LH2 complexes in the membranes, frame sizes 1000x1000 nm^2, 250x250 nm^2 (****A*** *and* ***B****, respectively) , full grey scale 6.1 nm;* ***C****: High-resolution topograph of LH2 complexes in the native membrane, frame size 100x100 nm^2, full grey scale 5 nm.*

The surface of the membranes was rather wavy and next to the relatively flat membrane areas curved bulges could be located as well. For example, in Fig. 2.10C the height difference between the lowest and the highest areas over the membrane surface (the darkest and the lightest areas in the image, respectively) could reach 4 nm (Fig. 2.11, upper panel). In the 2D-crystals on the same image size scale (100x100 nm^2) the height variations were approximately one order of magnitude less (Fig. 2.11, lower panel).

Zooming-in into the membranes revealed dense packing of LH2 complexes and, strikingly, the packing arrangement of the proteins in the membranes was very similar to the crystalline ordering found in LH2-only 2D-crystals with Type A periodicity (compare Figs. 2.2A and 2.10). Neither Type B (Fig. 2.2B) nor Type C (Fig. 2.2C) packing arrangements of the LH2 complexes was found in LH2-only native membranes.

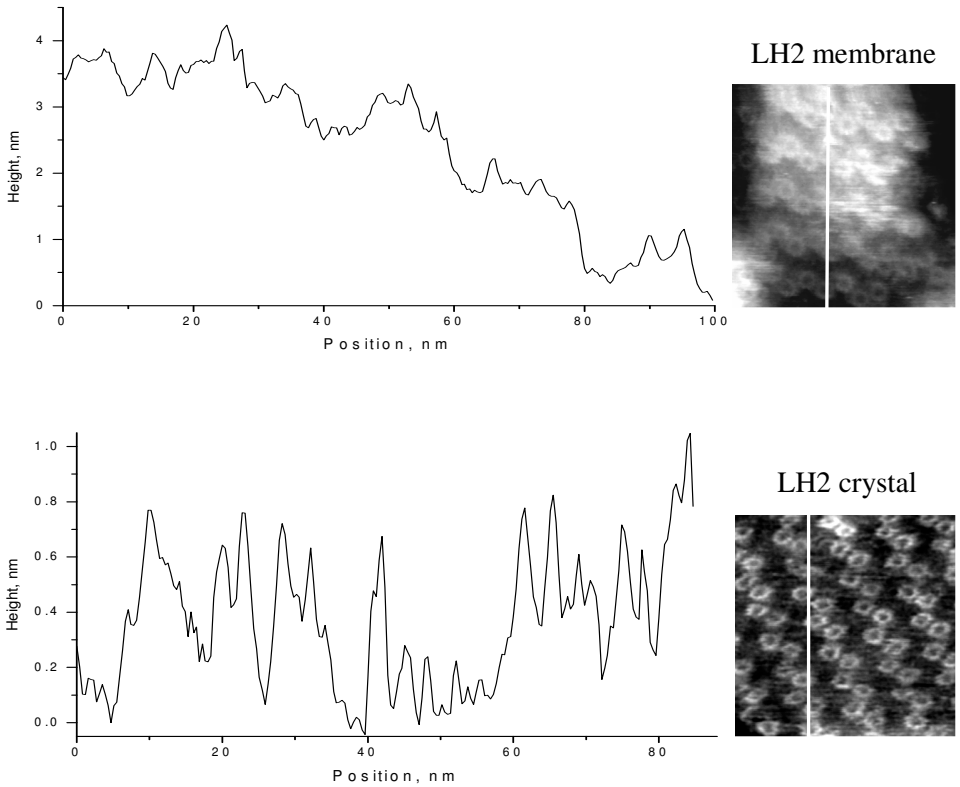

Fig. 2.11. *Comparison of surface roughness in LH2-only native membranes and 2D-crystals. Upper panel – height profile along the white line in AFM image of LH2 membrane (Fig. 2.10C); height variations within 100x100 nm^2 area could reach 4 nm. Lower panel – height profile along the white line in AFM image of LH2 crystal (Fig. 2.5); height variations within 100x100 nm^2 area could reach maximum 1 nm.*

Another example of a high magnification topograph of LH2-only membrane (also from band 2, 0.01% DDM) is shown in Figure 2.12. In this image the ring-like LH2 proteins occurred in the lipid bilayer at two different height levels above the lipids and higher LH2 rings could be recognized together with the lower LH2 rings (Fig. 2.12, arrows). The height difference between high and low rings was 0.9 ± 0.1 nm (n = 23). Due to the not sufficient resolution in this image (Fig. 2.12) the space in-between LH2 complexes filled with lipid molecules was poorly resolved, thus the calculation of the height of LH2 protrusions with respect to the lipid bilayer could not be carried out. However, a better contrast between LH2 complexes and lipid surface in Fig. 2.10C allowed us to calculate the height of the strongly protruding LH2 rings, which was 1.3 ± 0.2 nm (n = 24). Knowing the height difference between the strongly and the weakly protruding LH2 complexes, which was 0.9 nm, we can conclude that the weakly protruding LH2 had a height of ~ 0.4 nm above lipid bilayer. The average diameter of higher LH2

rings was ~ 7 nm. The contours of the lower rings were poorly resolved, but the distance between two neighboring pairs of higher LH2 complexes was ~ 14 nm, sufficient to accommodate two lower rings.

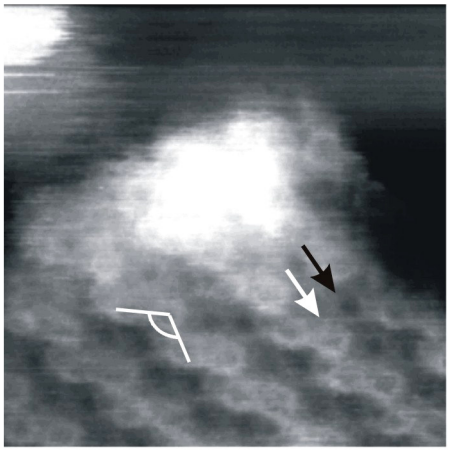

Fig. 2.12. *LH2 complexes in the native membrane (0.01% DDM, band 2), frame size 100x100 nm^2, full grey scale 5 nm. Two different height levels of LH2 rings in the membrane are clearly visible. The white arrow points to the high LH2 complex and the black arrow points to the low LH2 complex. The angle between adjacent high LH2 rings is shown.*

In order to further assess the packing arrangement of the LH2 complexes in this membrane fragment we measured the angle between three adjacent high LH2 complexes; this was found to be 122.1 ± 4.8° (n = 26, Fig. 2.12). This is markedly different from the angle found in the LH2 2D-crystals, which was ~ 93°, and indicated that the LH2 complexes were packed hexagonally in the native membranes.

Clearly there has been an effect of the higher detergent concentration upon the morphology of the membrane fragments generated and also upon the disposition of the LH2 complexes within the lipid bilayer.

2.4 Discussion

High resolution AFM imaging was used recently to study the structure of reconstituted LH2 complexes into the 2D-crystals. LH2 was obtained from different species of purple bacteria: *Rubrivivax gelatinosus* (Scheuring et al 2001), *Rhodobacter sphaeroides* (Scheuring et al 2003a) and *Rhodopseudomonas acidophila* (Gonçalves et al 2004; Stamouli et al 2003). In the work of Scheuring and co-workers (2001, 2003a) the addition of 20 mM of the detergent n-octyl-β-D-thioglucopyranoside (OTG) to the initial micellar lipid-protein-LDAO solution gave rise to a significantly increased size of the 2D-crystals. After detergent removal large vesicular crystals were obtained with sizes up to 5 µm. Also unilamellar sheets were present, probably originating from vesicular crystals that had fractured or were broken open (Scheuring et al 2001; Scheuring et al 2003a).

Stamouli et al. have reconstituted LH2 complexes into preformed egg phosphatidylcholine liposomes, without adding extra chemical agents such as OTG (Stamouli et al 2003). The relatively small liposomes, which were obtained in that study, opened up into a flat bilayer with a typical diameter of ~ 400 nm.

In our study of LH2 complexes from *Rhodobacter sphaeroides* reconstituted into the 2D-crystals no secondary detergents (such as OTG used by Scheuring et al) were used during crystallization. The solution of mixed proteins-DOPC(lipid)-β-OG(detergent) produced two types of LH2 2D-crystals upon dialysis to remove the β-OG, the majority were large tubular LH2 crystals and the minority small vesicular crystals (Fig. 2.1). Similar types of *Rhodobacter sphaeroides* LH2 2D-crystals were found by Walz et al. (1998) in cryo-EM data on LH2 crystals prepared by the same procedure as was used in our study. It was previously shown that during 2D-crystallization trials different types of 2D-crystals can be produced (Rigaud et al 2000) and that in most cases the results of 2D-crystallization (morphology of 2D-crystals, their quality and a type of a unit cell) are difficult to predict (Hasler et al 1998). We demonstrated in this chapter a coexistence of several types of LH2 2D-crystals, namely vesicles and tubes, while previous studies of LH2 crystals (Scheuring et al 2001; Scheuring et al 2003a; Stamouli et al 2003) documented only a single type of LH2 crystal. It is likely that the overall morphology of the 2D-crystals is dependent on the purple bacteria species used and conditions of crystallization.

Reconstituted 2D-crystal packing geometries

After deposition onto the mica surface, subsequent AFM imaging of LH2 tubular 2D-crystals revealed uniformly ordered arrays of complexes over the entire crystal surface. We have observed two different types of crystalline packing of LH2 proteins within tubular crystals, Type A and Type B, while in the open tubes as well as in vesicular crystals the long-range order was often broken (Fig. 2.2). The unit cell of crystalline packing of Type B (Fig. 2.2B) is in agreement with the data of Scheuring et al. (2003a) obtained on the *Rhodobacter sphaeroides* LH2 complex and also with the unit cell found in the cryo-EM study on *Rhodobacter sphaeroides* LH2 crystals (Walz et al 1998). In contrast, the crystalline packing of Type A has been observed in our study for the first time for LH2 complexes (Fig. 2.2A), although Scheuring and co-workers reported the crystals which showed coherence only over small regions, and lattice displacements of half a unit cell resembling zigzag packing of proteins were frequent (Scheuring et al 2001).

In the first high-resolution AFM study of LH2 complex from *Rubrivivax Gelatinosus* two different packaging arrangements in the crystals have been found (Scheuring et al 2001). In areas where two different sides of the aggregates were present, proteins were regularly packed in alternating orientations, with the unit

cell hosting two rings and with unit cell dimensions: a = 8.2 nm, b = 13.3 nm, γ = 90°. In areas where only weakly protruding complexes with respect to the lipid surface could be observed, proteins were unidirectionally inserted in a hexagonal packing pattern with unit cell dimensions of a = b = 7.6 nm and γ = 60°. Neither of these packaging arrangements has been found by us in the present work. In the AFM study of LH2 from *Rhodopseudomonas acidophila* (Stamouli et al 2003) only a low degree of order in the crystals was found. Small domains of LH2 aggregates occurred with unit cell dimensions of a = 13.4 nm, b = 16.4 nm and γ = 63°.

The conclusion from this comparison of unit cell types found for LH2 complexes in different studies is that LH2 complex does allow a packaging flexibility to exist, which is probably dependent on the subtle interplay of parameters during the crystallization process and differences in the protein sequences of the LH2 polypeptides, particularly that of the β-polypeptide which forms the outer envelope of the complex in the transmembrane region, varying from species to species.

Fig. 2.13 depicts two models which illustrate schematically the main differences between the two types of crystalline packing of LH2 complexes in the 2D-crystals, Type A and Type B, found in this study.

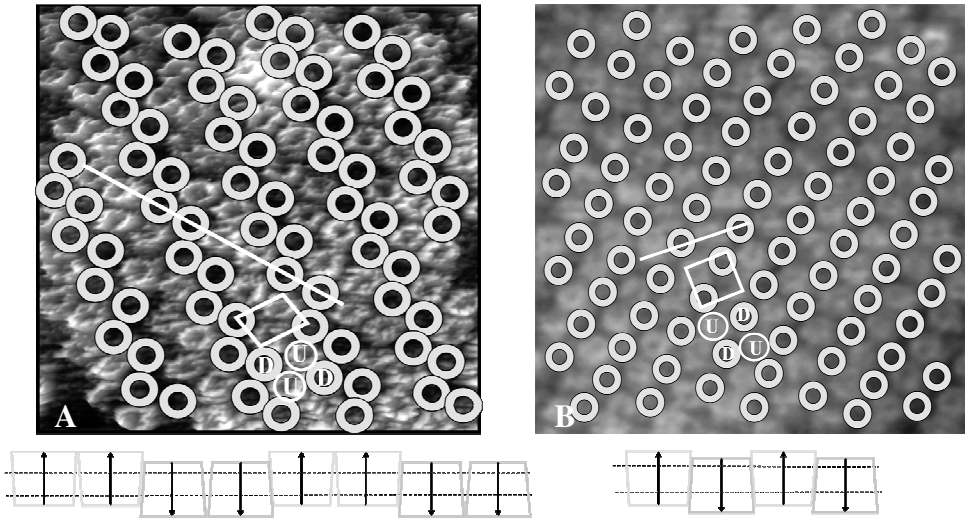

Fig. 2.13. *Schematic representation depicting differences in two types of crystalline packing in LH2 2D-crystals. The strongly protruding LH2 complexes (up rings) were originally well resolved in the AFM images, while weakly protruding LH2 complexes (which were badly resolved by AFM) were substituted in the images by the rings of approximately one LH2 ring size. Unit cells are outlined and four LH2 complexes (two in*

up and two in down orientation) housing one unit cell are marked with the corresponding letters U (up) or D (down). ***A:*** *Crystalline packing Type A, frame size 100x100 nm^2, full grey scale 2 nm;* ***B:*** *Crystalline packing Type B, frame size 100x100 nm^2, full grey scale 2 nm. Beneath each figure LH2 complexes are schematically shown inserted into the lipid bilayer in two opposite orientations following the white line shown in the image. LH2 complexes are shown as trapezoids with unequal diameters of the opposite sides of the complexes (in accordance with the LH2 crystal structure (McDermott et al 1995) and recent AFM images of LH2 2D-crystals (Scheuring et al 2001)). Up and down LH2 complexes are denoted by the corresponding arrows pointing to the opposite directions. Up rings protrude more above the plane of the lipid bilayer in comparison with the down rings.*

The space between the strongly protruding LH2 rings (the most apparent topographical features in the images) was filled in by the circles of approximately one LH2 complex diameter in order to visualize dense packing of LH2 proteins in the crystal 2D-plane (Fig. 2.13). The unit cell is outlined for both types of periodicities and the up and down LH2 complexes within one unit cell are marked with the corresponding letters, U (up) or D (down) (Fig. 2.13A and B). In both types of LH2 crystalline packing the unit cell comprises four LH2 complexes. Two of them protrude more above the lipid plane (up-oriented rings) than two other rings (down-oriented rings). As can be seen (Fig. 2.14, center and right), the primary difference between crystalline packing Type B and Type A is that in the former there is no close contact between adjacent up rings housing one unit cell while in the latter they are brought together very closely.

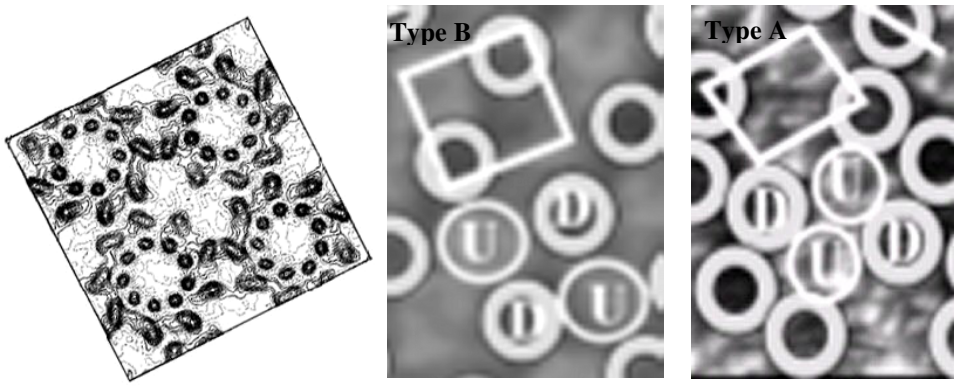

Fig. 2.14. *The unit cell of the Type B (center) and Type A crystal (right) is compared with the unit cell from Walz et al. (left, from Walz et al 1998). It is apparent that the Type B packing of the LH2 complexes is identical to EM data, thus we can gain an insight into how closely the complexes pack within the bilayer. Each complex has close contacts of eight of its β-polypeptides with the surrounding complexes.*

As can be seen in Fig. 2.15 of the LH2 of *Rhodopseudomonas acidophila* the β-polypeptides cross the transmembrane region of the complex at an angle (McDermott et al 1995). Thus when two LH2 complexes pack together in the membrane with their β-polypeptides interdigitating this will force the two complexes to lie at an angle to each other. This interaction of the β-polypeptides was reported by Walz et al. (1998) while Scheuring et al. observed tilting of the complexes in the bilayer (Scheuring et al 2003a). In this packing arrangement 8 of the 9 β-polypeptides make contact with the surrounding LH2 complexes, thus very little of the external surface of the complexes is exposed to lipid molecules. This is an energetically favorable configuration for the complexes to adopt when they form the 2D-crystal.

Similar intercalating of the β-polypeptides must be occurring where the up and down complexes pack together in the Type A crystals but there is an additional set of contacts between up-up as well as down-down complexes. As there is no equivalent information from EM studies we cannot conclude just how many protein-protein contacts there are, but as this type of crystal packing was not rare we can assume that the majority of the β-polypeptides are involved in favorable packing arrangements.

Fig. 2.15. *Rhodopseudomonas acidophila LH2 complex. [From Prof. R. Cogdell Internet web site http://www.gla.ac.uk/ibls/BMB/rjc/rcgallery.html]*

We observed that in most tubular crystals (Fig. 2.1A) a uniform crystalline lattice could be observed with conserved parameters over the whole area of the tube. In the open tubes (Fig. 2.1B, C), however, usually more than one lattice structure was present simultaneously and sometimes areas were found where all three lattice types coexisted within a distance of less than 500 nm (Fig. 2.3). We noticed as well that the lattice heterogeneity often occurred in the crystal areas where empty lipid bilayer was exposed. Empty lipid bilayer was, at the same time, very rarely observed in the tubular crystals. Thus, our measurements showed that the occurrence of fractured tubes was related to the structural heterogeneity, which apparently made these tubes more sensitive to the external forces during sample handling and/or adhesion to the substrate.

Structural data of the extrinsic regions of the LH2 complex

(i) height of the protrusions:

LH2 complexes in 2D-crystals were found to be inserted into the lipid bilayer at two different heights (Fig. 2.4). The strongly protruding LH2 complexes had an average height above the lipid bilayer 1 nm. This was in good agreement with the data of Scheuring et al. in LH2 crystals from *Rubrivivax gelatinosus* and *Rhodobacter sphaeroides* of 0.9 and 1 nm, respectively (Scheuring et al 2001; Scheuring et al 2003a). In the former work the strongly protruding face was assigned to the periplasmic side of the complex as a result of thermolysin digestion which only affected this face. Therefore we can also conclude that in our *Rhodobacter sphaeroides* LH2 2D-crystals the strongly protruding LH2 rings were exposing the periplasmic side of the complexes. Correspondingly, the weakly protruding LH2 rings, 0.5 nm above the lipid bilayer, were the cytoplasmic side. This value is close to the range of values found by Scheuring et al. for *Rhodobacter sphaeroides* LH2 2D-crystals, 0.2-0.4 nm, and may reflect different degrees of distortion of the protein caused by the use of tapping mode in our work and contact mode in Scheuring et al. (2003a).

(ii) internal and external diameters of the LH2 complexes:

The lateral dimensions of LH2 complexes were measured and we found that the strongly protruding aggregates had an average outer diameter ~ 7 nm. This value was in close agreement with the number reported in the 3D crystal structure of *Rhodopseudomonas acidophila* LH2 complex, which was 6.8 nm (McDermott et al 1995). Stamouli et al. reported "doughnut"-shaped *Rhodopseudomonas acidophila* LH2 complexes with an average outer diameter of ~ 7 nm (Stamouli et al 2003). Scheuring et al. found for *Rubrivivax gelatinosus* LH2 aggregates ring diameters of 5.4 nm for the weakly protruding rings and 4.9 nm for the strongly protruding rings (Scheuring et al 2001). In the 2D-crystals of *Rhodobacter sphaeroides* LH2 aggregates the average diameter of the strongly protruding rings was ~ 5.3 nm (Scheuring et al 2003a). It should be noted that the ring diameter in both these studies was measured from the highest parts of the aggregate, leading to consistently lower values in comparison with those reported by us, ~ 7 nm. Essentially, Scheuring et al. presented an average overall ring diameter, while we have reported separately both outer and internal LH2 ring diameters, ~ 7 and ~ 3 nm, respectively. An average from these two values is in the range of ~ 5 nm value found by Scheuring et al. The diameter of the LH2 complex reported by different authors is summarized in Table 2.1.

Table 2.1. *Summary of LH2 lateral dimensions reported in different sources*

LH2 diameter, nm	**Periplasmic face**	6.8	4.9	5.3	7.3	7.2
	Cytoplasmic face		5.4	n/a	n/a	n/a
Source		McDermott et al 1995	Scheuring et al 2001	Scheuring et al 2003	Stamouli et al 2003	This study

(iii) ellipticity of the LH2 complexes:

Ellipticities were observed for *Rubrivivax gelatinosus* LH2 aggregates of *b/a* = 0.95 for the cytoplasmic side and *b/a* = 0.91 for the periplasmic side (Scheuring et al 2001). Our high-resolution topographs of *Rhodobacter sphaeroides* LH2 aggregates, on the other hand, have shown that independently of the type of crystalline packing in the 2D-crystals, LH2 proteins appeared to be always circular. A very small deviation from circularity was found, *b/a* = 0.98, where *b* and *a* were both averaged values with an error. This small deviation from circularity was within the measurement error and may thus not be significant. It is important to stress that even in the disordered crystals (Type C, Fig. 2.2C), where LH2 rings were not so densely packed within the crystal plane and therefore were subjected to much smaller external packing forces, LH2 complexes still appeared to be circular and homogeneous in size. This observation indicated that within our detection limit LH2 complexes were inherently rigid and circular. This is in marked contrast to data derived from single molecule spectroscopy on individual *Rhodopseudomonas acidophila* LH2 complexes, where elliptical deformation of 8.5% of the LH2 rings was found (Ketelaars et al 2001).

Recent synchrotron small-angle X-ray scattering data indicated that the molecular shape of *Rhodobacter sphaeroides* LH2 complex in detergent solution clearly deviated from the ring-like crystal structure and the eccentricity for the LH2 complex in detergent solution was found to be 0.59 (Hong et al 2004), while in the 3D-crystals it was zero (McDermott et al 1995). It was concluded by the authors (Hong et al.) that an obvious tendency is that the more freedom exists for LH2 complexes to move, the larger deformation the LH2 complexes suffer. This might also explain the discrepancy of elliptical deformations observed by different groups.

WT LH2-only native membranes

LH2-only native membranes have been deposited onto the mica surface and have been imaged with AFM for the first time; this has allowed direct comparison of

the aggregation and structural properties of LH2 complexes purified and reconstituted into the 2D-crystals and within their native membranes directly isolated from *Rhodobacter sphaeroides* cells. The recent AFM study of native membranes isolated from *Rhodospirillum photometricum* (Scheuring et al 2004b, c) has allowed direct visualization of an intact photosynthetic membrane that has not been treated with detergent. In this work it can be seen that the nonameric LH2 complexes pack in a hexagonal arrangement in those parts of the membrane where they do not interact directly with the LH1-RC core complex.

Our study of LH2-only membranes required the use of a mild detergent treatment with DDM to break open the spherical chromatophores before AFM imaging could be attempted. It is notable that these fragments required a longer time to adsorb to mica than 2D-crystals before high resolution imaging could be conducted. We observed that even a small change in the detergent concentration (from 0.01% to 0.005%) led to a considerable change in the membrane fragments morphology (Fig. 2.8). AFM topographs of LH2-only membranes have revealed that intracytoplasmic vesicular membranes fractioned in the presence of 0.005% DDM produced either very small membrane patches or largely intact chromatophores (Fig. 2.8C, D). Medium-sized (100 – 500 nm), single-layered membrane fragments resulted from intracytoplasmic membranes treated with 0.01% DDM (Fig. 2.8A, B). Apparently there is a threshold point, between 0.005% and 0.01% DDM concentration, when the detergent is sufficiently concentrated to affect the membranes during the fractionation process.

.

The most unexpected result of this study of LH2-only native membranes was the observation of crystalline-like packing of LH2 complexes in the lipid bilayer in native membranes (Fig. 2.10, 2.12) that appeared to be very similar to the Type A crystalline packing of the LH2 rings in the 2D-crystals (Fig. 2.2A). Moreover, in the native membranes LH2 complexes were present in the lipid bilayer at two different height levels, just as in the 2D-crystals (Fig. 2.12). However, in spite of seeming similarity between the spatial organization of LH2 complexes in the 2D-crystals and native membranes, a closer inspection of crystalline lattices revealed a significant difference between two systems. We found that the angle formed by the adjacent strongly protruding LH2 complexes was ~ 93° in the 2D-crystals and ~ 122° in the native membranes, indicating hexagonal packing of LH2 complexes in the membranes (Fig. 2.16).

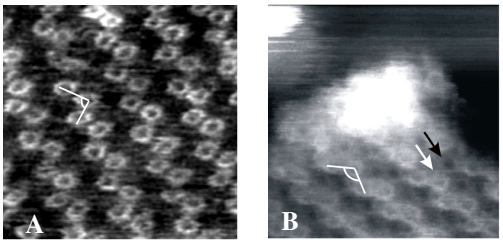

Fig.2.16. *Comparison of the angle formed by the adjacent strongly protruding LH2 complexes in the 2D-crystals (**A**) and native membranes (**B**).*

From the 3D crystal structure of the *Rhodopseudomonas acidophila* LH2 complex (McDermott et al 1995) it is known that LH2 has a slightly conical shape, with different diameters for opposite sides of the complex. This was also demonstrated in high-resolution AFM topographs of *Rubrivivax gelatinosus* LH2 2D-crystals (Scheuring et al 2001), where LH2 rings had diameters of 5.4 nm and 4.9 nm for opposite sides of the complex. The difference in sizes of periplasmic and cytoplasmic sides can be, in principle, used to determine if LH2 complexes have one or two orientations in the membrane by measuring diameters of the strongly and weakly protruding complexes. The current resolution of AFM topographs of LH2-only native membranes did not allow us to determine accurately the diameter of lower LH2 rings and to compare it with the diameter of higher rings. However we may derive the missing information from the high resolution images of photosynthetic native membranes obtained in Bahatyrova et al. (2004b) where only the cytoplasmic face of the membrane is exposed. We found that the LH2 complexes protruding on the cytoplasmic side of the membrane had the diameter of 7.6 ± 0.2 nm (n = 17). This value is larger than the diameter of 7.2 nm found for the periplasmic side of the LH2 complex embedded into the 2D-crystals, which is in agreement with previously reported data (Scheuring et al 2001).

There is also a clear discrepancy between the measured heights of the elevated rings in the LH2-only membranes and the up rings in the 2D-crystals, see Table 2.2, which points to a different arrangement of the LH2 complexes in the two bilayer systems. In the 2D-crystals the height difference between strongly and weakly protruding LH2 complexes is 0.5 nm, while in the native membranes this difference is larger, 0.9 nm.

Table 2.2. *Comparison of LH2 protrusions height in the 2D-crystals and native membranes*

	Height of strongly protruding rings, nm	**Height of weakly protruding rings, nm**	**Height difference between strongly and weakly protruding rings, nm**
LH2 2D-crystals	1	0.5	0.5
LH2 native membranes	1.3	0.4	0.9

Furthermore, the amount of the detergent used in this study for fractionation of the membranes was minimal and below its CMC, which is 0.017%. It is therefore highly unlikely that there was enough detergent to cause the LH2 complexes to totally dissociate from each other and then re-associate in an up- and down-packing arrangement. We suggest that some of the complexes have been vertically translated in the membrane plane as a response to the deposition of the curved membrane surface onto the flat mica surface.

Our hypothesis takes as its starting point a curved native membrane adsorbing to the mica, a process that begins at the contact area around its perimeter. The attractive forces between the periplasmic face of the LH2 complexes and the mica effectively pull them onto the surface. This brings further complexes next to the mica surface and they also adsorb. As the LH2 complex has an approximately conical shape, where the cytoplasmic face is wider than the periplasmic face, the flattening of the membrane will cause an increase of lateral pressure due to the reduction in surface area from the curved to the flat surface (Fig. 2.17, A-B->A'-B'). In response to this compression some of the LH2 complexes undergo vertical translation and tilting when they re-arrange themselves in the available space as shown in Fig.2.17.

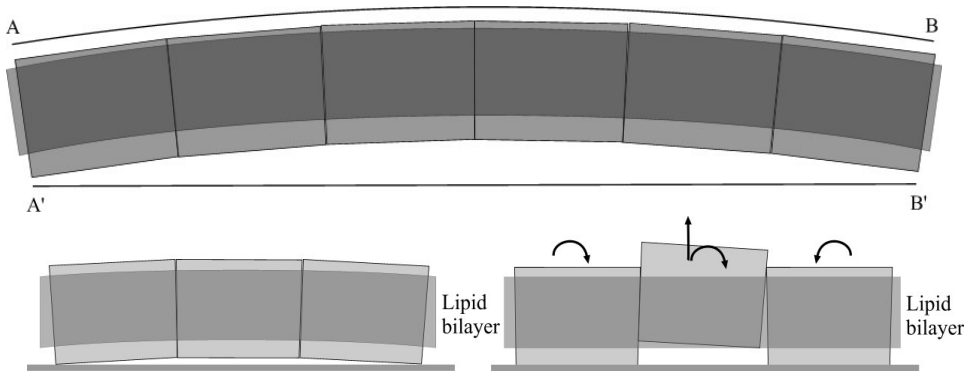

Fig. 2.17. *Schematic representation of a process of a curved membrane surface deposition onto the flat mica surface. As a result of a membrane flattening some proteins undergo vertical translation and tilting in the lipid bilayer.*

Although this re-arrangement results in a "high-low" pattern that is seemingly similar to the LH2-only 2D-crystal packing, the original hexagonal arrangement of the complexes is preserved as demonstrated by the unit cell angle of ~ 122^{o}, see Fig. 2.18, in contrast to ~ 93^{o} for the Type A 2D-crystal. The difference in height between strongly and weakly protruding LH2 complexes was of the order of 1 nm in all the samples measured. This indicates that the vertical translation is not a random response but there is a clear preference for this particular packing configuration. This is very likely to be related to the shape of the LH2 complex and exposed hydrophobic residues such as Phe, Tyr or Trp on the external face of the complex near the C-terminus of the β-polypeptide, which could interact favorably with each other through π-π stacking.

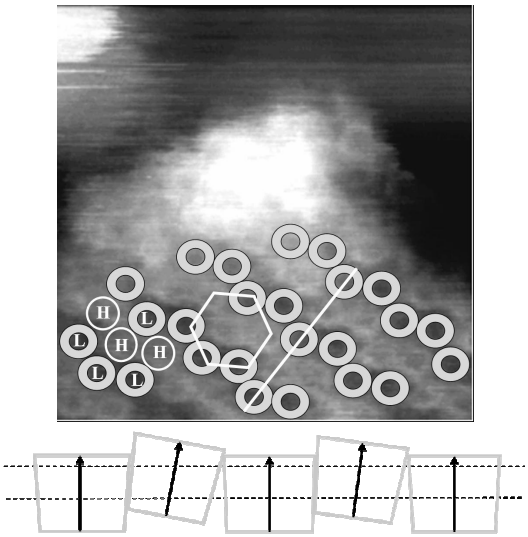

Fig. 2.18. *Schematic representation depicting dense packing of LH2 rings in the native membrane, frame size 100x100 nm^2, full grey scale 5 nm. Higher LH2 complexes were well resolved in the AFM images, while lower LH2 complexes (which were not sufficiently well resolved by AFM) were substituted in the images by the rings of approximately one LH2 ring size. The hexagonal unit cell is outlined and seven LH2 complexes comprising one unit cell are marked with the corresponding letters H (high) or L (low). Beneath the figure LH2 complexes are schematically shown inserted into the lipid bilayer in one orientation following the white line shown in the image. LH2 complexes are shown as trapezoids with unequal diameters of the opposite sides of the complexes (according to the LH2 crystal structure (McDermott et al 1995) and recent AFM images of LH2 2D-crystals (Scheuring et al 2001)). As all LH2 rings face only one side, they are marked with the arrows pointing only to one direction. Higher protruding LH2 rings alternate with lower protruding LH2 rings. Some of the LH2 rings are shown tilted according to the scheme presented in Fig. 2.17.*

2.5 Conclusions

In this chapter we have compared the manner with which the LH2 complex packs when it is reconstituted into a 2D-crystal, which leads to two regular and one irregular pattern, with the arrangement in native membrane fragments. In the former system purely physical forces lead to the oppositely oriented insertion of the proteins, while in the latter the biologically driven unidirectional insertion is apparent.

The comparison of the LH2 lateral dimensions from the reconstituted bilayer and the natural bilayer has shown that, within experimental error, the LH2 complex preserves a uniform circular shape and invariable size.

The imaging of highly curved membranes is not possible by AFM and it was necessary to transform the membrane fragments to a more planar form suitable for high-resolution imaging. This led to a change in the appearance of the membrane but this did not perturb the hexagonal organization of LH2 complexes. This set of data collected when imaging LH2-only native membranes will be particularly useful when imaging other native membranes that have a degree of curvature.

It is the mark of an educated mind
to rest satisfied with the degree of precision
which the nature of the subject admits
and not to seek exactness
where only an approximation is possible.
Aristotle

Chapter 3

Flexibility and size heterogeneity of the LH1 light harvesting complex revealed by AFM

Previous electron microscopic studies of bacterial LH1-RC complexes demonstrated both circular and elliptical conformations of the LH1 ring, and this implied flexibility has been suggested to allow passage of quinol from the Q_B site of the RC to the quinone pool prior to reduction of the cytochrome bc_1 complex. We have used atomic force microscopy to demonstrate that these are just two of many conformations for the LH1 ring, which displays large molecule-to-molecule variations, in terms of both shape and size. This AFM study has used a mutant lacking the reaction center complex, which normally sits within the LH1 ring providing a barrier to substantial changes in shape. This approach has revealed the inherent flexibility and lack of structural coherence of this complex in a reconstituted lipid bilayer at room temperature. Circular, elliptical and even polygonal ring shapes as well as arcs and open rings have been observed for LH1; in contrast, no such variations in structure were observed for the LH2 complex under the same conditions. The basis for these differences between LH1 and LH2 is suggested to be the H-bonding patterns that stabilize binding of the bacteriochlorophylls to the LH polypeptides. The existence of open rings and arcs provides a direct visualization of the consequences of the relatively weak associations that govern the aggregation of the protomers ($\alpha_1\beta_1Bchl_2$) comprising the LH1 complex. The demonstration that the linkage between adjacent protomer units is flexible and can even be uncoupled at room temperature in a detergent-free membrane bilayer provides a rationale for the dynamic separation of individual protomers, and we may now envisage experiments that seek to prove this active opening process.

This chapter is based on Svetlana Bahatyrova, Raoul N. Frese, Kees O. van der Werf, Cees Otto, C. Neil Hunter, John D. Olsen. 2004. Flexibility and size heterogeneity of the LH1 light harvesting complex revealed by atomic force microscopy: functional significance for bacterial photosynthesis. J. Biol. Chem. 279: 21327-21333.

3.1 Introduction

Photosynthetic organisms harvest light energy and convert it to a chemically useful form, using LH and RC complexes. In the purple photosynthetic bacteria the RC, the site of photochemistry, receives excitation energy from the LH1 complex, which receives energy in turn from the LH2 complex (reviewed in Blankenship et al 2002). The atomic structure of the *Rhodopseudomonas acidophila* LH2 complex (McDermott et al 1995) and the cryo-EM structure of the *Rhodobacter sphaeroides* complex (Walz et al 1998) both revealed a circular arrangement of nine protomers, each consisting of an α- and a β-polypeptide. The LH2 α-polypeptides formed an inner ring, with the β ring outermost. Altogether, 27 Bchl molecules are bound to this structure (McDermott et al 1995). More recent work has established that LH1 surrounds the RC using an arrangement of 16αβ protomers and 32 Bchls (Jamieson et al 2002) when there is no PufX protein. In other bacteria an LH1 ring of 15 αβ protomers, together with either PufX or a putative PufX homologue (W), form a continuous ring of protein round the RC (Roszak et al 2003; Siebert et al 2004). The demonstration of both circular and elliptical forms of this LH1 complex provided evidence for its flexibility (Jamieson et al 2002). This property of the LH1 complex was suggested to be a significant factor in the export of quinol, the product of RC photochemistry, to the cytochrome bc_1 complex (Jamieson et al 2002). For organisms such as *Rhodospirillum rubrum*, which assemble an $(\alpha\beta)_{16}$ LH1 complex completely enclosing the RC, such flexibility would clearly be an essential feature of this LH complex and would imply a dynamic series of conformations *in vivo.* However, only the extremes of this dynamic population have been reported and the flexibility hypothesis requires the imaging of several conformations at room temperature.

For other photosynthetic bacteria such as *Rhodobacter sphaeroides*, *Rhodobacter capsulatus* and *Rhodopseudomonas palustris* other possibilities for quinol export became apparent when it was found that these bacteria assemble another polypeptide, PufX (W), into the LH1 complex. It was discovered that PufX$^-$ mutants were unable to photosynthesize (Farchaus and Oesterhelt 1989; Farchaus et al 1992), and subsequently such mutants were found to be impaired in their ability to shuttle quinones/quinols in and out of the Q_B site of the RC (Lilburn and Beatty 1992; Barz et al 1995b). It was suggested that PufX forms part of the LH1 ring, providing a portal for quinol (Cogdell et al 1996). This concept would appear to be supported by work on mutants with an LH1 complex that is too small to completely surround the RC; these mutants can therefore allow free movement of quinones/quinols to the RC Q_B site and so they are fully capable of photosynthetic growth, even in the absence of PufX (McGlynn et al 1994). Studies on LH1-RC-PufX complexes in native membranes show that PufX causes a specific orientation of the RC, which is the likely cause of the long range

organization of the core complexes (Frese et al 2000; Siebert et al 2004) and plays a role in organizing the core complex into dimers in detergent-solubilized systems (Francia et al 1999; Scheuring et al 2004a).

It is not known whether the LH1 complex of *Rhodobacter sphaeroides* is flexible, and if so, to what extent; perhaps there is no need if PufX does indeed provide a quinol portal. In terms of LH1 flexibility we are confined at present to the knowledge, based upon cryo-electron microscopy studies of 2D-crystals, that the *Rhodospirillum rubrum* LH1 complex lacking PufX can assume both circular and elliptical forms. This observation is subject to the limitations that the crystals are frozen in glucose at ~ 77K, and that LH1 molecules in disordered regions will not be represented. The use of AFM to image the surface of 2D-crystals presents us with the opportunity to obtain high signal-to-noise data without the need for processing the data, and particularly without the need to obtain large highly ordered crystals. Previous studies have amply illustrated the usefulness of AFM for imaging 2D-crystals of the LH2 complexes of *Rubrivivax gelatinosus* (Scheuring et al 2001), *Rhodobacter sphaeroides* (Scheuring et al 2003a) and *Rhodopseudomonas acidophila* (Gonçalves et al 2004; Stamouli et al 2003). Scheuring et al. achieved the imaging of native membranes of *Rhodopseudomonas viridis* containing LH1-RC complexes by AFM and were able to show that LH1 formed an ellipse round the RC, but that it became circular upon removal of the RC (Scheuring et al 2003b).

In view of the possible functional significance of alterations in conformation of the LH1 ring, it is important to visualize all of the possible shapes and aggregation states of which LH1 is capable. This should be compared with the peripheral LH2 complex, using the same methodology. Scheuring et al. have extensively characterized large planar 2D-crystals of the LH2 complex from *Rhodobacter sphaeroides* by AFM (Scheuring et al 2003a). In our work, we have examined different crystal forms of the LH2 complex, to establish whether alterations in crystal packing produce distortions of the LH2 complex. In this regard, it is already known that lateral packing forces exerted in 2D-crystals can distort LH1-RC complexes into circles or ellipses, depending on whether the crystal form is tetragonal or orthorhombic, respectively (Jamieson et al 2002). Recently, high-resolution AFM was used to image 2D-crystals of the LH1-RC complex of *Rhodospirillum rubrum* (Fotiadis et al 2004). It was shown that the LH1-RC complex may adopt an irregular shape in regions of uneven packing forces in the crystal, reflecting a likely flexibility when in the natural membrane. This study also imaged a few LH1-only complexes, formed as a consequence of removing the RC with the AFM tip, which showed some of the possibilities for distorting this complex. In order to examine this in more detail it is important to obtain images of many LH1 complexes free of the RC; it is only then that the inherent flexibility and even deformability of LH1 will be revealed, since the RC,

which sits fairly tightly within the LH1 ring, normally provides a barrier to substantial deformation.

We have used AFM to compare 2D-crystals of LH1 and of LH2 of *Rhodobacter sphaeroides*. We find that the LH2 crystals have three different packing forms and despite the differing packing forces, the complexes are essentially always circular. In contrast, LH1 molecules displayed a wide range of both ring sizes and packing geometries that generated circular, elliptical and even polygonal ring shapes as well as arcs and open rings. From these data we conclude that the LH1 ring is intrinsically highly deformable and we relate this property to the manner in which it is assembled and further to its operation within the photosynthetic unit. For further corroboration of our findings LH1-only native membranes have been imaged by AFM and similar heterogeneity of LH1 rings in terms of both shape and size was found.

3.2 Materials and methods

Biological samples were prepared in the laboratory of Prof. Dr. C. N. Hunter (University of Sheffield, UK).

Strains and plasmids

The *Rhodobacter sphaeroides* strains have been described previously: DD13 ($LH2^-$, $LH1^-$, RC^-) (Jones et al 1992); DPF2, LH2-only (Jones et al 1992); *E. coli* S17–1 (Simon et al 1983); DD13(pRKEK1), LH1-only (Jones et al 1992).

Bacterial growth

The LH2-only strain DPF2 was grown semiaerobically and the intracytoplasmic membranes prepared according to the methods in Olsen et al. (1994). The plasmid pRKEK1 was introduced into the double deletion strain DD13 by conjugative transfer**.** Colonies were examined for the presence of the LH1 WT complex using a Guided Wave 260 fibre-optic spectrophotometer and a homebuilt plate holder. Representative colonies were then grown semi-aerobically in liquid culture and intracytoplasmic membranes were isolated as previously described (Olsen et al 1994), except that in this work we used a lower growth temperature of 30°C, and then concentrated the membranes by centrifugation at 186,000g for 4.5 hours after diluting the sucrose present to less than 5%, prior to LH purification.

Purification and 2D-crystallization of LH1 and LH2 complexes

LH2 was purified and crystallized as described in Walz et al. (1998). For LH1, approximately 500 absorbance units of concentrated LH1-only membrane sample were solubilized with 1.5 ml of 20% β-OG with gentle stirring at 10°C and then loaded onto a pre-equilibrated 15 ml DEAE column. The column was washed for an hour, at a flow rate of 1 ml/min, with 155 mM NaCl, 10 mM TRIS pH 7.5, 1% β-OG then eluted with a 155-400 mM NaCl salt gradient over 60 minutes, at 1ml/min. The best fractions were determined by the ratio of the absorbance at ~ 850 nm vs. 280 nm and these were used for 2D-crystallization trials using the lipid DOPC.

Detergent treatment of chromatophores to produce LH1-only membrane fragments for AFM

Chromatophores have been treated as described for LH2-only membranes in Chapter 2. Membranes were solubilized with 0.04% DDM. The sucrose density gradient produced 3 bands which are labeled 1, 2, and 3 (Fig. 3.1). Membrane fractions from band 3 were examined by AFM.

Fig. 3.1. *Solubilization of LH1-only membranes with DDM with subsequent fractionation by ultracentrifugation on sucrose density gradient [Image courtesy of John Olsen, University of Sheffield].*

Atomic force microscopy and image processing

For AFM measurements LH2 2D-crystals have been prepared as was described in Chapter 2. LH1-only crystals and native membranes were handled identically to the LH2-only native membranes (as described in Chapter 2).

AFM imaging parameters have been described in Chapter 2. All the AFM images presented in this chapter are processed by applying a low-pass filter and represented in 3D-view using Scanning Probe Image Processor program, unless otherwise specified.

3.3 Results

3.3.1 Morphology of 2D-crystals formed from LH1 complexes; comparison with LH2 2D-crystals

The 'empty' LH1 complex containing no RC formed a homogeneous population of planar single layered crystals between 100 and 700 nm in width (an example of a crystal ~ 300 nm in diameter is shown in Fig. 3.2A).

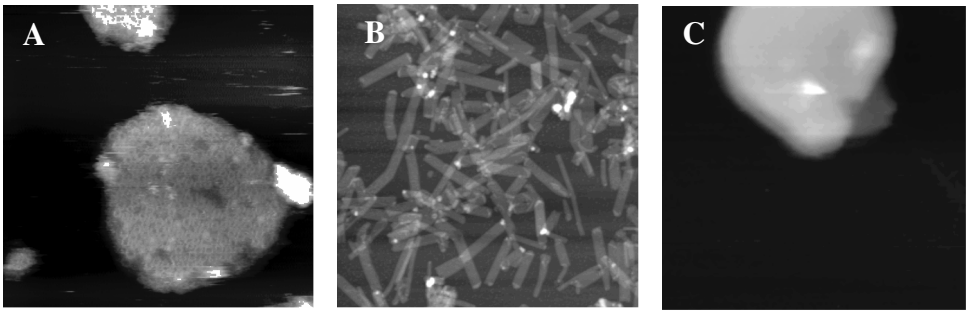

Fig. 3.2. *Examples of LH1 and LH2 2D-crystals.* ***A****: LH1 crystal, frame size 500x500 nm^2, full gray scale 11 nm;* ***B****: LH2 tubular crystals, frame size 20x20 µm^2, full gray scale 20 nm;* ***C****: LH2 vesicular crystals, frame size 1000x1000 nm^2, full gray scale 30 nm. The images represent raw, unprocessed data.*

The height of LH1 crystals above the mica surface was 6.7 ± 0.4 nm (n = 81; Table 3.1). Most of the LH1 crystals displayed dense packing of LH1 complexes, while some of the crystals also contained empty areas of lipid bilayer with an average height above the mica surface of 4.1 ± 0.2 nm (n = 20; Table 3.1). In contrast, tubular crystals (Fig. 3.2B) were found most frequently for the LH2 complex, some of which had ruptured, forming single-layered sheets up to 1 µm wide. Empty lipid patches were also observed for LH2 crystals, with an average height of 4.1 ± 0.1 nm (n = 16), which corresponds well with the number obtained from the analysis of LH1 crystals. Vesicular LH2 crystals (Fig. 3.2C) were observed less frequently and consisted of small round patches (average diameter ~ 200 nm).

Table 3.1. *LH2 and LH1 crystals height above the mica surface measured with the AFM*

LH2	**Average height (nm)**	**Sample size**
lipid bilayer	4.1 ± 0.2	16
vesicular 2D-crystals	15.9 ± 0.8	11
single-layered 2D-crystals (broken tubes)	7.2 ± 3.3	30
tubular 2D-crystals	16 ± 2.4	32
LH1		
lipid bilayer	4.1 ± 0.2	20
planar sheets	6.7 ± 0.4	81

3.3.2 Variations in packing in 2D-crystals

The different packing arrangements of LH1 complexes are shown in Fig. 3.3. No long-range crystalline ordering was observed for LH1, unlike the situation for LH2 (see Fig. 3.4; Walz et al 1998; Scheuring et al 2003a). In rare cases, LH1 rings formed small areas of well-ordered crystalline lattices with a tentative assignment of hexagonal packing (Fig. 3.3A). This could only be observed in crystals of larger than average size, i.e. more than 500 nm. This ordering was also accompanied by a marked preference for a single orientation, as determined by the height of the protruding face of the complex. The majority of LH1 rings (86%) were positioned in the lipid membrane in the "down" orientation, characterized by a height from the lipid surface to the highest point of LH1 of 0.8 ± 0.1 nm (n = 261). In the opposite orientation this height was 1.4 ± 0.1 nm (n = 43). It should be emphasized that LH1 rings, which tended to be circular in the well-ordered areas of crystals (see Fig. 3.3A), still displayed some heterogeneity in size. For example, the left and right arrows in Fig 3.3A indicate ring sizes of 12.6 and 14.1 nm, respectively.

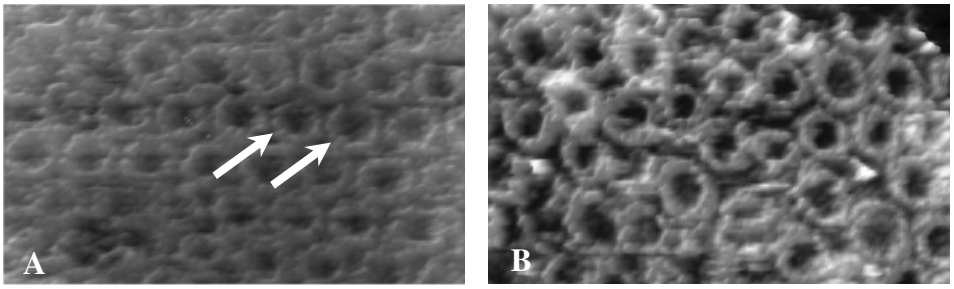

Fig. 3.3*. Variations in packing for LH1 crystals.* ***A****: Ordered (hexagonal), frame size 65x130 nm^2, full gray scale 1.8 nm;* ***B****: Disordered packing, frame size 65x130 nm^2, full gray scale 3.2 nm. The right and left arrows indicate large and small LH1 complexes, respectively.*

The high level of disorder of LH1 aggregates typified by Fig 3.3B was accompanied by heterogeneity of the LH1 complexes in terms of differing ring sizes, with each size category displaying at least two different shapes. Broken rings and also incomplete arcs were found.

Crystalline packing of LH2 complexes was clearly resolved and AFM images indicated that this fell into 3 categories: Type A, a zigzag pattern, Type B, a rectangular pattern and Type C, disordered. These are displayed separately in Fig. 3.4.

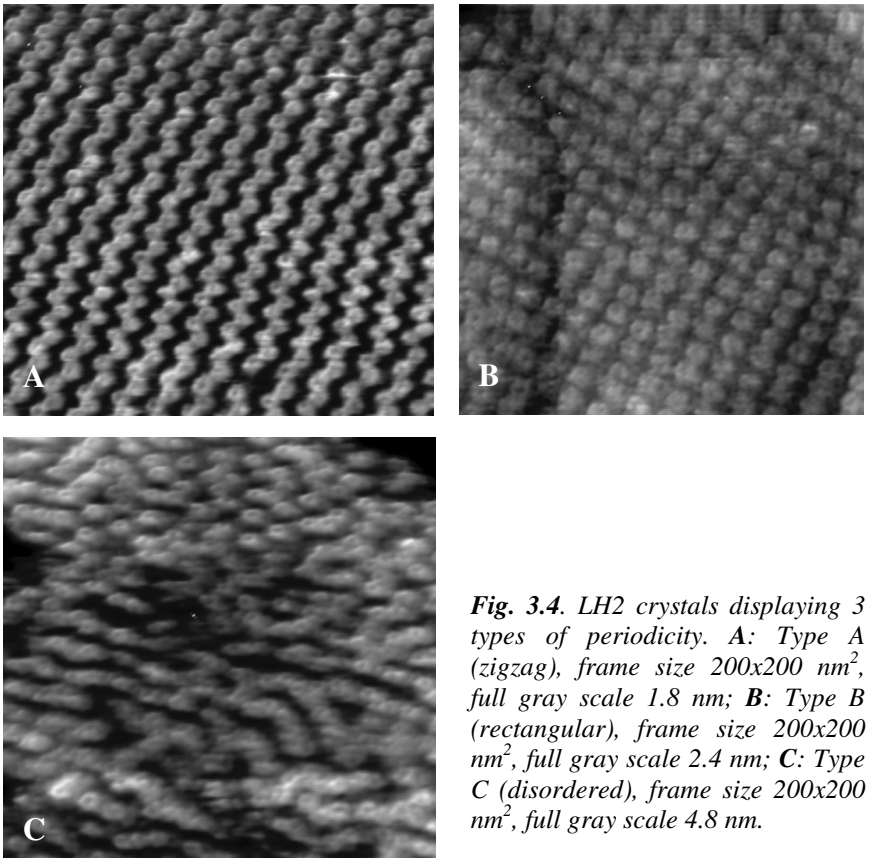

***Fig. 3.4**. LH2 crystals displaying 3 types of periodicity. **A**: Type A (zigzag), frame size 200x200 nm^2, full gray scale 1.8 nm; **B**: Type B (rectangular), frame size 200x200 nm^2, full gray scale 2.4 nm; **C**: Type C (disordered), frame size 200x200 nm^2, full gray scale 4.8 nm.*

A Fourier transform of AFM images of Type A crystals directly allowed the definition of a unit cell (a = 19.9 nm, b = 15.9 nm, γ = 87°). The unit cell encompasses four LH2 rings, two facing upwards and two downwards, which are clearly resolved. One face of the complex protrudes more than the other; the height from the lipid surface to the extremity of LH2 ("up") was 1.0 ± 0.1 nm (n = 105), and in the opposite orientation ("down") this was 0.5 ± 0.1 nm (n = 96). This up-down configuration has been reported before from 2D EM data (Walz et

al 1998) and from subsequent AFM studies on LH2 2D-crystals (Scheuring et al 2001; Scheuring et al 2003a). The primary difference between Type B and Type A crystal packing is that in the former there is no close contact between adjacent "up" rings in the unit cell, while in Type A they are brought together very closely. Type C crystals did not show any distinct periodical pattern (Fig. 3.4C), as the LH2 complexes were incorporated into the lipid bilayer in a random, chaotic way.

3.3.3 Detailed characteristics of LH1 and LH2 rings; a variety in shape, size and conformation for LH1 complexes

Fig. 3.5A shows a high-resolution image of LH1 complexes embedded in a representative, disordered 2D-crystal.

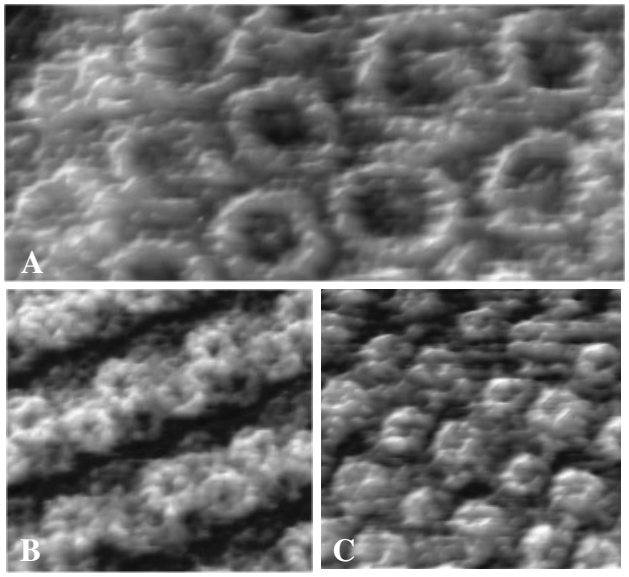

***Fig. 3.5**. High magnification topographs of LH1 and LH2 complexes. **A**: LH1 rings (disordered area), frame size 35x70 nm^2, full gray scale 1.8 nm; **B**: LH2 rings (Type A), frame size 50x50 nm^2, full gray scale 1.7 nm; **C**: LH2 rings (Type B), frame size 50x50 nm^2, full gray scale 2 nm.*

LH1 complexes displayed a high level of heterogeneity in shapes, size and conformation. In contrast, LH2 complexes showed no such heterogeneity. Figs. 3.5B and C show high magnification images of LH2 rings. The most noteworthy finding was that under no circumstances, not even for disordered regions of 2D-crystals, did the LH2 complex display the heterogeneity in size and shape we observed for LH1. Regardless of the type of packing or disorder, all LH2 rings appeared to be circular and of identical diameter, within experimental error. Without the use of single particle averaging methods we found that in some of the

LH2 rings the resolution was high enough to count the number of units per LH2 ring, confirming the nonameric nature of the ring.

The variety of types of LH1 complex imaged by AFM could be observed from our analysis of ~ 300 individual LH1 complexes from ~ 10 different membrane patches. An overview of the variation in LH1 complexes is represented in Fig. 3.6. Circles (Figs. 3.6A-C), polygonal rings (Fig. 3.6D), open rings (Fig. 3.6E), ellipses (Figs. 3.6F-H), and more anomalous structures such as arcs (Figs. 3.6I, J) were all observed. Polygonal rings are deformed rings, in which circular or elliptical ring architectures were considerably distorted. The ellipses and circles formed the two major groups, comprising 41 and 35% of the total number of complexes, respectively. Polygonal and open rings were observed less frequently, at 19 and 5% respectively.

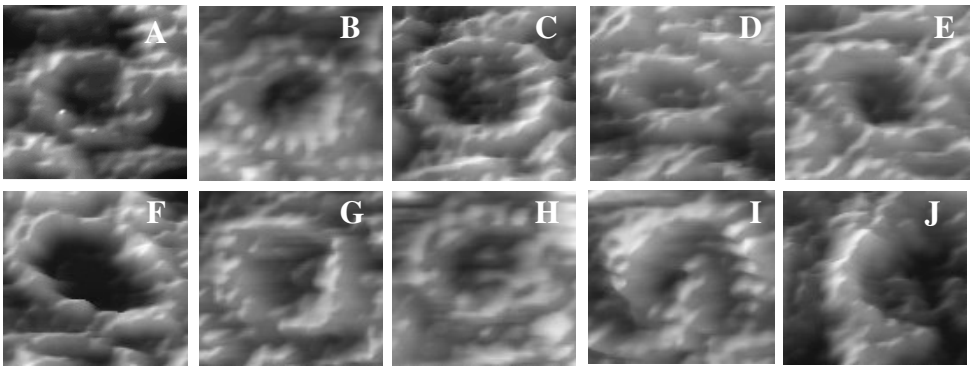

Fig. 3.6*. An overview of LH1 complexes, displaying the wide variation in shape and size. All 10 images have an image size of 18x18 nm.* ***A****: Small circular. Percentage of total – 6%. Dimensions 11.6 ± 0.5 nm, n = 17.* ***B****: Medium circular. Percentage of total – 22%. Dimensions 12.6 ± 0.5 nm, n = 66.* ***C****: Large circular. Percentage of total – 7%. Dimensions 14.5 ± 0.8 nm, n = 23.* ***D****: Polygonal. Percentage of total – 19%. Dimensions n/a, n = 57.* ***E****: Open. Percentage of total – 5%. Dimensions 12.7 ± 1.3 nm, n = 17.* ***F****: Small elliptical. Percentage of total – 10%. Dimensions 13.3(±1.1)x10.0 (±1.1) nm, n = 30.* ***G****: Medium elliptical. Percentage of total – 18%. Dimensions 13.8(±1.2)x10.9 (±1.2) nm, n = 55.* ***H****: Large elliptical. Percentage of total – 13%. Dimensions 14.4(±1.1)x11.4 (±1.1) nm, n = 39.* ***I****: Two intersecting arcs.* ***G****: Single arc.*

The differing ring sizes observed for LH1 had outer diameters of 11.6 ± 0.5 nm, 12.5 ± 0.3 nm, and 14.6 ± 0.8 nm, which are further referred to as small, medium and large. In the circular LH1 rings, the fraction of small rings (Fig. 3.6A) was 14%, medium rings (Fig. 3.6B) - 64%, and large rings (Fig. 3.6C) - 22%. Using the known size of the αβ-protomer we suggest that the small rings contain 15 subunits, the medium 16 and the large 18 subunits. For ellipses the occurrence of small, medium and large (Figs. 3.6F-H) was 24, 45 and 31 % respectively. The

circularity of some of the LH1 complexes was confirmed by the practically equal diameters for two orthogonal directions. For the elliptical complexes the ratio between short (*b*) and long (*a*) axes was found to vary slightly for different sizes: small ellipses, *b/a* = 0.75, medium and large ellipses, *b/a* = 0.8.
Table 3.2 details parameters that were measured for LH1 and LH2 complexes. The height of weakly protruding LH1 rings above the lipid bilayer was 0.8 nm, which is similar to the height of empty LH1 rings on the periplasmic side for the *Rhodopseudomonas viridis* complex (Scheuring et al 2003b). The height of stronger protrusions of the LH1 complexes observed here and attributed to the cytoplasmic face of the complex was 1.4 nm. The inner diameters of cytoplasmic and periplasmic faces of the small rings were 6.1 and 6.6 nm, respectively; medium rings 6.5 and 7.3 nm, and large rings 7.6 and 9 nm. Thus, in each case the inner diameter of the strongly protruding cytoplasmic surface of the LH1 rings was noticeably smaller than that of the weakly protruding periplasmic surface.

Table 3.2. *LH2 and LH1 individual ring dimensions measured with the AFM*

LH2		**Type A**	**Type B**	**Type C**
Periplasmic face	Lipid to protein top	1 ± 0.1 nm, n = 105		
	Ring centre to protein top	0.4 ± 0.1 nm, n = 84		
	Outer diameter	7.4 ± 0.3 nm, n = 68	7.3 ± 0.3 nm, n = 31	7.1 ± 0.3 nm, n = 90
	Inner diameter	3.2 ± 0.2 nm, n = 62	3.3 ± 0.3 nm, n = 28	3.0 ± 0.2 nm, n = 87
Cytoplasmic face	Lipid to protein top	0.5 ± 0.1 nm, n = 96		
LH1		**small**	**medium**	**large**
Periplasmic face	Lipid to protein top	0.8 ± 0.1 nm, n = 261		
	Ring center to protein top	0.8 ± 0.2 nm, n = 261		
	Outer diameter	11.6 ± 0.5 nm, n = 13	12.5 ± 0.3 nm, n = 56	14.6 ± 0.8 nm, n = 21
	Inner diameter	6.5 ± 0.4 nm, n = 13	7.2 ± 0.4 nm, n = 56	8.9 ± 0.5 nm, n = 21
Cytoplasmic face	Lipid to protein top	1.4 ± 0.1 nm, n = 43		
	Ring center to protein top	0.8 ± 0.2 nm, n = 43		
	Outer diameter	11.6 ± 0.5 nm, n = 4	13.0 ± 0.9 nm, n = 10	15.2 ± 0.8 nm, n = 2
	Inner diameter	6.1 ± 0.9 nm, n = 4	6.5 ± 0.6 nm, n = 10	7.6 ± 0.2 nm, n = 2

3.3.4 Imaging of LH1-only native membranes

We performed high-resolution AFM imaging of LH1-only native membranes directly isolated from *Rhodobacter sphaeroides* cells and solubilized in the presence of 0.04% DDM detergent. A comparison of the LH1 complex in its native membrane and in the 2D-crystal environment, similar to that performed for the LH2 complex in Chapter 2, could be made. LH1-only native membranes, just as LH1-only 2D-crystals, were firmly adhered to the surface of the freshly cleaved mica. Membrane patches with lateral dimensions varying from 100 to 500 nm could be easily found on the mica surface (Fig. 3.7A). The average height of the membranes above the mica was 6.9 ± 0.5 nm (n = 19), corresponding to a single layer of the lipid membrane. High-magnification topographs of the membrane surface revealed dense packing of LH1 complexes in the lipid bilayer (Fig. 3.7B). The ring-like structure of LH1 complexes in the native membrane was clearly resolved. We found that LH1 rings were positioned in the lipid membrane at two different height levels, with the height difference between higher and lower LH1 complexes of ~ 1 nm. The ratio between high and low LH1 rings was variable in different membrane patches. In some of the membranes approximately half of the rings were higher, while in the rest of the membrane patches the fraction of higher LH1 rings was only ~ 25%. The lower rings protruded from the lipid bilayer with the height of 0.7 ± 0.2 nm (n = 26) and the higher rings had a height above the lipids of 1.7 ± 0.2 nm (n = 25). The depth of the ring central hole was 1.9 ± 0.3 nm (n = 26) and 1.5 ± 0.3 nm (n = 25) for lower and higher rings, respectively. The outer diameter of LH1 rings was 12.5 ± 0.4 nm (n = 26) and 13.0 ± 0.7 nm (n = 25) (lower and higher rings, respectively). The inner diameter was 7.9 ± 0.8 nm (n = 26) and 7.6 ± 0.5 nm (n = 25) (lower and higher rings, respectively).

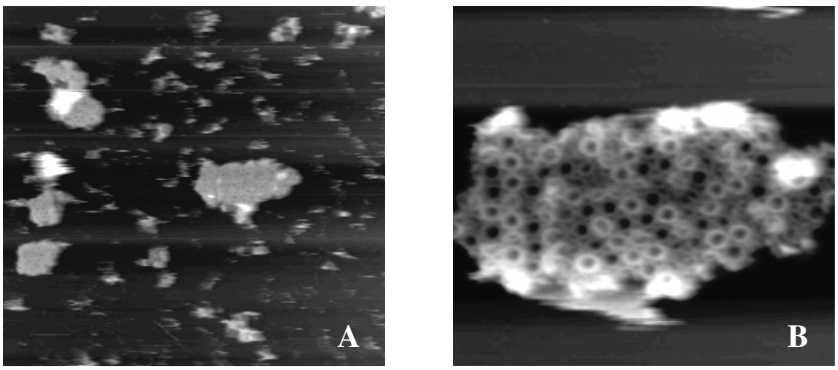

Fig. 3.7. *AFM images of LH1-only native membranes.* ***A****: An overview of LH1 membranes, frame size 1000x1000 nm^2, full grey scale 15.4 nm;* ***B****: Packing of LH1 complexes in the native membranes, frame size 250x250 nm^2, full grey scale 6.1 nm.*

The LH1 complexes in the native membranes displayed heterogeneity in terms of both shape and size, as can be seen in Figure 3.7B and 3.8. LH1 rings of different sizes and shapes (circular, elliptical, open, arcs, intersecting arcs) could be found.

High-magnification topographs of LH1-only membrane are shown in Fig. 3.8. Both individual LH1 rings and also their individual subunits were clearly resolved. Two different membrane areas display LH1 complexes which show a diversity of shapes and sizes as was observed also for LH1 2D-crystals.

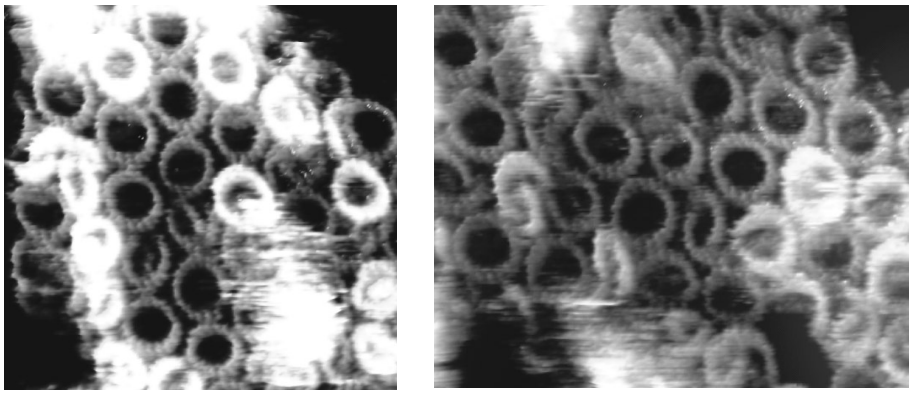

Fig. 3.8. *High magnification topographs of LH1 complexes in the native membranes, frame size 100x100 nm^2 (left) and 80x100 nm^2 (right), full grey scale 5.4 nm.*

3.4 Discussion

The flexibility, which has been suggested to be a functionally essential property of the LH1 complex, would require a dynamic series of conformations *in vivo.* We have used AFM to examine a population of LH1 molecules in a membrane environment at room temperature. Our work highlights the extraordinary variety of shapes and sizes exhibited by the isolated LH1 complex. This has not been visualized directly before by AFM, since previous studies have concentrated on the LH1-RC complex, either in native membranes of *Rhodopseudomonas viridis* (Scheuring et al 2003b) or in 2D-crystals formed from the *Rhodospirillum rubrum* complex (Fotiadis et al 2004), and on the *Rhodobacter sphaeroides* LH1-RC-PufX complex (Scheuring et al 2004a; Siebert et al 2004). Ketelaars et al. (2002) also noted that only 30% of the single LH1-RC complexes of *Rhodopseudomonas acidophila* that they analyzed showed a fluorescence-excitation spectrum consistent with a circular structure; the remainder were interpreted as either rings deformed in a C_2 manner or incomplete rings.

AFM images were recorded using tapping mode imaging in liquid, and by applying the lowest force possible. Previous AFM studies of bacterial LH complexes (Scheuring et al 2001; Scheuring et al 2003a, b; Stamouli et al 2003) have employed contact mode AFM, so it was important to establish that tapping mode AFM is also effective. A comparison of contact and tapping mode AFM concluded that the former method tends to offer superior resolution, but that tapping mode AFM, in which the tip touches the sample only at the end of a downward movement, is capable of imaging without detectable deformation of polypeptide domains (Möller et al 1999).

It is likely that the presence of the RC inside the LH1 ring greatly restricts the range of conformations possible for LH1, necessitating removal of the RC, in this case by genetic means, in order to avoid employing detergent treatments for RC removal. It should be stressed that the particular LH1-only strain used in this study did not contain the PufX gene and thus the complex studied here is analogous to the LH1 complex from *Rhodospirillum rubrum* or *Rhodopseudomonas viridis*. Attempts were made to form ordered 2D sheets reconstituted from monomeric LH1-only complexes. Such crystals have already been reported (Walz et al 1998) with sufficient order to be analyzed by negative stain EM. However, it appears to be difficult to form very highly ordered 2D sheets from LH1-only complexes. For example, there is evidence from transmission EM that the LH1-only strain of *Rhodopseudomonas viridis* produces membranes that are much more disordered than for the wild type containing the LH1-RC complex (Ostafin et al 2003). The AFM images of LH1 arrays in Figs. 3.2 and 3.3 illustrate the inherent difficulties of reconstituting lattices with a high degree of order, since the isolated LH1 complex exhibits heterogeneity in both ring size and conformation. Although this is a disadvantage for crystallographic approaches, or any method that employs averaging procedures, it provides fascinating material for analysis by AFM.

It is surprising that even in the well-ordered regions of the 2D-crystals of LH1-only complexes there is apparently little tendency to aggregate in the alternating ‘up-down-up’ arrangement often seen for LH2 and LH1-RC complexes (Fotiadis et al 2004; Jamieson et al 2002; Scheuring et al 2003a; Walz et al 1998). It is possible that this mode of packing arises from small differences in diameters of these complexes at the cytoplasmic and periplasmic faces, coupled with a certain amount of rigidity. Together, these might favour alternating associations in a 2D lattice. The obvious flexibility of LH1 seen in the gallery of images in Fig. 3.6 might preclude any such up-down lattice, and may explain the preponderance of one topology in our crystals.

WT LH1-only native membranes

Comparison of LH1-only 2D-crystals and native membranes demonstrated that in both systems the LH1 complex displayed a wide range of ring sizes and conformations. The observation of diverse LH1 rings in their native membrane environment confirms the inherent property of the LH1 ring architecture to be highly flexible and heterogeneous.

We observed that LH1 complexes in the native membranes were inserted into the lipid bilayer at two different height levels, similar to the pattern we found in the LH1 2D-crystals. As in the LH2 2D-crystals and LH2 native membranes, described in Chapter 2, the observation of LH1 complexes positioned at two different height levels in the native membrane was not expected by us. For the LH2 complex, this phenomenon was observed earlier for LH2 2D-crystals (Scheuring et al 2001; Scheuring et al 2003a; Walz et al 1998). The two different heights of LH2 proteins above the lipid bilayer in the 2D-crystals were explained by the insertion of the proteins in two opposite orientations, thus facing both sides, periplasmic and cytoplasmic. Following the same reasoning we conducted in Chapter 2 for LH2 complexes, we assume that it is highly unlikely that the same pattern (alternation of up-(cytoplasmic) and down-(periplasmic) rings) found in LH1 2D-crystals exists in the native membranes as well. The two different height levels of LH1 rings observed in their native membranes can be explained by an assumption that some of the LH1 rings have been elevated in the lipid bilayer plane, and some have been depressed with regard to the others. Such a vertical translation of membrane proteins in the native membranes probably occurs due to the deposition of the membrane patches onto the flat mica surface (see Fig. 2.17, Chapter 2). For a further proof that LH1 complexes have not been flipped over in the native membranes but that they have undergone vertical translation in the membrane 2D plane, we note that from the model structure of the LH1 complex it is known that the N-terminal helix of the β-polypeptide lies at an angle to the membrane normal pointing towards the centre of the ring (Conroy et al 2000). This means that on the cytoplasmic face of the LH1 complex the inner diameter of the ring should be smaller than on its periplasmic face. We have measured inner diameters for higher and lower LH1 rings in the native membranes and have found that they were identical within our measurement error, 7.6 ± 0.5 nm and 7.9 ± 0.8 nm, respectively. This finding supports our suggestion that the LH1 rings face only one side in the native membranes with some of the rings sitting in the lipid bilayer higher than the others. In contrast, in the LH1 2D-crystals inner diameters of higher and lower rings differed from each other thus representing both faces of the LH1 rings (Table 3.2).

There is a clear difference between the measured heights of strongly protruding LH1 rings in the 2D-crystals and in the native membranes (Table 3.3), as has been also seen in the LH2-only 2D-crystals and membranes (Chapter 2, Table 2.2). The height difference between strongly and weakly protruding LH1 rings in the 2D-crystals is 0.6 nm, while in the native membranes this difference is 1 nm. These two values are in the range of values found for LH2-only crystals and membranes (0.5 and 0.9 nm), which points to the similar origins of both LH complexes arrangement in the two bilayer systems, which is very likely to be related to the shape of the LH complexes and exposed hydrophobic residues as was explained in detail in Chapter 2 for LH2-only membranes.

Table 3.3. *Comparison of LH1 protrusions height in the 2D-crystals and native membranes*

	Height of strongly protruding rings, nm	**Height of weakly protruding rings, nm**	**Height difference between strongly and weakly protruding rings, nm**
LH1 2D-crystals	1.4	0.8	0.6
LH1 native membranes	1.7	0.7	1

Structural basis for variations in size and shape of the LH1 complex, and comparison with the LH2 complex

We have examined three different crystal forms, and could find no evident variations in either size or shape for the LH2 complex. Clearly, there must be substantial differences between the protein architectures of LH1 and LH2, which are not apparent from a superficial examination of the primary sequences. We suggest that the one crucial difference between these complexes is the arrangement of H-bonds between the C-terminal regions of LH complexes and the C_2 acetyl carbonyls of the bound Bchls. As already noted (Pugh et al 1998), a combination of resonance Raman and mutagenesis approaches has shown that a network of H-bonds stabilizes each $\alpha_1\beta_1Bchl_2$ unit within LH1, so that the four possible H-bonds to each pair of Bchls are donated by the α- and β-polypeptides that bind the same Bchls (Olsen et al 1994; Olsen et al 1997; Sturgis et al 1997). Thus, these four H-bonds are "internal" to the $\alpha_1\beta_1Bchl_2$ unit, and provide a significant driving force to stabilize this complex (Davis et al 1997). In contrast, the H-bonding arrangements for the nonameric LH2 complexes from *Rhodobacter sphaeroides* and *Rhodopseudomonas acidophila* each involve one H-bond internal to an αβ pair of polypeptides, but with the other bond directed towards the neighbouring αβ pair. This difference is depicted in Fig. 3.9, which shows a portion of the ring of the *Rhodopseudomonas acidophila* complex (Papiz et al 2003) in Fig. 3.9A and schematically in Fig. 3.9C, and of the LH1 complex in Fig. 3.9B, modeled from EM, NMR, mutagenesis and AFM data (Fotiadis et al

2004) and schematically in Fig. 3.9D. The effect of these differing arrangements is that each $\alpha_1\beta_1$Bchl$_2$ unit within LH1 has a certain degree of autonomy within the complex. This is depicted schematically by showing separate $\alpha_1\beta_1$BChl$_2$ units in Fig. 3.9D, and a continuity of interlinked H-bonds in Fig. 3.9C. This difference is borne out by the facts that LH1 can be readily dissembled into individual $\alpha_1\beta_1$BChl$_2$ units, often termed B820 (Miller et al 1987), and that it can also be fractionated into a series of LH1 oligomers that vary in size from $(\alpha\beta)_{2\text{-}3}$ to $(\alpha\beta)_{10\text{-}11}$ (Westerhuis et al 1999; Westerhuis et al 2002). Neither of these types of subdivision of a nonameric LH2 complex has been reported, although the octameric LH2 of *Rhodospirillum molischianum* has been successfully dissociated into B820 subunits (Todd et al 1998). Fig. 3.9 provides a rationale for the *Rhodospirillum molischianum* LH2 dissociation, since its H-bonding arrangement resembles that of LH1 (Germeroth et al 1993). In the light of these differences between LH1 and nonameric LH2 complexes it is easier to understand why LH2 displays no variation in either its size or shape detectable by AFM, and why LH1 behaves as a loosely connected series of $\alpha_1\beta_1$Bchl$_2$ units, capable of forming the circular, elliptical, polygonal and open rings represented in Fig. 3.9.

Biological significance of the flexibility and deformability of LH1

The LH1-RC complex is already known to adopt both circular and elliptical conformations, as seen in the EM projection maps (Jamieson et al 2002) and more recently in 3D-crystals (Roszak et al 2003). This implied flexibility of the LH1 complex was suggested to be important for its function, by allowing the export of quinol formed as a result of RC photochemistry (Jamieson et al 2002). AFM topographs of the membrane-bound *Blastochloris viridis* LH1-RC complex demonstrated a similar ellipticity, which altered to a circular shape upon removal of the RC (Scheuring et al 2003b). The shapes of the LH1-only complex in Fig. 3.6 reveal a much more flexible structure than was previously suspected. It was not clear why an ability to slightly deform LH1 of *Blastochloris viridis* or *Rhodospirillum rubrum* into circular or elliptical shapes would, by itself, allow the passage of quinol from the enclosed RC to the external quinone pool. Our demonstration that the linkage between adjacent $\alpha_1\beta_1$BChl$_2$ units is flexible and also even breakable at room temperature in a detergent-free membrane bilayer provides a rationale for the transient opening and closing of LH1 units adjoining the Q_B site of the RC. The existence of open rings and arcs in our samples serves to illustrate this point, since it shows that LH1 can indeed form stable, but interrupted oligomers, as was proposed by Westerhuis et al. (Westerhuis et al 2002) on the basis of LDS solubilized LH1-only complexes. In addition, this temporary uncoupling is compatible with the presence of the PufX polypeptide, which interrupts the continuity of the ring of Bchls but effectively becomes a part of the LH1 ring system by associating closely with the LH1 α-polypeptide (Recchia et al 1998), perhaps providing a weak link.

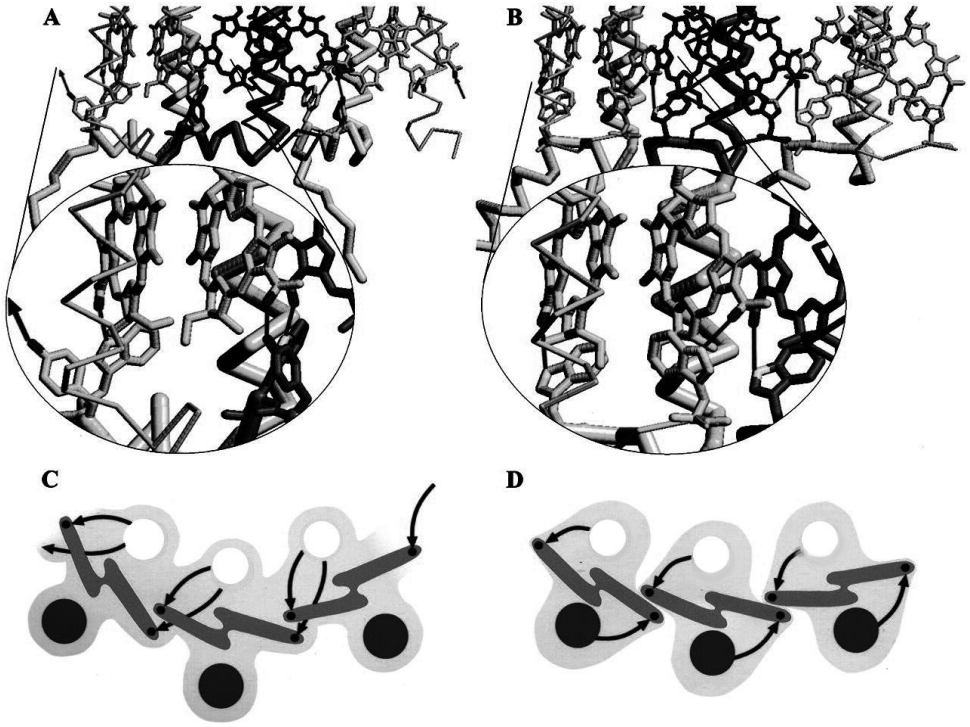

Fig. 3.9. *Diagram illustrating the differences in H-bonding between nonameric LH2 complexes (**A** and **C**) and 16-membered LH1 complexes (**B** and **D**). This diagram shows the arrangement of H-bonds between the C-terminal regions of LH complexes and the C2 acetyl carbonyls of the bound Bchls.* ***A:*** *The H-bonding arrangement for the nonameric LH2 complexes from Rhodobacter sphaeroides and Rhodopseudomonas acidophila involves one H-bond internal to each αβ pair of polypeptides, but with the other bond directed towards the neighbouring αβ pair (**C**). Each pair of LH polypeptides and their BChls is colour coded in a different shade of grey;* ***B:*** *The H-bonding arrangement for the LH1 complex, with colour coding as in (**A**). The four possible H-bonds to each pair of BChls are donated by the α- and β-polypeptides that bind the same BChls. Thus, these four H-bonds are "internal" to the $\alpha_1\beta_1BChl_2$ unit (**D**);* ***C:*** *A schematic representation of (**A**), with the α-polypeptide in white, the β-polypeptide in black, Bchls in dark grey, and the H-bonds denoted by arrows showing the linkage between adjacent protomers;* ***D:*** *A schematic representation of (B), colours as in (**C**), showing the H-bonds as being confined to individual protomers, one from the α-polypeptide and the other from the β-polypeptide. The effect of these differing arrangements is that each $\alpha_1\beta_1BChl_2$ unit within LH1 has a certain degree of autonomy within the complex, when compared to LH2.*

AFM topographs of LH1+PufX 2D-crystals of *Rhodobacter sphaeroides* also showed open rings, though at the current resolution we cannot determine whether these occur adjacent to PufX (Fig. 3.10).

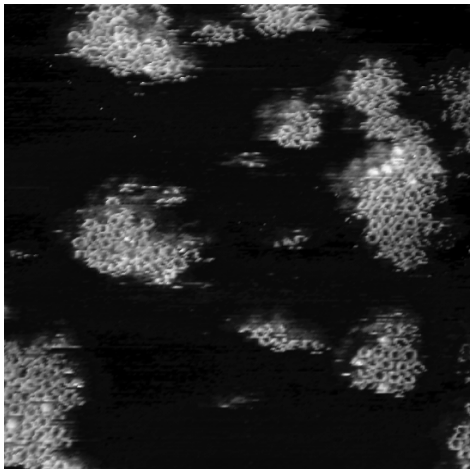

***Fig. 3.10**. AFM image of LH1+PufX 2D-crystals, frame size 500x500 nm^2, full grey scale 5 nm.*

Origin and significance of variable ring sizes for LH1

None of the above would necessarily lead to an observation of different ring sizes, yet the data clearly show the existence of open rings as well as a variety of ring diameters. It might be argued that the different ring sizes, and indeed the open rings, are merely artifacts of the purification procedure. We do not believe that the complexes undergo radical dissociation/re-association during our preparation, as there is no sign of a peak at either 777 or 820 nm in the post-purification material that was used for the 2D crystallization trials (Fig. 3.11).

The conditions that are known to dissociate LH1 of *Rhodobacter sphaeroides* into B820 subunits necessitate the use of either a carotenoidless mutant LH1 or the extraction of lyophilized chromatophores with petroleum ether in order to obtain efficient dissociation of the complex (Chang et al 1990). We suggest that the presence of native carotenoids in our complexes protects them against the concentration of β-OG used. Indeed Scheuring et al. (2004a) used 3% β-OG to isolate and purify dimeric core complexes of *Rhodobacter sphaeroides*, indicating that delicate higher orders of organization are preserved, even at this high concentration of β-OG.

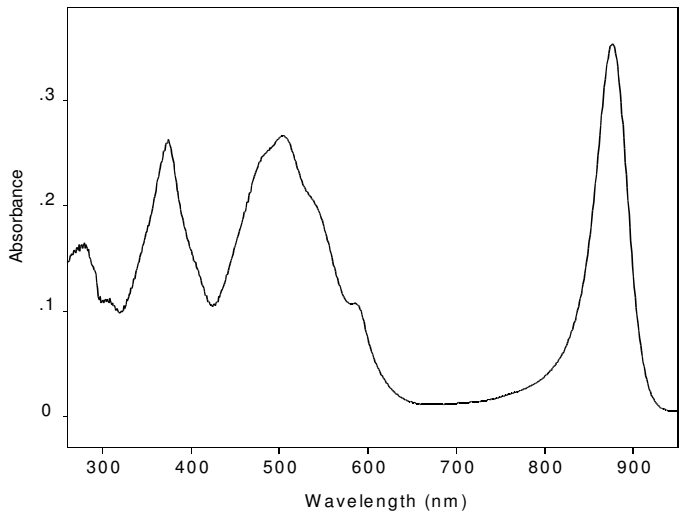

Fig. 3.11. *RT absorbance spectrum of post-purification LH1 complexes.*

The dimensions of the large LH1-only ring measured by AFM would be compatible with enclosing an RC complex and there may be no imperative for the assembly of $\alpha_{16}\beta_{16}BChl_{32}$ units. A recent AFM analysis of reconstituted 2D-crystals of *Rhodobacter sphaeroides* LH1-RC-PufX complexes demonstrated the existence of a small proportion of larger diameter (13.4 nm) rings (Siebert et al 2004). The AFM study of Scheuring et al. on native membranes of *Blastochloris viridis* reported 16-fold rings (Scheuring et al 2003b), although the data processing could have masked the presence of other ring sizes. Currently it is not known how the assembly system senses when the correctly-sized ring is nearing completion, and how it halts this process. It is known that LH1 can assemble *in vitro* from its constituent $\alpha_1\beta_1BChl_2$ units (Miller et al 1987), but currently, the mode of *in vivo* assembly of LH1 is not known, although it has been shown that there is an assembly factor for the LH1-RC complex (Young et al 1998; Young and Beatty 1998). We have observed variability in LH1 aggregation in membranes where both PufX and the RC are absent, thus one or both of these components might be an important factor in determining the LH1 ring size of *Rhodobacter sphaeroides*. Perhaps the absence of the RC complex deprives the assembly system of a guide or template on which to assemble LH1, and in its absence some variation in oligomerization takes place. Our AFM images of the native membranes of LH1-only complex showed diversity in LH1 ring size as it was observed in the LH1-only 2D-crystals, which supports our assumption that in the native system RC complex or PufX protein (or both of them) defines the template for the proper LH1 ring size.

3.5 Conclusions

To conclude and summarize, we have used AFM to demonstrate large variations from molecule to molecule in the LH1 complex, in terms of both shape and size. Freed from enclosing the RC, the inherent flexibility and lack of structural coherence of this complex become apparent. In particular, the existence of open rings and arcs provides a direct visualization of consequences of the relatively weak associations that govern the association of the $\alpha_1\beta_1Bchl_2$ protomers comprising the LH1 complex. These associations, which are known to be significantly different for the readily dissociated LH1 complex and the stable nonameric LH2 complex, are suggested to arise from the H-bonding patterns that stabilize binding of the Bchls to the LH polypeptides. This relative instability, exaggerated here by the genetic removal of the RC, forms the basis for a dynamic separation of individual $\alpha_1\beta_1Bchl_2$ protomers, thus allowing passage of quinol from the RC to the quinone pool prior to reduction of the cytochrome bc_1 complex.

Harrisberger's Fourth Law of the Lab:
Experience is directly proportional
to the amount of equipment ruined.
Unknown

Chapter 4

The native architecture of a photosynthetic membrane

In photosynthesis, the harvesting of solar energy and its subsequent conversion into a stable charge separation are dependent upon an interconnected macromolecular network of membrane-associated chlorophyll-protein complexes. Although the detailed structure of each complex has been determined (Allen et al 1987; Deisenhofer et al 1985; McDermott et al 1995; Roszak et al 2003), the size and organisation of this network is unknown. We used atomic force microscopy to directly visualise a native bacterial photosynthetic membrane. This first view of any multi-component membrane shows the relative positions and associations of the photosynthetic complexes and reveals crucial new features of the organisation of the network – we found that the membrane is divided into specialised domains each with a different network organisation and wherein one type of complex predominates. Two types of organisation were found for the peripheral LH2 complex. In the first, groups of 10-20 molecules of LH2 form light capture domains that interconnect linear arrays of dimers of core reaction centre-light harvesting 1 (LH1-RC-PufX) complexes; in the second, they were found outside these arrays in larger clusters. The LH1 complex is ideally positioned to function as an energy collection hub, temporarily storing it prior to transfer to the RC where photochemistry occurs: the elegant economy of the photosynthetic membrane is demonstrated by the close packing of these linear arrays, which are often only separated by narrow 'energy conduits' of LH2 just 2-3 complexes wide.

This chapter is based on Svetlana Bahatyrova, Raoul N. Frese, C. Alistair Siebert, John D. Olsen, Kees O. van der Werf, Rienk van Grondelle, Robert A. Niederman, Per A. Bullough, Cees Otto and C. Neil Hunter. 2004. The native architecture of a photosynthetic membrane. Nature. 430:1058-1062.

4.1 Introduction

Photosynthetic purple bacteria can contain two types of complex, LH1-RC and LH2, with both LH complexes comprising roughly circularly arranged α-helices with bound carotenoid and bacteriochlorophyll pigments (Jamieson et al 2002; McDermott et al 1995; Roszak et al 2003; Walz et al 1998). In order to investigate the functionally crucial organisation of these complexes, native photosynthetic membranes from the wild-type purple bacterium *Rhodobacter sphaeroides* were imaged by AFM, a technique that allows the topography of biological samples to be acquired in buffer solution at room temperature and under normal pressure.

4.2 Materials and methods

Biological samples were prepared in the laboratory of Prof. Dr. C. N. Hunter (University of Sheffield, UK).

Bacterial growth

Cells of *Rhodobacter sphaeroides* NCIB 8253 were grown photosynthetically at moderate light intensity (500 Wm^{-2} for 18-20 hours) and then switched to high light intensity (825 Wm^{-2}) for 4 hours. Intracytoplasmic membrane vesicles with an LH1/LH2 molar ratio of 0.78 were isolated by rate-zonal sucrose density gradient centrifugation (Niederman et al 1979). Membranes were pelleted by ultracentrifugation at 100,000 x g for 4 hours and resuspended with gentle homogenisation in 50 mM HEPES buffer at pH8 containing 0.03% β-dodecyl maltoside (buffer A) to 16 absorbance units/cm/ml at 875nm. 250 µl of this sample was loaded onto a 20/25/30/35/40/50% w/w sucrose density step gradient in buffer A and centrifuged for 20 hours at 200,000 x g using a Beckman SW41 rotor. The fraction containing large membrane fragments was harvested from the 40/50% interface using a blunted hypodermic syringe and frozen at -20ºC using 45% sucrose as cryoprotectant until required for AFM.

Atomic Force Microscopy

For AFM measurements the sample solution was adsorbed to the surface of freshly cleaved mica. Adsorption time, adsorption and recording buffers were the same as used for LH2-only membranes (described in Chapter 2) and for LH1-only 2D-crystals and membranes (described in Chapter 3).

AFM topographs were obtained using tapping mode in liquid. The images with the highest resolution could be achieved when the free tapping amplitude was 1-2 nm and the amplitude setpoint was adjusted to minimal forces, resulting in the

damping of the free amplitude by only 5-10%. Images contain 256 x 256 pixels and were recorded at a typical line frequency of 5-7 Hz.

4.3 Results and discussion

Fig. 4.1A shows a cluster of several membrane patches, each of a size approximating to the surface area of an intracytoplasmic membrane vesicle (chromatophore). The bright areas represent photosynthetic complexes; even at this low magnification this remarkable view of native photosynthetic membranes shows that they are composed at least in part of linear arrays of dimeric complexes.

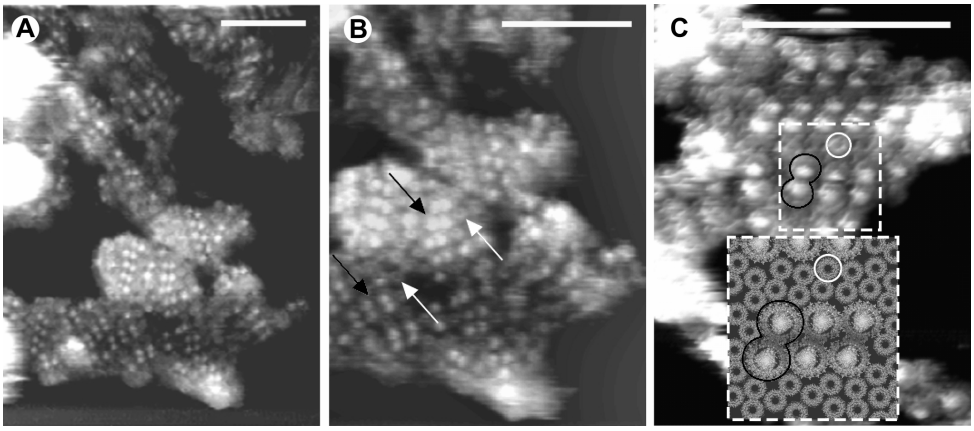

Fig. 4.1. *AFM of native photosynthetic membranes.* ***A:*** *Large-scale view of several membrane fragments.* ***B:*** *Higher magnification view showing a region of dimeric LH1-RC-PufX core complex arrays (black arrows) and associated LH2 complexes (white arrows).* ***C:*** *3D-view of core complex arrays surrounded by LH2 complexes. The inset panel is a representation of the region denoted by the dashed box, using model structures derived from atomic resolution data (Allen et al 1987; McDermott et al 1995; Roszak et al 2003). A typical LH1-RC-PufX dimer is delineated in both images by the black outline and a representative LH2 complex by white circle. Scale bar = 100 nm in all panels. For all images the z-range is 6 nm (from darkest to lightest).*

This arrangement was mirrored in all the membrane patches we examined and a gallery of additional images is displayed in Fig. 4.2.

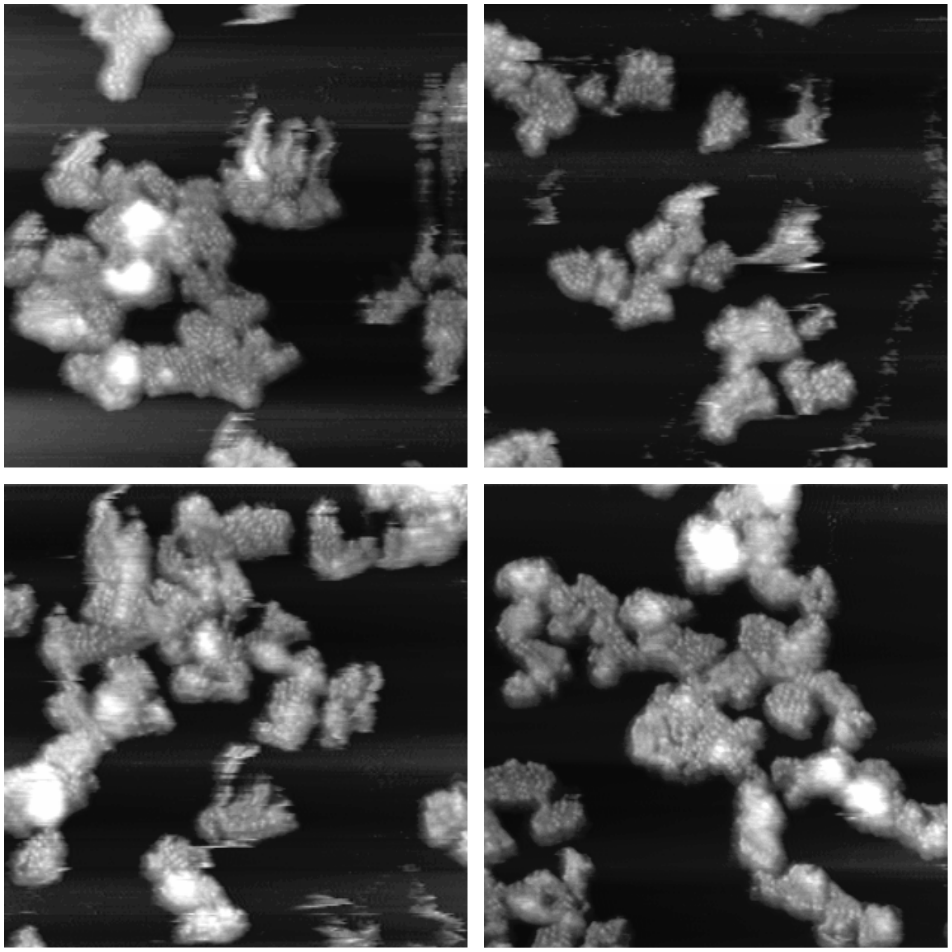

Fig. 4.2. *The four panels depict typical membrane patches on mica, with a scan area 1x1 μm^2. On this scale the arrays of core complexes are readily visible and show up as double lines of brightness, which are the protruding H-subunits of the RC's in the arrays. At this magnification it is not possible to resolve the smaller LH2 rings that occur between the arrays of core complexes. For all images the z-range is 15 nm.*

Fig. 4.1B clearly shows how the light harvesting and photochemical functions of a membrane are apportioned, and reveals the arrangement of photosynthetic complexes. Two types can be seen; large circular complexes with a bright and therefore protruding central protein, and smaller rings with no central density and

a diameter of ~ 7 nm. The antenna complexes were identified by comparison with AFM data compiled on purified LH2, LH1 and LH1-RC complexes (Bahatyrova et al 2004a; Fotiadis et al 2004; Siebert et al 2004a) and the 3D-structures for the LH2, and LH1-RC-PufX complexes (Allen et al 1987; Deisenhofer et al 1985; McDermott et al 1995; Roszak et al 2003). The larger features are LH1-RC-PufX complexes, each approximately 12 nm in diameter and comprising an LH1 ring surrounding a central bright region representing a RC complex. These LH1-RC-PufX complexes are usually dimeric, and the dimers are arranged in rows such as those indicated (red arrows) in Fig. 4.1B. Typically, rows of up to 6 dimers of LH1-RC-PufX complexes are found, forming a domain of 240-360 Bchls. This is in close agreement with singlet-singlet annihilation experiments on a mutant containing only the LH1-RC-PufX complex that established domain sizes of ≥330 LH1 Bchls at room temperature (Vos et al 1988).

Rather than being interspersed randomly throughout the membrane, many of the LH2 complexes are clustered in regions between the rows of LH1-RC-PufX dimers, as outlined in Fig. 4.1C. Typically these regions consist of 10-20 LH2 complexes representing 270-540 Bchls; the same order of magnitude of connected Bchls (≥365) was deduced from singlet-singlet annihilation measurements of mutant LH2-only *Rhodobacter sphaeroides* membranes (Vos et al 1988). We suggest that the LH2 complexes situated between rows of LH1-RC-PufX dimers form a relatively invariant complement of light harvesting antenna, and that the arrangement of complexes depicted in Fig. 4.1C represents the basic requirement for the efficient harvesting, transmission and trapping of light energy in this bacterium. However, by itself, this would not account for all the LH2 present; a comparison of the starting absorbance spectrum with one roughly estimated from the number of LH2 and LH1 rings in Figs. 4.1 – 4.3 indicates that up to 50% of the expected LH2 has not been accounted for in such images.

The circled region in Fig. 4.3A shows that there are other regions consisting largely of LH2 that are not 'sandwiched' between rows of LH1-RC-PufX complexes. Individual LH2 rings can be discerned within the higher magnification image in Fig. 4.3B, such as the one indicated with an arrow. These LH2-enriched domains could represent the variable antenna, known for many years to form in response to lowered light intensity (Aagaard et al 1972). In addition to making contact with each other some of the LH2 rings are in close physical association with the LH1-RC-PufX complexes, see upper black arrow in Fig. 4.1B, thus facilitating transfer of excitation energy from LH2 to LH1 and then to the RC. Even at this intermediate level of detail, the physical and organisational basis for harvesting, transferring and utilizing light energy is clearly evident.

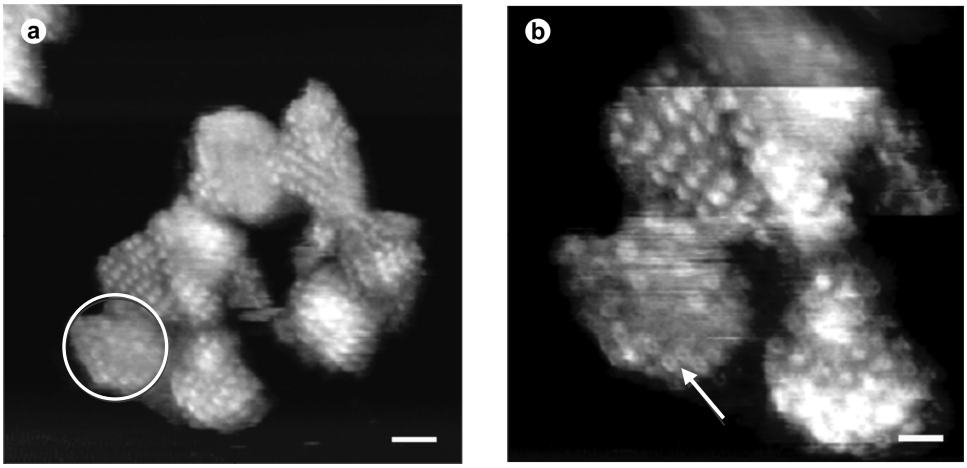

Fig. 4.3. *Membrane patches showing two types of arrangement of photosynthetic complexes.* ***A:*** *The circled region is mainly composed of LH2 complexes.* ***B:*** *Higher magnification image of the same membrane patch in which an arrow points to an LH2 ring within the LH2-only domain. This higher resolution scan clearly shows that there are no core complexes in these regions. The scale bar in* ***A*** *represents 50 nm and in* ***B*** *25 nm.*

A model of the bacterial photosynthetic membrane has been formulated in Fig. 4.1C (inset) by arranging the structural information available for the individual photosynthetic components (Allen et al 1987; McDermott et al 1995; Roszak et al 2003) in a manner consistent with the AFM data. These direct images of an intact photosynthetic membrane resemble one of the models proposed in 1977 by Monger and Parson (Monger and Parson, 1977) on the basis of fluorescence quenching experiments conducted on *Rhodobacter sphaeroides* membranes. From a quantitative point of view the model in Fig. 4.1C explains why fluorescence quenching studies of *Rhodobacter sphaeroides* membranes concluded that there were up to 3000 light harvesting Bchls connected for energy transfer (Hunter et al 1985). This work also estimated that a single photosynthetic membrane vesicle would contain 30 reaction centres, in rough agreement with the number observed in the membrane patches in Figs. 4.1 – 4.3. The AFM data suggest that 100 or more LH2 molecules would form the dominant antenna within such a vesicle, partitioned between the linear rows of LH1-RC-PufX dimers (Fig. 4.1C) and the LH2-enriched areas in Fig. 4.3B. There is extensive physical continuity between individual LH2 complexes (27 Bchls for each ring) and between LH2 and LH1-RC-PufX dimers (60 LH1 Bchls per dimer). Thus, the LH2 rings appear to cooperate to form an extended array for collecting photons, and, once transferred 'downhill' to an LH1-RC-PufX dimer, the excited state can hop the relatively large distance of ~ 3.5 nm from LH1 Bchls to the special pair of Bchls within the RC (Visscher et al 1989), thereby eliciting conversion to photochemical energy

(Beekman et al 1994). It is possible that the linear arrays of LH1-RC-PufX complexes cooperate in the overall process of energy trapping, since if any particular RC is already undertaking photochemical charge separation and is thus unavailable for receiving excitation energy from its LH1 ring (in a 'closed' state), the LH1 excitation can migrate along a succession of such dimers until an 'open' RC is reached. This arrangement of LH1-RC-PufX dimers might also provide a structure with the largest number of effective connections between LH1 rings. In addition, it becomes clear why mutants lacking LH2 form tubular membranes containing linear rows of dimers aligned in parallel (Frese et al 2000; Siebert et al 2004); this is a natural consequence of removing the LH2 complexes that normally separate rows of LH1-RC-PufX dimers.

The AFM was used to examine a small area of membrane containing only a few photosynthetic complexes; for clarity the data are represented in 3D (Fig. 4.4).

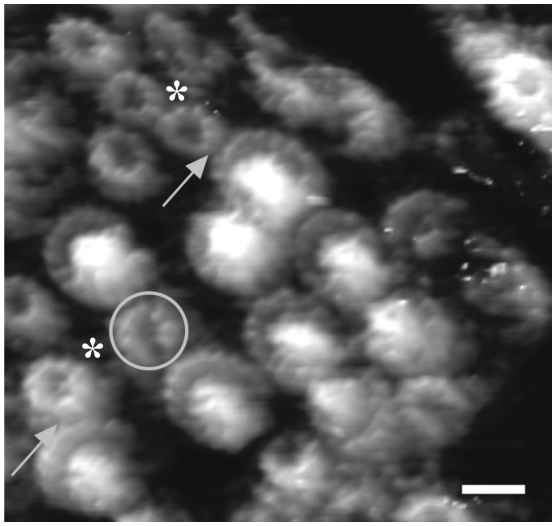

Fig. 4.4. *3D representation of a small region of membrane showing LH1-RC-PufX core complex dimers and monomers with associated LH2 complexes. Contact points for energy transfer between LH2 and LH1-RC-PufX complexes are indicated by arrows. LH2 rings marked by asterisks are composed of nine units. The LH2 in the circle is sandwiched between two LH1-RC-PufX complexes. The average tilt of 7 LH1 complexes is 4.8°; the average height of LH1 above the lipid membrane = 1.4 ± 0.3 nm. The maximum subunit height = 1.8 ± 0.3 nm (n = 7) and the minimum subunit height = 1.1 ± 0.1 nm (n = 7). The average tilt of 3 LH2 complexes is 3.8°. For LH2 the average height of LH2 rings above the lipid membrane = 1.5 ± 0.1 nm (n = 11). For 3 tilted rings the maximum subunit height = 1.7 ± 0.1 nm and the minimum subunit height = 1.2 ± 0.1 nm. The average height of the RC-H subunit above the lipid membrane is 3.7 ± 0.3 nm (n = 9). The scale bar is 10 nm.*

The rows of dimeric LH1-RC-PufX complexes, which are the most prominent features in low magnification topographs of photosynthetic membranes (Fig. 4.1A and B), can now be seen in greater detail. Each dimer in Fig. 4.4 is ~ 23 nm across, corresponding to the LH1-RC-PufX dimer complexes ~ 20 nm in width previously revealed by negative stain EM (Siebert et al 2004). The central protruding feature is ~ 4 nm above the lipid bilayer, which corresponds to the RC-H subunit (Fotiadis et al 2004). Thus it is the cytoplasmic face of the membrane that lies uppermost, and the periplasmic face that has adhered to the mica substrate. Inspection of the LH1-RC-PufX dimers shows that in some cases the bright central density is missing. This has been seen before in AFM images of bacterial RCs, and it arises when the AFM tip dislodges an extrinsic subunit, revealing the underlying L- and M- subunits (Fotiadis et al 2004; Scheuring et al 2003b). As seen already in Fig. 4.1 some of the LH2 complexes make contact with LH1-RC-PufX complexes, at points indicated by the arrows in Fig. 4.4, fulfilling their role not only as gatherers of relatively high energy excitations, but also as energy conduits to the lower energy LH1 complex surrounding the RC. Although LH2 complexes associate mainly with other LH2 complexes some can be found singly, for example sandwiched between two LH1-RC-PufX complexes (Fig. 4.4, circle). At the contact points between LH2 and LH1-RC-PufX complexes, the distance between the B850 Bchls of LH2 and the B875 Bchls of LH1 was calculated to be between 2.7 and 3.2 nm on the basis of the energy transfer rate, which is 3 ps (Hess et al 1995). Remarkably, the subunit structure of both LH2 and LH1 rings emerges, even in the native membrane environment. The LH2 rings such as those marked by asterisks in Fig. 4.4 appear to be composed of nine units *in vivo*, consistent with previous structural data (McDermott et al 1995; Walz et al 1998).

We also investigated the disposition of individual photosynthetic complexes with respect to the native membrane bilayer, information that has escaped the attention of crystallographic methods. Curiously, some, but not all, LH2 complexes appear to be slightly tilted in the native membrane, estimated to be between 3 and 4° from the vertical. This tilting is a surprise, notwithstanding the fact that LH2 is tilted in 2D-crystals reconstituted from detergent purified LH2 complexes (Scheuring et al 2003a; Walz et al 1998). This phenomenon is not confined to the LH2 complex; close inspection of 7 LH1 rings within a series of native LH1-RC-PufX dimers reveals an average 4.8° tilt of each LH1 ring towards the monomer-monomer interface. We cannot determine whether the enclosed RC is also tilted although we note that purified, detergent-solubilized RCs crystallised in a cubic lipidic phase lie 11° from the vertical (Katona et al 2003). This small degree of tilt in each LH1-RC-PufX complex obscures the central part of each dimer from analysis, preventing the identification of the PufX polypeptide, which is thought to be somewhere in this region (Siebert et al 2004a). It is not clear if the tilting of LH2 and LH1-RC-PufX complexes has any functional significance, but the

mutual inward tilt of the LH1-RC-PufX complexes suggests that it is a consequence of the dimerization process. The tilting of these photosynthetic complexes might be accompanied by a slight degree of buckling of the lipid bilayer in the immediate vicinity of the complex, and could arise as a consequence of applying the sample to the mica surface, which imposes a flattened profile onto a piece of membrane that was originally curved. This could be exacerbated in LH2-rich regions, which are expected to be particularly curved (Sturgis and Niederman, 1996). An interaction with the mica surface could also account for the very low lateral mobility of the photosynthetic complexes in the membrane patches that we observed. This point is illustrated by Fig. 4.5, which displays 4 of a sequence of 18 consecutive images obtained from the same membrane patch. The reproducibility of the data is remarkable, even on the scale of a single LH2 complex.

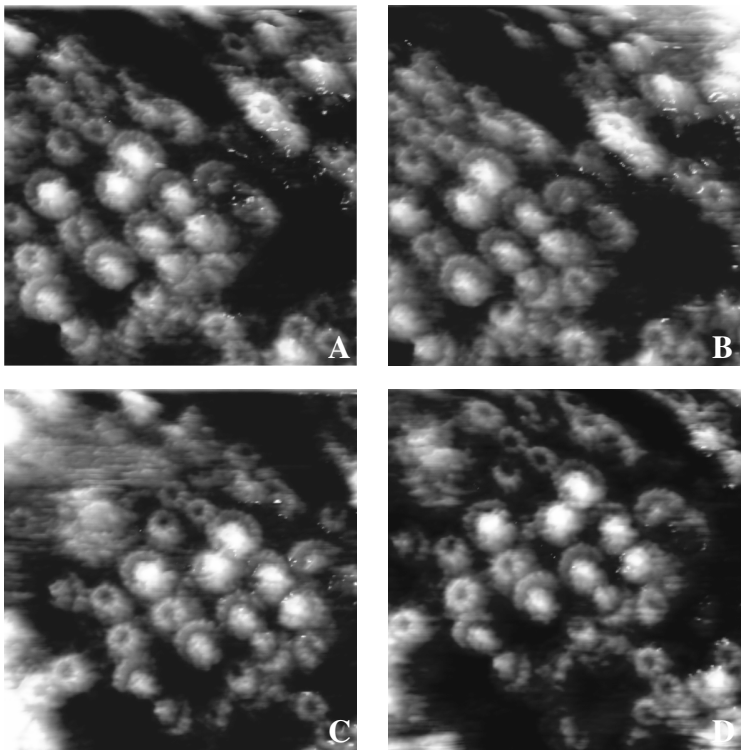

Fig. 4.5. *The selected area was repeatedly scanned several times. The four sequential scans shown (from A to D) are shown using a three-dimensional representation. There is no evidence of the LH complexes moving between scans though the images do show the slight drift of the piezo-head between images. All frames have size of 100x100 nm^2.*

A similar lack of lateral mobility was noted by Müller et al. (2003), who studied the bacterial ATP-synthase in a reconstituted lipid bilayer and found remarkably low diffusion in comparison with eukaryotic membranes. They also noted that those molecules that formed close associations with others did not tend to move and some of the isolated mobile molecules ceased moving when they associated with larger groups. We suggest that the close packing of many of the LH complexes probably prevents lateral diffusion of individual components.

4.4 Conclusions

To conclude, this study has directly visualised the organisation of bacterial photosynthetic membranes. Further questions can now be addressed; for example, how does the increased level of LH2 in low light grown cells affect this architecture? Where is the other component of the cyclic electron transfer chain, the cytochrome bc_1 complex, located in the cell? Where is the ATP synthase? How is this simple yet effective photosynthetic membrane assembled? Further work will be necessary to answer these questions. In the case of the cytochrome bc_1 complex only low amounts were detected by western blot analysis of the membrane patches (results not shown), and there could be a potential problem detecting cytochrome bc_1 complexes by AFM, since the very recent structure of this complex from the photosynthetic bacterium *Rhodobacter capsulatus* reveals relatively little surface topology on the cytoplasmic side of the membrane (Berry et al 2004). In the case of the ATP synthase it has been reported that intracytoplasmic membrane vesicles of *Rhodobacter capsulatus* contain on average only one F_OF_1-ATP synthase. Indeed, 37% of the chromatophore vesicles had no ATP synthase at all (Feniouk et al 2002), which would make them difficult to locate and image by AFM.

In view of the highly organised arrangements of photosynthetic complexes seen in recent electron microscopic investigations of bacterial and plant membranes (Boekema et al 2000; Siebert et al 2004) which demonstrate crystallographic order, our results present a slightly more chaotic landscape. A high degree of order is clearly not essential for transmitting excitation energy; the bacterial photosynthetic membrane fulfils the basic requirements of being physically extensive, in order to maximize the likelihood of harvesting photons, while fostering multiple contacts between its LH components, so that energy can migrate between complexes. In the context of its energy transfer function this is a very robust architecture, since associations between LH rings place few demands on the contact sites, as long as the distances between rings are minimised. Thus, the two-dimensional organisation we have visualised here by AFM will always present multiple possibilities and pathways for fast and efficient transfer and trapping of energy.

You can observe a lot by watching.
Yogi Berra

Chapter 5

The role of PufX in the supramolecular organization of a photosynthetic membrane

In this chapter we discuss results obtained by high-resolution AFM imaging on membranes where one or more components of the WT PSU have been genetically removed. In this way we are able to determine the contribution of the missing components to the overall architecture of the PSU. The peripheral LH2 complex forms the bulk antenna and its removal has previously been shown to alter the membrane morphology from spherical to tubular (Hunter et al 1988; Siebert et al 2004). PufX has been demonstrated to organize the LH1-RC core complexes of *Rhodobacter sphaeroides* into dimers which associate into larger well-ordered arrays in photosynthetically grown cells regardless of whether LH2 is present or not (Jungas et al 1999; Bahatyrova et al 2004b). When PufX is absent the cells cannot be grown photosynthetically, so to compare the effect of eliminating this protein all the cells examined in this chapter were grown semiaerobically. We have now shown that LH2 also has an ordering effect on the core complexes when the small integral membrane protein PufX is absent from the LH1-RC core in these semiaerobically grown cells. The overall principles of supramolecular organization of the protein complexes responsible for light harvesting, energy transfer and electron transfer in the semiaerobically grown photosynthetic membranes are compared with the photosynthetically grown native membranes.

5.1 Introduction

The effect of the growth conditions on the supramolecular organization of the ICM

Many species of purple photosynthetic bacteria repress synthesis of their photosystem if the molecular oxygen level is high, i.e. near ambient. Oxygen limitation is the major determining factor for expression of genes necessary for the initiation of intracytoplasmic membranes (ICM) development and LH and Bchl production in *Rhodobacter sphaeroides* purple bacteria. An internal network of ICM (chromatophores) can develop when grown either anaerobically in the light (photosynthetically) or aerobically in the dark under low oxygen partial pressure (semiaerobically) (Kiley and Kaplan, 1988). ICM invaginations develop in response to the insertion of LH complexes and contain all the membrane components required for the photosynthetic reactions.

Semiaerobically grown bacteria are expected to develop an ICM system almost identical to the photosynthetically grown membranes with the possible absence of cytochrome bc_1 complexes as the cell does not rely on cyclic electron transfer for its energy. Indeed, recent EM work on semiaerobically grown $LH2^-$ mutants of *Rhodobacter sphaeroides* that express only $LH1^+RC^+PufX^+$ and $LH1^+RC^+PufX^-$ core complexes demonstrated that cytochrome bc_1 complex was absent from the purified tubular membranes (Siebert et al 2004). The same authors reported that when the $LH1^+RC^+PufX^+$ $LH2^-$ strain was grown photosynthetically the tubular membranes, as analyzed by silver stain SDS-PAGE, were shown to have an essentially identical protein composition to tubular membranes from semiaerobically grown cells as no cytochrome bc_1 complex was detected .

However, it was suggested that the cytochrome bc_1 complexes are likely to be present elsewhere in other membrane fractions (Siebert et al 2004). Interestingly, recent high-resolution AFM topographs of photosynthetically grown native membranes from *Rhodobacter sphaeroides* (Bahatyrova et al 2004b, see Chapter 4) and *Rhodospirillum photometricum* (Scheuring et al 2004b, c) also failed to detect the presence of cytochrome bc_1 complexes within the dense network of LH and RC complexes. This may indicate that these complexes are not present within the chromatophores or that they occur in a highly curved piece of the membrane that is not suitable for imaging by AFM.

We expect that the growth of the bacterial cells in the dark (semiaerobical growth) is favorable for the overproduction of peripheral LH2 complexes (Sturgis and Niederman, 1996). This can result in the extra LH2-only domains away from the LH1-RC-PufX core complexes in the ICM in comparison with the cells grown in the light (photosynthetic growth).

The role of PufX in the supramolecular organization of the ICM

It has been shown that PufX-containing species of purple bacteria can only grow photosynthetically when the PufX protein is present (Farchaus et al 1992; Lilburn et al 1992; McGlynn et al 1994) and this was a consequence of its effect on quinone/quinol exchange (Barz et al 1995a, b). However, reversion mutations that either impair or abolish production of LH1 can grow photosynthetically (Lilburn and Beatty 1992, Barz and Oesterhelt 1994, Lilburn et al 1995) and truncations of the C-terminus of the LH1 α-polypeptide that destabilized the LH1 complex (McGlynn et al 1996) were able to grow photosynthetically. Lilburn et al. (1995) suggested that PufX prevented the complete enclosure of the RC by LH1 so that quinones/quinols could be freely exchanged. This established the concept of the quinone portal as the primary function of PufX. Furthermore, as we already discussed in detail in Chapter 1, section 1.4.3, in these bacterial cells the supramolecular organization of photosynthetic apparatus is strongly dependent on the presence/absence of the PufX protein (Francia et al 1999; Frese et al 2000; Siebert et al 2004; Scheuring et al 2004a). While it is clear that PufX drives the dimerization of the LH1-RC-PufX core complexes in *Rhodobacter sphaeroides* the actual position of the protein within the complex is the subject of debate. Scheuring and co-workers place a PufX dimer at the junction of the two LH1-RC core complexes, while Seibert et al. place PufX molecules in the region of the LH1 ring that has low protein density in negatively stained samples. Higher resolution EM data or a 3D structure of the *Rhodobacter sphaeroides* LH1-RC-PufX core complex will be necessary to answer this question unambiguously. The LH1-RC-W core complex from *Rhodopseudomonas palustris* has been crystallized (Roszak et al 2003) and the polypeptide W is in a position analogous to that proposed for PufX by Seibert et al. (2004). However W has yet to be proven to be a PufX homologue. When relating these data to the supramolecular organization of the complete PSU it must be remembered that LH2 is missing in all the above studies on the dimerization of core complexes by PufX. This deficiency is addressed in this work where we examine the membranes isolated from four different types of *Rhodobacter sphaeroides* cells, all grown semiaerobically: *i)* $LH2^-$, $PufX^+$; *ii)* $LH2^-$, $PufX^-$; *iii)* $LH2^+$, $PufX^+$; *iv)* $LH2^+$, $PufX^-$.

The photosynthetic membranes directly isolated from these four cell types have never been analyzed before by high-resolution AFM imaging. Native membranes have been fractionated in the presence of a small amount of a DDM detergent in order to break spherical ICM open and to obtain membrane fragments with less curvature suitable for deposition onto the mica surface and subsequent high-resolution AFM imaging.

We demonstrated for the first time by direct AFM imaging of native membranes that, in both $LH2^+$ and $LH2^-$ membranes, PufX plays a significant role in organizing LH1-RC core complexes by causing their dimerization when PufX is present. In contrast, when the PufX gene was deleted, LH1-RC cores were essentially monomeric and packed in a hexagonal array similar to the LH1-RC complexes of *Rhodopseudomonas viridis* membranes (Scheuring et al 2003b). Additionally, general features of the supramolecular architecture of native membranes from semiaerobically grown cells could be resolved and compared with the native photosynthetic membrane architecture found in photosynthetically grown cells (discussed in Chapter 4).

5.2 Materials and methods

Biological samples were prepared in the laboratory of Prof. Dr. C. N. Hunter (University of Sheffield, UK).

Mutant preparation

Mutant preparation is documented in full detail in Jones et al. (1992) and McGlynn et al. (1996).

Cell growth

The DD13/G1 double deletion strain, which does not synthesize LH2, LH1, or RC complexes (Jones et al 1992), was complemented with the appropriate genes encoding RC, LH1, LH2 and/or PufX as described (McGlynn et al 1996). Transconjugants were grown under oxygen-limited conditions and selected for in antibiotic and vitamin supplemented media. The cultures were grown in 2 l conical flasks in the dark, by shaking at 80% capacity at 150 rpm at 30°C. Cultures were subjected to an extra 48 h growth period upon reaching a cell density of ~1.4 absorbance units at 680 nm. Cells were harvested by centrifugation at 4000 x g for 25 min, washed twice in 1 mM Tris, 2 mM EDTA, pH7.5, resuspended and frozen in 10 mM Tris 20 mM EDTA, pH7.5 (membrane buffer).

Membrane isolation

Cells were supplemented with 500 µl of protease inhibitor cocktail (Sigma) per 25 ml of cells along with a few crystals of DNAse I prior to passage through a French press thrice at 3000 psi. Whole cells and cell wall material were pelleted at 10.000 x g for 10 min. The supernatant was placed onto a 15/40/50% w/w sucrose/membrane buffer density gradient and spun for 4 h at 100 000 x g. The

pigmented band at the 15/40% interface was harvested using a blunted hypodermic syringe. These unsolubilized membranes were stored at -20 ºC until required.

Membrane solubilization and fractionation

Unsolubilized membranes were diluted tenfold in membrane buffer and centrifuged for 4 h at 100.000 x g. The resulting pellet was resuspended overnight in 50 mM HEPES at pH8 containing 1% α-DDM (buffer A) and gently homogenised. Membranes were fractionated on 20/25/30/35/40/45% w/w sucrose/buffer A gradient systems with load volumes of approximately 15 units of membrane per gradient (1 unit is defined as an absorbance of 1 unit at 875nm/cm/ml). Samples were centrifuged for 20 h at 200 000 x g; all the pigmented bands were harvested (Fig. 5.1) and frozen.

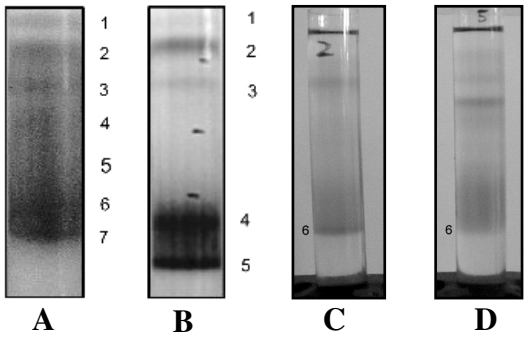

Fig. 5.1. *Solubilization of membranes with 1% DDM with subsequent fractionation by ultracentrifugation on sucrose density gradients.* ***A:*** *$LH2^+X^+$ membranes;* ***B:*** *$LH2^+X^-$ membranes;* ***C:*** *$LH2^-X^+$ membranes;* ***D:*** *$LH2^-X^-$ membranes [Image courtesy of Alistair Siebert, University of Sheffield].*

Atomic Force Microscopy

For AFM measurements fragments of native membranes from band 7 ($LH2^+X^+$, Fig. 5.1A), band 5 ($LH2^+X^-$, Fig. 5.1B) and band 6 (both $LH2^-X^+$ and $LH2^-X^-$, Fig. 5.1C, D) have been deposited onto the surface of freshly cleaved mica. Adsorption time, adsorption and recording buffers were the same as used for LH2-only membranes and LH1-only crystals and membranes (as described in Chapters 2 and 3).

AFM imaging parameters have been described in Chapter 2.

5.3 Results

5.3.1 AFM imaging of native membranes lacking peripheral LH2 complexes

General description of native membranes morphology

$LH2^-$ native membranes, both $PufX^+$ and $PufX^-$, adhered to the mica surface were measured by tapping mode AFM. A representative image of LH1-RC $PufX^+$ membranes is shown in Fig. 5.2A. Numerous membrane patches of different sizes, from very small ones, less than 50 nm, to somewhat larger patches, up to 200 nm, could be encountered. Some of the patches were clustered together. Three different height levels above the mica surface (Fig. 5.2C, position 0 for mica "zero" level) were found. Some of the membrane fragments were adsorbed to the mica quite flat over their entire surface and the height of these patches was ~ 8-10 nm corresponding to the single lipid bilayer sheet (Fig. 5.2C, position 1). At the same time, many of the patches could not be fully adhered to mica, and only the edges of these fragments could make more or less firm contact with the substrate while the central part remained rather curved. The height of these partially curved membrane patches was ~ 20-25 nm (Fig. 5.2C, position 2). Also quite a few very high patches, with the height up to 40 nm, could be found (Fig. 5.2C, position 3). These could be intact chromatophore spheres.

An image of LH1-RC $PufX^-$ membranes is displayed in Fig. 5.2B. The overall lateral and vertical dimensions of $PufX^-$ membranes were found to be similar to the dimensions of $PufX^+$ membranes.

Organization of LH1-RC core complexes in the native membranes

High magnification topographs of LH1-RC native membranes revealed the essential difference in the 2D-organization of LH1-RC core complexes in the membranes with and without the PufX protein (Fig. 5.3). It is important first to note that high-resolution AFM topographs could only be achieved when scanning flat (or just slightly curved) membrane patches, i.e. the fragments which were tightly attached to the mica. Detailed information on the protein organization in the very high and highly curved fragments (with the height up to 40 nm) in the majority of cases could not be obtained due to their weak attachment to the substrate. Thus, in order to obtain reliable high-resolution information zooming in to the small areas was mostly conducted on the flat membrane fragments. In the $PufX^+$ membranes bright topological protrusions organized as pairs (dimers), were the most apparent features (Fig. 5.3A). Protruding protein densities had the height ~ 3 nm above the lipid surface and had a size of ~ 8 nm and thus were attributed to the H-subunits of RC's which are encircled *in vivo* by the LH1 rings

(not resolved here). Typically, LH1-RC dimers were aligned linearly and formed rows consisting of up to 6 core dimers. Rarely, disordered areas in the membranes could be found where LH1-RC dimers did not form aligned rows and thus the long-range ordering of the proteins was broken.

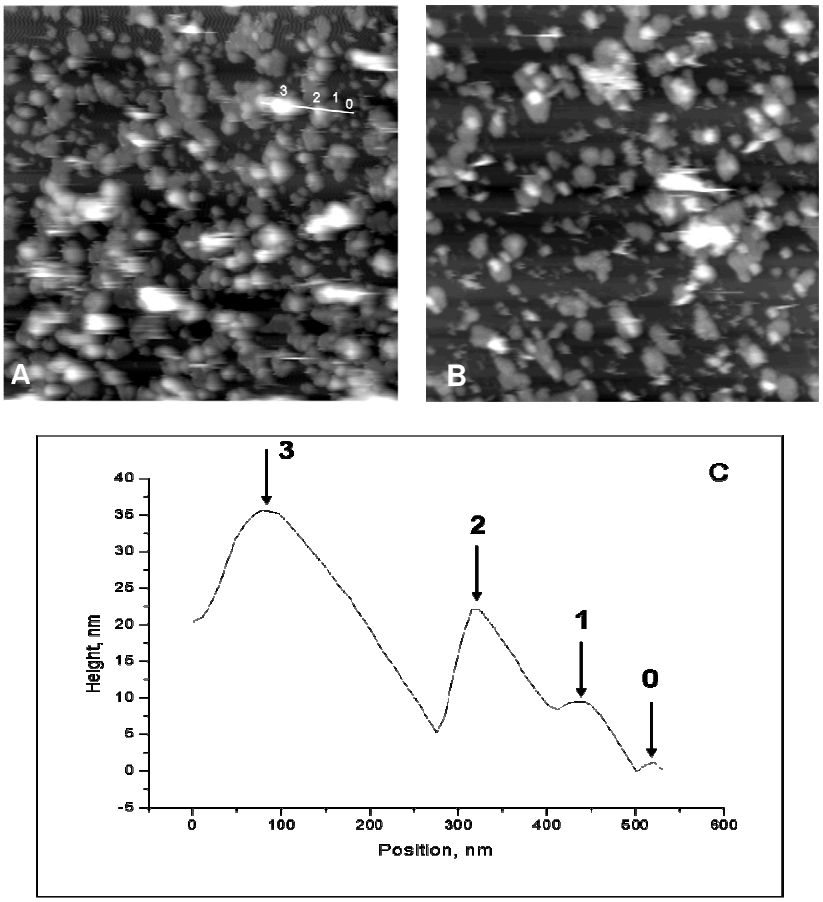

Fig. 5.2. *AFM images of LH1-RC native membranes adhered to the mica surface.* ***A****: Overview of LH1-RC PufX$^+$ membranes, frame size 2500x2500 nm^2, full grey scale 48 nm. Profile line across an area with several membranes is shown with four different height levels marked (0-3);* ***B****: Overview of LH1-RC PufX$^-$ membranes, frame size 2500x2500 nm^2, full grey scale 39 nm;* ***C****: Section analysis along the height profile in* ***A*** *revealing three different heights of the membranes above the mica level, where 0 – mica level, 1 – flat membranes, 2 – curved membranes, 3 – highly curved membranes (chromatophores).*

Organization of the LH1-RC cores in the PufX$^-$ membranes was very different when compared to the PufX$^+$ membranes, as can be seen in Fig. 5.3B. In contrast to the LH1-RC dimers and linear arrays of rows of dimers (PufX$^+$ membranes, Fig. 5.3A), in the PufX$^-$ membranes LH1-RC complexes were not dimeric but monomeric and formed a hexagonal lattice in the membrane (Fig. 5.3B).

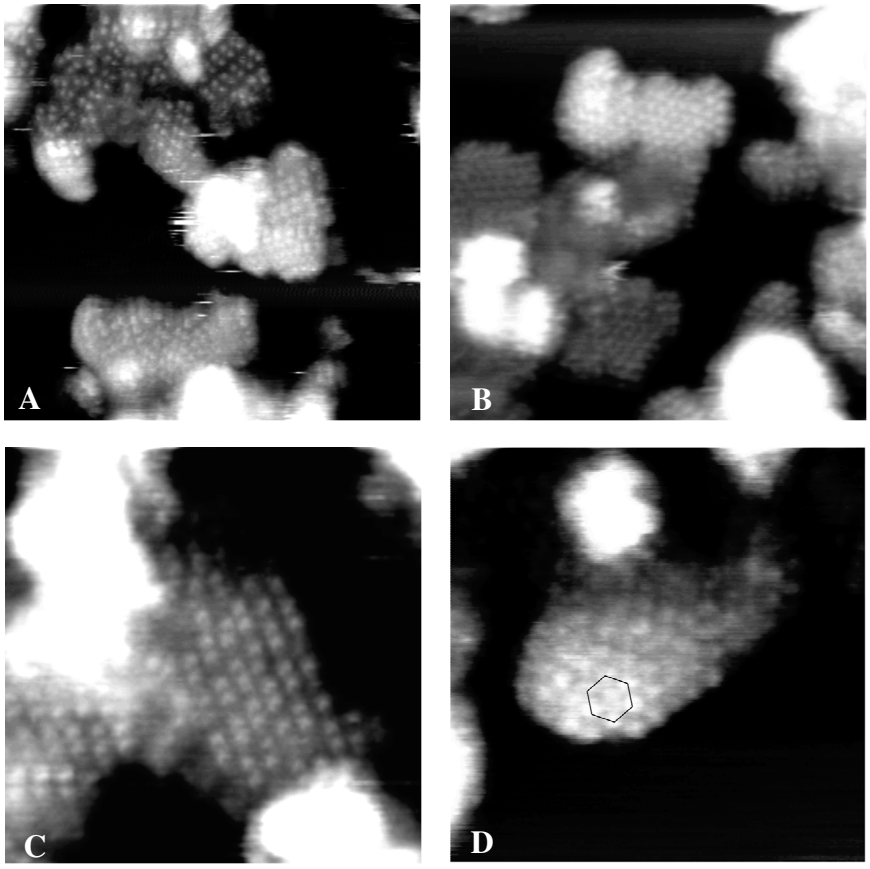

Fig. 5.3. *High magnification topographs of LH1-RC native membranes.* ***A, C****: PufX$^+$ membranes, frame sizes 500x500 and 250x250 nm^2, full grey scales 12 and 6 nm (for A and C, respectively);* ***B, D****: PufX$^-$ membranes, frame sizes 500x500 and 250x250 nm^2, full grey scales 12 and 6 nm (for B and D, respectively). In* ***D*** *the hexagonal lattice is outlined.*

Two additional images of smaller scan areas, 250x250 nm^2 (Fig. 5.3C, D), properly illustrate the intrinsic difference in the protein distribution patterns in the PufX$^+$ and PufX$^-$ membranes, where in the former linear arrays of rows of core dimers are formed and in the latter core complexes are monomeric and form a quasi-crystalline hexagonal lattice. This arrangement was reflected in all the membrane patches we examined (~ 40).

5.3.2 AFM imaging of native membranes containing peripheral (LH2) complexes

General description of native membranes morphology

Photosynthetic membranes (containing both LH1-RC core complexes and peripheral LH2 complexes either with or without PufX) were imaged using tapping mode AFM in liquid. Overview images of LH1-RC $LH2^+$ $PufX^+$ and $PufX^-$ membranes are shown in Fig. 5.4A and B, respectively. Membrane patches had an average size of ~ 200 nm, though very small fragments (less than 50 nm) and quite big membranes (~ 500 nm, as in Fig. 5.4B) could be encountered. Single-layered patches had an average height of ~ 8 nm above the mica surface. Also there were many bright spots on the surface, with height of 20 nm and more. These spots may represent weakly attached and highly curved membrane patches similar to the $LH2^-$ membrane fractions shown in Fig. 5.2A, position 3.

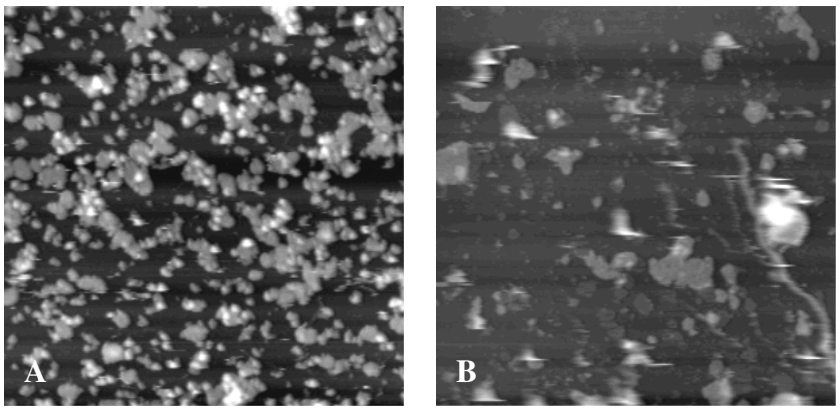

Fig.5.4. *AFM images of LH1-RC native membranes containing LH2 complexes adhered to the mica surface.* ***A****: $PufX^+$ membranes, frame size 2500x2500 nm^2, full grey scale 25 nm;* ***B****: $PufX^-$ membranes, frame size 2500x2500 nm^2, full grey scale 33 nm.*

The surface of the membranes was quite wavy and curved, as can be seen in two examples shown in Fig. 5.5, where a profile line drawn across a typical membrane surface (Fig. 5.5B) clearly demonstrates how the surface height level above the mica constantly varies all over the plane of the membrane patch (Fig. 5.5B, C). The height difference between membrane "waves" in their maximal and minimal positions could reach 5 nm and more.

Already at low magnification (500x500 nm^2 scan area) fine detail of the membrane substructure could be distinguished. In both types of the membranes ($PufX^+$ and $PufX^-$) the predominant features were individual bright protrusions with heights ~ 3-4 nm above the lipid bilayer and lateral size ~ 8 nm (Fig. 5.5A, B). These numbers correspond to the protruding RC H-subunit on the cytoplasmic face of the membranes, thus the membranes were adhered to the mica surface with their periplasmic face and the cytoplasmic face was facing the scanning AFM tip. Therefore, LH1-RC core complexes could be identified by their protruding RC H-subunits; however LH2 complexes could not be resolved at this magnification.

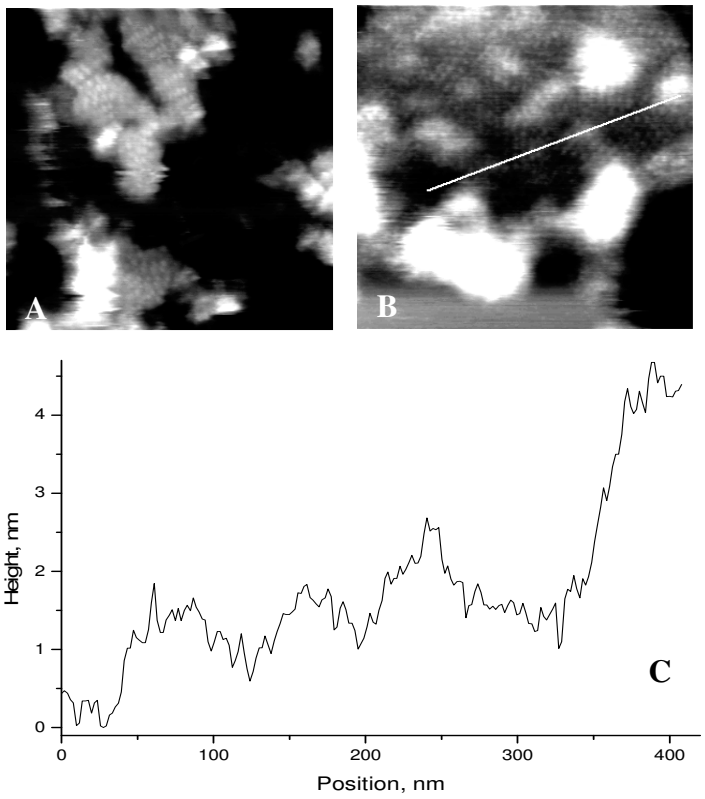

Fig. 5.5. *Surface topology in the native membranes. In both $PufX^+$ and $PufX^-$ membranes the top layer of the membranes is not flat but corrugated.* ***A****: Example of the wavy surface in $PufX^+$ membranes, frame size 500x500 nm^2, full grey scale 12 nm;* ***B****: Example of the wavy surfaces in $PufX^-$ membranes, frame size 500x500 nm^2, full grey scale 12 nm;* ***C****: Height profile drawn across a white line in* ***B****, which shows the surface topology and height variations up to 4 nm within one membrane patch.*

In case of $PufX^+$ membranes LH1-RC core complexes were organized as linear arrays of rows of dimers, while in the $PufX^-$ membranes monomeric core complexes formed quasi-crystalline hexagonal lattice (Fig. 5.5A, B). More examples of the AFM images demonstrating rows of core dimers and hexagonal packing of core monomers are shown in Fig. 5.6 (upper panel – $PufX^+$ membranes, lower panel – $PufX^-$ membranes).

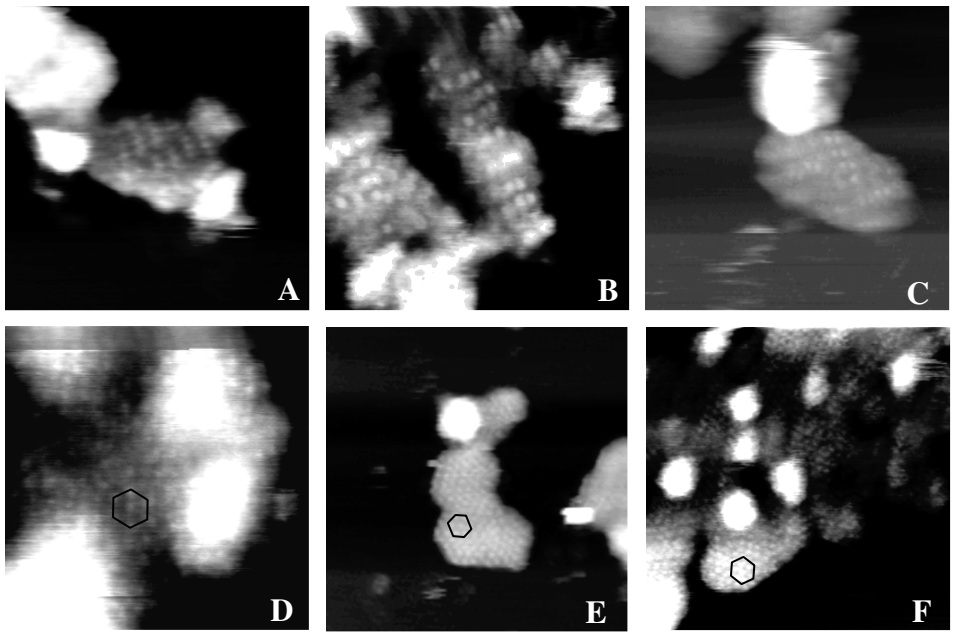

Fig. 5.6. *Medium magnification images of LH1-RC native membranes containing LH2 complexes.* ***A - C:*** *$PufX^+$ membranes, rows of LH1-RC core complexes dimers are resolved;* ***D - F:*** *$PufX^-$ membranes, hexagonal packing of LH1-RC core complexes monomers is resolved.* ***A - D*** *- frame size 250x250 nm^2, full grey scale 6 nm;* ***E - F*** *– frame size 500x500 nm^2, full grey scale 12 nm.*

High magnification AFM images of the native photosynthetic membranes are presented in Fig. 5.7. The organization of the $PufX^+$ membranes becomes visible in detail: rows of the LH1-RC core complexes (arrows) were bounded by the LH2 rings (*) (Fig. 5.7A). The width of the rows of LH1-RC dimers was found to be ~ 23 nm, coinciding with the size of core dimer (Siebert et al 2004, Scheuring et al 2004a). The diameter of LH2 rings was ~ 7 nm which is in agreement with LH2 atomic structure (McDermott et al 1995). The distance between LH1-RC core dimers and LH2 complexes was ~ 5-7 nm.

A high resolution AFM topograph of $PufX^-$ membrane is shown in Fig. 5.7B. In contrast to the $PufX^+$ membranes, the LH1-RC core complexes, did not form

dimers but were monomeric. The LH1-RC monomers in PufX$^-$ membranes were organized hexagonally in the membrane plane (Fig. 5.7B). The distance between LH1-RC monomers was ~ 2 nm (Fig. 5.7B). No LH2 rings could be detected in the close vicinity to the core monomers. The LH1 rings did not contain prominently protruding densities within the ring as was detected in the images of PufX$^+$ membranes (Fig. 5.7A). This could indicate the complete absence of RC's in the LH1 rings, the nanodissection of the RC H-subunits by the AFM tip or that we are facing the periplasmic side of the membrane, where the RC surface is at a lower level than the surrounding LH1 ring. It is more likely that the periplasmic face of the membrane was exposed to the scanning tip, as: *i*) the height of the LH1 ring above lipid layer is 0.9 ± 0.2 nm (n = 11), which corresponds to the protrusion of the LH1 ring on the periplasmic face of the membrane (Bahatyrova et al 2004a, Fotiadis et al 2004, Scheuring et al 2003b); *ii*) the dissection of only RC-H subunit would leave density within the ring both laterally and vertically (L- and M- subunits, see Fotiadis et al 2004), while in our images the central density in the LH1 rings is not higher than the ring itself, but even lower, with the depth of the central hole 0.4 ± 0.1 nm (n = 11), which is much lower than in the case of RC-H subunit nanodissection; *iii*) similarly, if the entire RC was removed then the central hole depth would be ~ 2 nm.

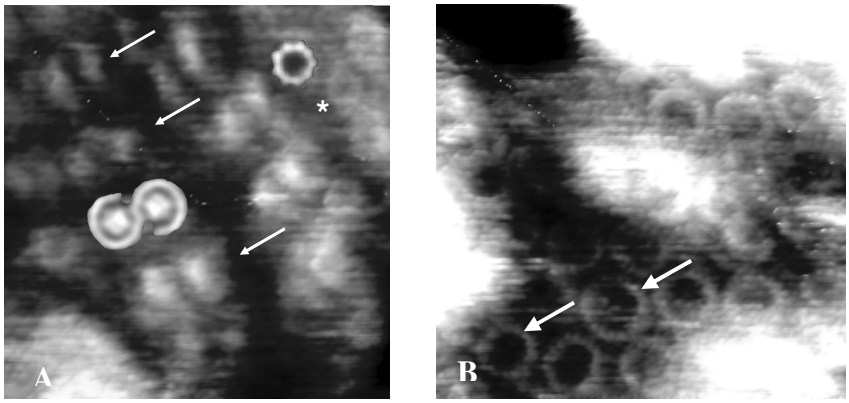

Fig. 5.7. *High resolution topographs of LH1-RC native photosynthetic membranes containing LH2 complexes.* ***A:*** *PufX$^+$ membranes, LH1-RC core complexes form rows of dimers (arrows), while LH2 complexes are located peripherally (*), frame size 100x100 nm^2, full grey scale 6 nm;* ***B:*** *PufX$^-$ membranes, LH1-RC core complexes are hexagonally packed in the membrane, no LH2 detectable, frame size 100x100 nm^2, full grey scale 6 nm.* ***A*** *contains a superposition of a core complex dimer excised from a projection map of a native membrane obtained by negative stain EM (Siebert et al 2004). A similar superposition of an individual LH2 complex is shown, from Walz et al 1998.*

In Fig. 5.7B we also note that in the native membranes LH1 rings display some heterogeneity at least in terms of size (arrows pointing to two LH1 rings with different sizes). The same flexibility and heterogeneity of LH1 rings were observed by us in LH1-only 2D-crystals and native membranes (Bahatyrova et al 2004a; Chapter 3).

A minor amount of disordered areas were observed for both types of the membranes ($PufX^+$ and $PufX^-$), where no long-range order of the core complexes could be found. However, in such disordered regions the dimeric and monomeric nature of the LH1-RC core complexes was preserved. These disordered areas showed close contact between the bulk LH2 and core complexes. Figure 5.8 shows examples of such areas for both types of the membranes.

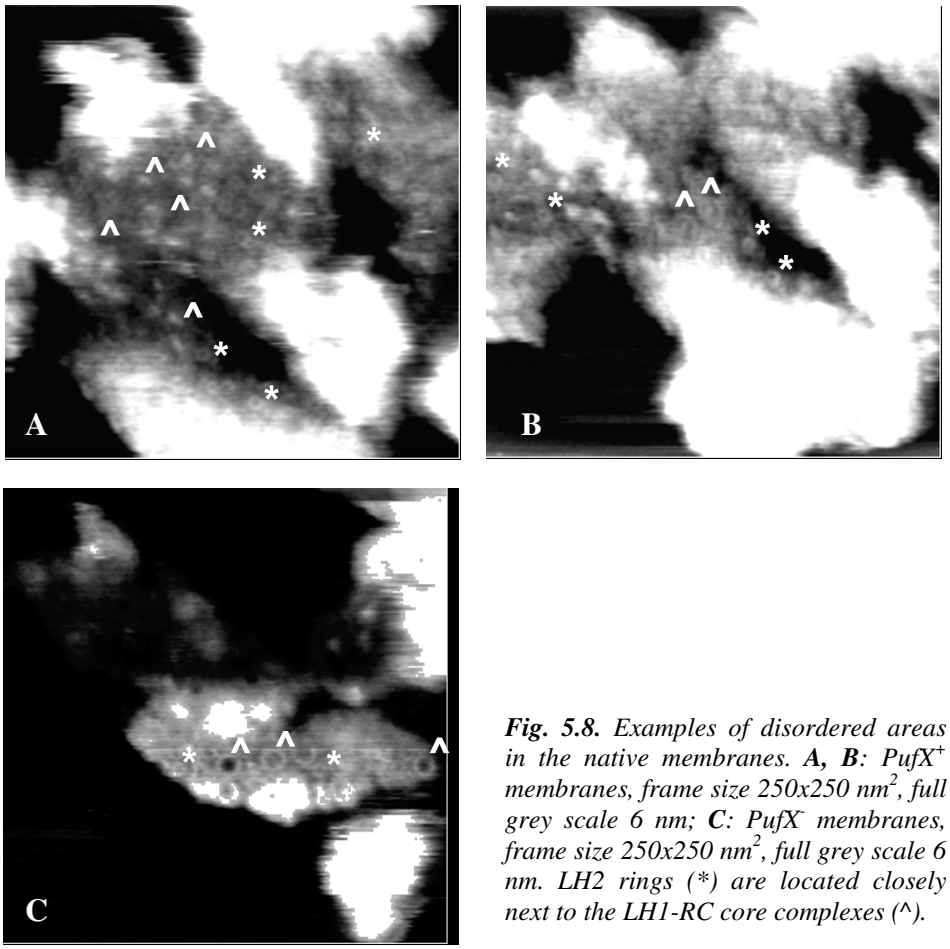

Fig. 5.8. *Examples of disordered areas in the native membranes.* ***A, B****: $PufX^+$ membranes, frame size 250x250 nm^2, full grey scale 6 nm;* ***C****: $PufX^-$ membranes, frame size 250x250 nm^2, full grey scale 6 nm. LH2 rings (*) are located closely next to the LH1-RC core complexes (^).*

LH2-only domains could be found as separate membrane patches (as shown in Fig. 5.9) and also in close proximity to the membrane areas where LH1-RC core complexes could be detected. This is illustrated, for instance, in Fig. 5.8A, where the central part of the membrane patch contains LH1-RC core complexes (arranged as dimers) with several LH2 rings located in the close vicinity to the core complexes. At the same time also very high areas (white spots on the image) could be found adjacent to the areas containing both cores and LH2s. Several LH2 rings could be resolved just on the edges of these bright areas, as for instance in the lowest part of the image in Fig. 5.8A, and it is likely that also the rest of this highly curved area was filled only with LH2 rings, as LH2-containing membranes are particularly curved (Sturgis and Niederman, 1996).

We also observed numerous patches consisting of only LH2 complexes, where LH1-RC core complexes could not be detected. These LH2-only domains were generally small and quite curved (Fig. 5.9).

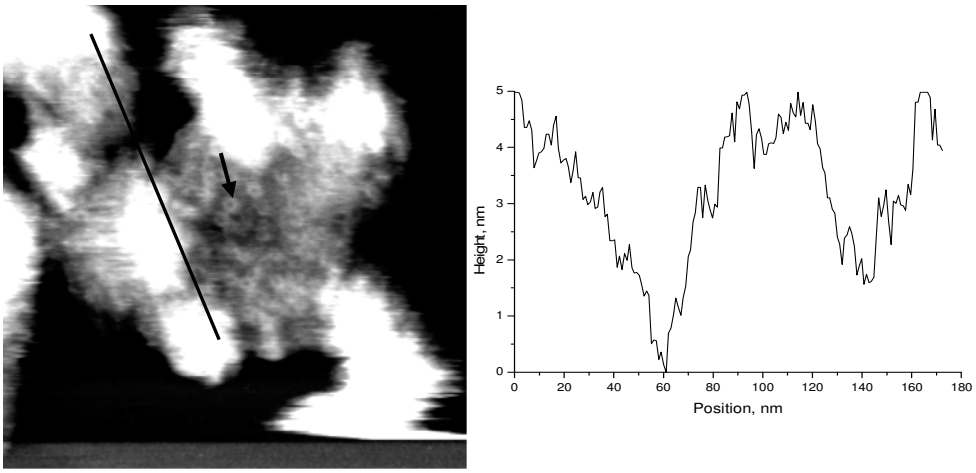

Fig. 5.9. *LH2-only domains in the native membranes (PufX$^+$), frame size 250x250 nm^2, full grey scale 6 nm. Single LH2 ring is marked with an arrow. Height profile drawn across a black line shows the surface topology and height variations up to 5 nm.*

Interestingly, LH2 complexes were sometimes found to form zigzag-like packing in the membrane (Fig. 5.10) resembling Type A crystalline packing found in LH2-only native membranes and 2D-crystals (discussed in Chapter 2). In Fig. 5.10A the membrane patch on the left contains several LH1-RC core complexes and the patch on the right, besides cores, reveals two zigzag rows formed by LH2 rings (circle). Fig. 5.10B is a zoom-in of the LH2 containing area from Fig. 5.10A.

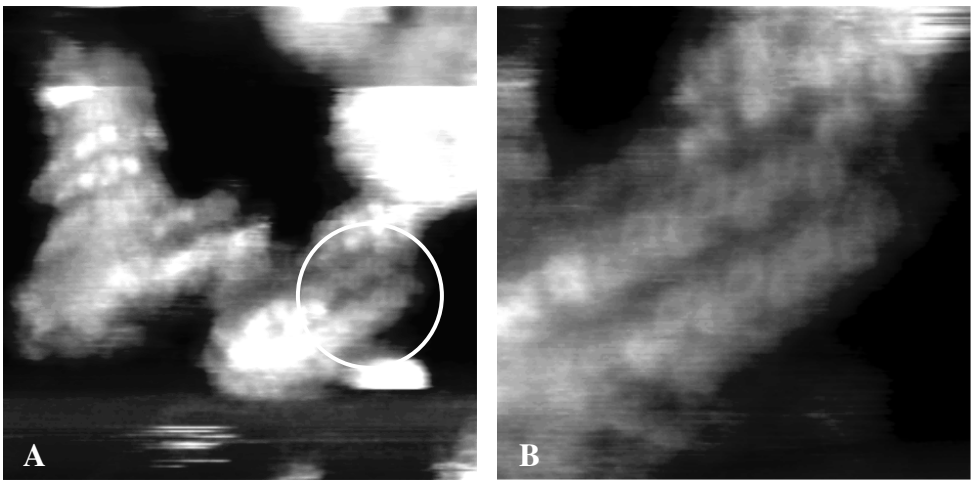

Fig. 5.10. *LH2 complexes displaying zigzag-like packing in native membranes (PufX$^+$), frame sizes 250x250 nm^2 and 100x100 nm^2 (**A** and **B**, respectively), full grey scale 6 nm. **B** is a zoom-in of the area in **A** marked with a circle.*

Another interesting observation was made in PufX$^-$ native membranes. In Fig. 5.11 two additional examples of high-resolution topographs of PufX$^-$ membranes are shown. Hexagonal packing of LH1-RC core monomers is clearly resolved. LH2 complexes could not be detected in this area, but several high and curved bulges all over the membrane surface suggest that LH2 rings might be located there, forming local LH2-only domains interspersed in-between the cores. The LH1-RC core complexes in this membrane patch seem to be packed more densely when compared to the image in Fig. 5.7B. Indeed, the distance between LH1-RC core monomers in this case is ~ 1 nm, while the monomers from the membrane patch in Fig. 5.7B were separated by the distance ~ 2 nm. Interestingly, some of the LH1 rings appear to be completely empty, with the depth of the central hole reaching 2 nm (arrows in Fig. 5.11A).

The rest of the LH1 rings do contain central density inside the rings, which is presumed to be the RC L- and M-subunit surfaces, which lie slightly below the level of the surrounding LH1 ring (asterisks in Fig. 5.11A), a result that is in agreement with the data of Fotiadis et al. (2004). This indicates that the membrane was adhered to the mica surface with its cytoplasmic face (where RC-H subunits protrude out of the LH1 ring with the height ~ 3-4 nm), and thus the periplasmic face of the membrane was exposed to the buffer solution and scanning AFM tip. This observation can be further supported by the height of the LH1 complex above the lipid bilayer in the membrane, which was ~ 0.9 nm,

corresponding to the height of the protruding LH1 ring on the periplasmic face of the membrane (Bahatyrova et al 2004a; Fotiadis et al 2004).

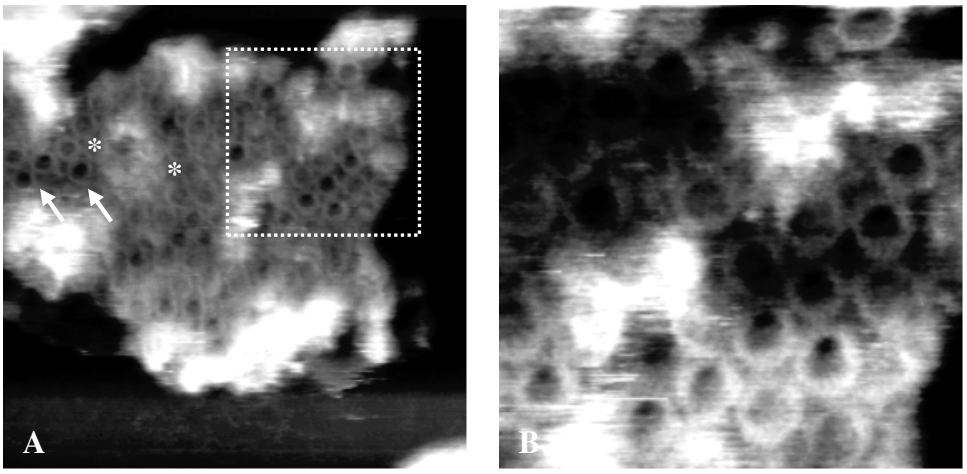

Fig. 5.11. *Example of PufX$^-$ native membrane, frame sizes 250x250 nm^2 and 100x100 nm^2, full grey scale 6 and 2.5 nm (**A** and **B**, respectively). LH1-RC core complexes are hexagonally packed with smaller distances between adjacent cores in comparison with larger packing distances found in the membrane patch shown in Fig. 5.7B. Empty LH1 rings (no RC inside) are marked by an arrow; LH1-RC cores with the periplasmic face of the RC are marked by an asterisk. **B** – zoom-in in **A** to the area marked with the broken square. Note how the overall organization of the LH1-RC monomers stays intact within the membrane after consecutive zooming-in.*

There are three possible explanations for the absence of RC's in some LH1 rings: *i)* that the semiaerobic growth conditions overproduced LH1 so that there were insufficient RC's produced to fill every available LH1 ring; *ii)* that some RC's have been lost during sample preparation; *iii)* that the missing RC's have been nanodissected by the action of the AFM tip. As the sample preparation and imaging conditions were identical for the PufX$^+$ and PufX$^-$ strains used and large numbers of empty rings were not observed in the PufX$^+$ strain, the first possibility seems most likely. This explanation is supported by the simultaneous imaging of both faces of the membrane shown in Fig. 5.12. The central region, marked 2, is clearly the cytoplasmic face as evidenced by the protruding H-subunits, while the flanking regions, marked 1, are of the periplasmic face. Both faces show the hexagonal packing typical of the PufX$^-$ strains and there are 'gaps' in the arrays of H-subunits as well as 'holes' in the centers of the LH1 rings where the RC's are missing (asterisks in Fig. 5.12). Nanodissection would preferentially remove the protruding H subunits rather than extract the low lying L- and M-subunits.

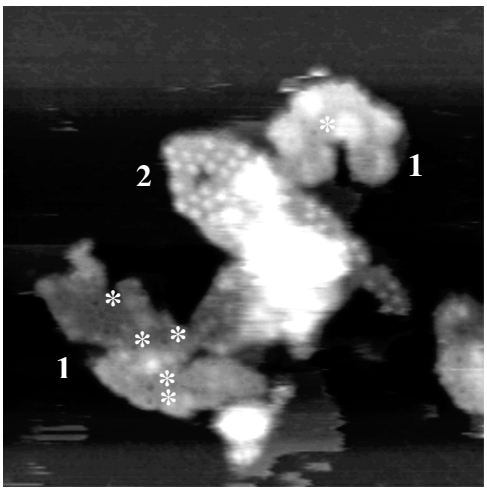

Fig.5.12. *Native membranes (PufX$^-$) exposing both periplasmic and cytoplasmic sides.* ***1*** *– periplasmic face, no protruding RC-H subunits detected, some empty LH1 rings are resolved (*);* ***2*** *– cytoplasmic face, protruding RC-H subunits are arranged in the quasi-crystalline hexagonal pattern. Frame size 500x500 nm^2, full grey scale 12 nm.*

5.4 Discussion and conclusions

We obtained high-resolution AFM topographs of semiaerobically grown native membranes from *Rhodobacter sphaeroides* either containing or lacking peripheral LH2 complexes. The role of the PufX protein in the spatial organization of the membrane components was studied by direct comparison of AFM images of the membranes in which the PufX gene was either preserved or deleted, given that PufX$^-$ membranes are capable of only semiaerobic growth but not photosynthetic. The difference between PufX$^+$ and PufX$^-$ membranes was clearly resolved: in the former membranes LH1-RC core complexes were dimeric, while in the latter membranes LH1-RC core complexes were monomeric. This was monitored for both LH2-lacking (Fig. 5.3) and LH2-containing membranes (Fig. 5.5 and 5.6). Recently, several authors have reported EM data on *Rhodobacter sphaeroides* LH1-RC-PufX native tubular membranes and 2D-crystals and have demonstrated the dimeric nature of the core complex when PufX was present (Jungas et al 1999; Siebert et al 2004; Scheuring et al 2004a). However, native membranes containing LH2 complexes could not be analyzed previously by EM, as LH2 complexes disturb the natural crystallinity observed for LH2$^-$ tubular membranes. Thus, our AFM images of LH2-containing native membranes from *Rhodobacter sphaeroides* are the first ever reported high-resolution images directly demonstrating dimerization of LH1-RC complexes in the presence of PufX even under semiaerobic growth conditions. The observation of dimeric core complexes in photosynthetically grown cells is significant since these dimers increase the efficiency of the photosynthetic process: when one RC is closed, excitations can migrate rapidly to a neighboring core complex. The distance between dimers is

close enough to ensure dimer-dimer energy transfer. It is interesting to note that the same organization prevails in semiaerobically grown cells indicating that this is a property of the LH proteins, particularly PufX, rather than a directed response governed by the growth conditions.

General features of the spatial organization of the individual components in the semiaerobically grown native membranes were resolved. In $LH2^-$ membranes LH1-RC core dimers were organized in linear arrays of rows consisting up to 6 dimers in $PufX^+$ membranes (Fig. 5.3A, C), while in the $PufX^-$ membranes core monomers were packed hexagonally in the membrane (Fig. 5.3B, D). Such long-range ordering of LH1-RC-PufX cores in the native membrane has been previously reported in freeze fracture EM images (Westerhuis et al 2002) and LD data (Frese et al 2000). In $LH2^+$ membranes the organization was identical, within the limits of the resolution achieved, as that for photosynthetically grown cells (see Chapter 4), where arrays of core complexes were linked by narrow 'channels' of LH2 to the separate bulk LH2 antenna.

In $LH2^+$ $PufX^-$ membranes LH1-RC core monomers formed a hexagonal lattice in the membrane, although no LH2 complexes could be detected within areas of hexagonally arranged LH1-RC cores (Fig. 5.7B, 5.11). Possibly, the majority of LH2 complexes were located in highly curved LH2-only domains (as in Fig. 5.9) which are extremely difficult to measure with AFM. In the disordered areas of the membranes some LH2 complexes could be found in very close proximity to the LH1-RC cores (Fig. 5.8) and in these regions there was no evidence of the core complexes forming hexagonal arrays. In the absence of PufX the core complexes appear to pack together preferentially, thus excluding the LH2 complexes.

Another intriguing observation was that some LH2 complexes in the native membranes were found to be inserted into the lipid bilayer in a zigzag manner (Fig. 5.10). Such arrangement of LH2 complexes was also found in LH2-only native membranes and 2D-crystals and was explained by the vertical translation of some of the rings (high-low positioning in the native membranes) and by the insertion of LH2 rings into the lipid bilayer in two opposite orientations (up-down configuration in the 2D-crystals) respectively. The former effect is most probably caused by the deposition of the curved membranes onto the flat mica surface in conjunction with the detergent used for membrane fractionation (see Discussion in Chapter 2).

As we discussed in the introduction to this chapter, the overall organization of the photosynthetic complexes in the native membranes grown under two different conditions (photosynthetically or semiaerobically) was expected to be rather similar. If we now compare results obtained on photosynthetically grown membranes (described in Chapter 4) with semiaerobically grown membranes

(described in this chapter) we can conclude that general principles of supramolecular organization of individual components within the photosynthetic membrane are identical in both systems. The membrane is divided into specialized domains and LH1-RC-PufX core dimers form linear arrays with LH2 complexes interspersed in-between them. Additionally, separate LH2-only domains can be encountered serving as additional energy harvesting regions. No cytochrome bc_1 complexes could be detected in either photosynthetically or semiaerobically grown membranes. This is in agreement with recent EM and AFM studies on native membranes from different species of purple bacteria where no cytochrome bc_1 complexes were detected (Siebert et al 2004; Scheuring et al 2004b, c). It raises questions about the location of this complex in the photosynthetic chromatophores and it is likely that it is located in some other membrane fractions.

We would like also to conclude that these results show that it was possible to overcome the major problem in imaging curved surfaces such as most biological membranes by means of the AFM technique. By applying tapping mode AFM in liquid we were able to record high-resolution AFM images on intrinsically curved membranes after they have been largely flattened out upon deposition onto the mica surface.

Any sufficiently advanced technology
is indistinguishable from magic.
Arthur C. Clarke

Chapter 6

Outlook and future directions in AFM on bacterial photosynthesis

In this thesis we presented high-resolution AFM topographs of different bacterial photosynthetic systems. These images promoted a deeper insight into the structural and functional properties of the photosynthetic complexes and the functional significance of these properties for the bacterial photosynthesis. A new model of a bacterial native membrane organization was derived based on the direct AFM topographs of photosynthetic membranes. Nevertheless, there are many questions which are still open in the field of the bacterial photosynthesis, and we can now envisage new experiments which can be carried out by AFM to answer them. In this chapter we will discuss some of these questions, such as *i)* the assembly of LH complexes in the ICM and the assembly factors responsible for the assembly process; *ii)* remaining questions in the bacterial photosynthetic membrane organization; *iii)* some practical recommendations on the high-resolution AFM tapping mode in liquid imaging of membrane proteins.

6.1 How are the pigment-protein complexes assembled in the photosynthetic membrane?

As was mentioned in Chapter 1, section 1.4.2, very little is known about biogenesis and assembly of pigment-protein complexes in the photosynthetic membranes. Some of the questions that still have to be answered are the following: *i)* how are the photosynthetic complexes assembled from their constituents: bacteriochlorophylls, carotenoids and αβ-polypeptides? ; *ii)* is it a synchronous or a step-like process? ; *iii)* how is the assembly process controlled in the photosynthetic membrane? Recently, the gene encoding LhaA protein in *Rhodobacter sphaeroides* cells was inactivated leading to the abolishment of LH1-RC-PufX complex assembly, while the assembly of the LH2 complex was completely unaffected (Tucker and Hunter, unpublished). These experiments showed that LhaA is an assembly factor for LH1 complex formation. The structure of LhaA is unknown, though it was shown to be similar in architecture to the members of the major facilitator superfamily of proteins (Abramson et al 2003; Hirai et al 2002; Huang et al 2003; Tucker and Hunter, unpublished).

During AFM imaging of LH1-only 2D-crystals (described in Chapter 3), we obtained high-resolution images of LH1 complexes, where some unidentified membrane proteins were found in addition to LH1 rings (Fig. 6.1).

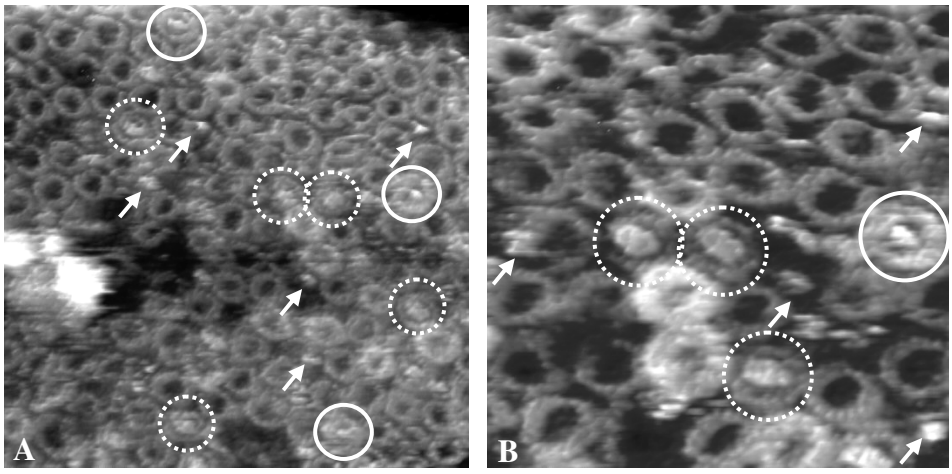

Fig. 6.1. *AFM images of LH1-only 2D-crystals. Besides LH1 rings, some unidentified proteins were found, which were located inside LH1 rings facing periplasmic side (dashed circles), inside LH1 rings facing cytoplasmic side (closed circles), and next to LH1 rings (arrows).* ***A:*** *Scan size 180x180 nm^2, full grey scale 6 nm;* ***B:*** *Scan size 90x90 nm^2, full grey scale 5 nm.*

Most of these topographical features were located inside LH1 rings, but some of the objects were also found next to the LH1 complexes (Fig. 6.1). These features cannot be RC's, as the deletion-complementation system used for the growth of the mutant strains (Jones et al 1992) does not allow crystals to contain any other proteins, except LH1 in this case. We hypothesize that the observed features might be assembly factors for LH1 complexes, LhaA. This is supported by the presence of LhaA in the crystalline material as identified in western blots using LhaA antibodies (Tucker and Hunter, unpublished). It is possible that in the absence of both RC and PufX in this mutant strain, some LhaA's are "trapped" in the LH1 ring during/after the completion of the ring assembly process. Furthermore, it is known that subunit IV of cytochrome bc_1, PufX and the H-subunit of the RC are the first proteins which are synthesized in the PSU followed by the synthesis of LH1 αβ-polypeptides encircling the RC (Pugh et al 1998). If we imagine the process of LH1 assembly, in which LhaA delivers, for example, bacteriochlorophylls to the site of LH1 construction, then, in principle, LhaA should be located in close vicinity of the LH1 ring when the ring construction is finished. We could not, however, detect any unidentified proteins in the images of native membranes containing LH1-RC-PufX cores and peripheral LH2 complexes (Bahatyrova et al 2004b). However, it is known that the upper pigmented band (UPB) of the photosynthetic membranes (ICM at the very early stage of its maturation) is enriched in assembly factor molecules as the LH complexes have to be assembled before full maturation of the ICM occurs (Tucker and Hunter, unpublished). Thus by imaging of UPB membranes there will be a higher probability of detecting LhaA proteins in these membranes.

Clearly, direct imaging of the LhaA-LH1 assembly-product complex by AFM could support this hypothesis. One approach to facilitate the identification and analysis of this novel complex can be the use of His-tagged assembly factors which can then be labeled with gold nanoparticles as topographical markers for AFM imaging. The topology and energy transfer properties of assembly complexes within membranes can be studied using the combined AFM/confocal microscopy setup developed in our group (Kassies et al 2004). GFP-labeled assembly factors can be topographically mapped by AFM and fluorescent images of labeled membranes can be simultaneously obtained. The use of high-resolution AFM in combination with other imaging and biochemical techniques will uniquely enable the collection of topographic data, which will give rise to completely new models on how assembly factors assemble and insert large protein complexes into membranes.

6.2 Outstanding questions on the organization of bacterial photosynthetic membrane

Although our studies of a native bacterial photosynthetic membrane from *Rhodobacter sphaeroides* (Chapters 4 and 5) showed the relative positioning of the main components of the photosynthetic membrane (LH2 and LH1-RC-PufX core complexes) there are still several questions to be answered on the overall organization of the photosynthetic membrane.

The location of the cytochrome bc_1 complex could not be detected, though our AFM images clearly showed that they do not form LH1-RC-PufX-bc_1 supercomplexes as was previously thought (Jungas et al 1999). However, the work of Siebert et al. (2004) did not exclude the possibility of such supercomplexes in some other types of membrane within the cell, and the challenge is to purify and examine each type of membrane from these bacteria, not just the images of ICM vesicles presented in Chapters 4 and 5. Cytochrome bc_1 complexes can be His-tagged and labeled by gold nanobeads for easier AFM identification.

It is not known how the overall organization of the photosynthetic membrane responds to variations in environmental conditions such as changes in oxygen tension and light intensity. Imaging of membranes purified from cells grown under widely varying conditions can be conducted, which will reveal the adaptability of this organization and, for example, will show how the membranes accommodate increased levels of LH2 complexes as a response to low light intensities. Another interesting aspect of this investigation can be examination of how the rows of LH1-RC-PufX core complex dimers are formed and to what extent these rows assemble in response to low light intensity.

Other species of purple bacteria (*Rhodopseudomonas palustris, Rhodobacter capsulatus, Rhodospirillum molischianum*) can be also imaged in order to compare the organization of the photosynthetic membrane from these species with the organization of the photosynthetic membrane from *Rhodobacter sphaeroides*. In *Rhodospirillum molischianum* the gene encoding PufX protein is absent and a totally different organization of the membrane proteins can be expected, as PufX plays a key role in the photosynthetic membrane organization in *Rhodobacter sphaeroides* as was shown in Chapter 5 of this thesis. In *Rhodopseudomonas palustris* a protein called W was found which might be an analogue to the PufX protein from *Rhodobacter sphaeroides* (Roszak et al 2003) and high resolution AFM imaging would be able to reveal the similarities and differences between these two systems. *Rhodobacter capsulatus,* the second species of purple bacteria which contains PufX, is expected to have identical organization of the photosynthetic membrane as in *Rhodobacter sphaeroides*.

6.3 Recommendations on high-resolution imaging of membrane proteins

In this thesis high-resolution AFM images of photosynthetic membrane proteins have been obtained. Moreover, the lateral organization of individual pigment-protein complexes in the native multi-component bacterial photosynthetic membrane was revealed by AFM. The shape and protruding termini of LH and RC complexes, just several nanometers in size, as well as their individual subunits could be clearly resolved. While performing AFM imaging on various photosynthetic systems (2D-crystals and native membranes) we found that *i)* the tip sharpness and *ii)* the amount of free tapping amplitude damping were especially crucial for the achievement of high-resolution topographs.

AFM tip sharpness

One of the most common artifacts which often accompanies AFM imaging is the tip convolution effect, when the apparent size of the feature in the image is much broader than its real size due to the fact that the size of the scanning probe is larger than the feature itself. For example, DNA molecules appear to have a width of ~ 20 nm instead of 2 nm (Bennink et al 2003; Nikova et al 2004). The AFM tips that were used in our experiments had a radius of curvature of ~ 20-40 nm (Veeco NanoProbe Tips, tip specification datasheet). This value is much larger than the smallest topographic feature which could be resolved by us in many of the high-resolution images, a distance between adjacent αβ-polypeptides subunits in LH1 and LH2 ring-like proteins, which was ~ 2 nm. The same discrepancy between the global size of the probe and the actual size of the finest details resolved by this probe is apparently present in all recently reported high-resolution AFM topographs of membrane proteins. It is clear that, only when the size of the scanning probe is smaller or equal to the size of the scanned feature, the tip convolution effect will be eliminated. Therefore, the tip which demonstrates the resolution of tiny details without their convolution should have very small protrusion(s) only couple of nanometers in size or even less at the very apex of the tip.

When performing imaging in liquid environment, the medium which is the most suited for biological samples such as membrane proteins, the AFM tip can pick up proteins or their fragments rather easily. This was, for example, directly demonstrated by the nanodissection of the bacterial RC H-subunit (Scheuring et al 2003b; Fotiadis et al 2004). Such an event of the tip contamination can have a two-sided effect: in some occasions, after the tip picks up something from the surface the resolution decreases dramatically and often can not be restored, but sometimes such an extra particle on the tip apex is even advantageous, since the actual scanning of the sample will be performed by this tiny protrusion. It

becomes clear, that it is not possible to control the shape of the AFM tip during imaging and to maintain its shape throughout the measurements. The tip's shape constantly undergoes changes during imaging, even if the other scanning parameters (the amount of the free tapping amplitude, damping of the amplitude, or scanning speed) are kept unchanged. Correspondingly, the resolution of the fine details changes with the alteration of the tip's shape. We can illustrate this by a set of 18 consecutive images of the same area of a native membrane (Fig. 6.2; four images out of this collection of the images were shown in Chapter 4, Fig. 4.5).

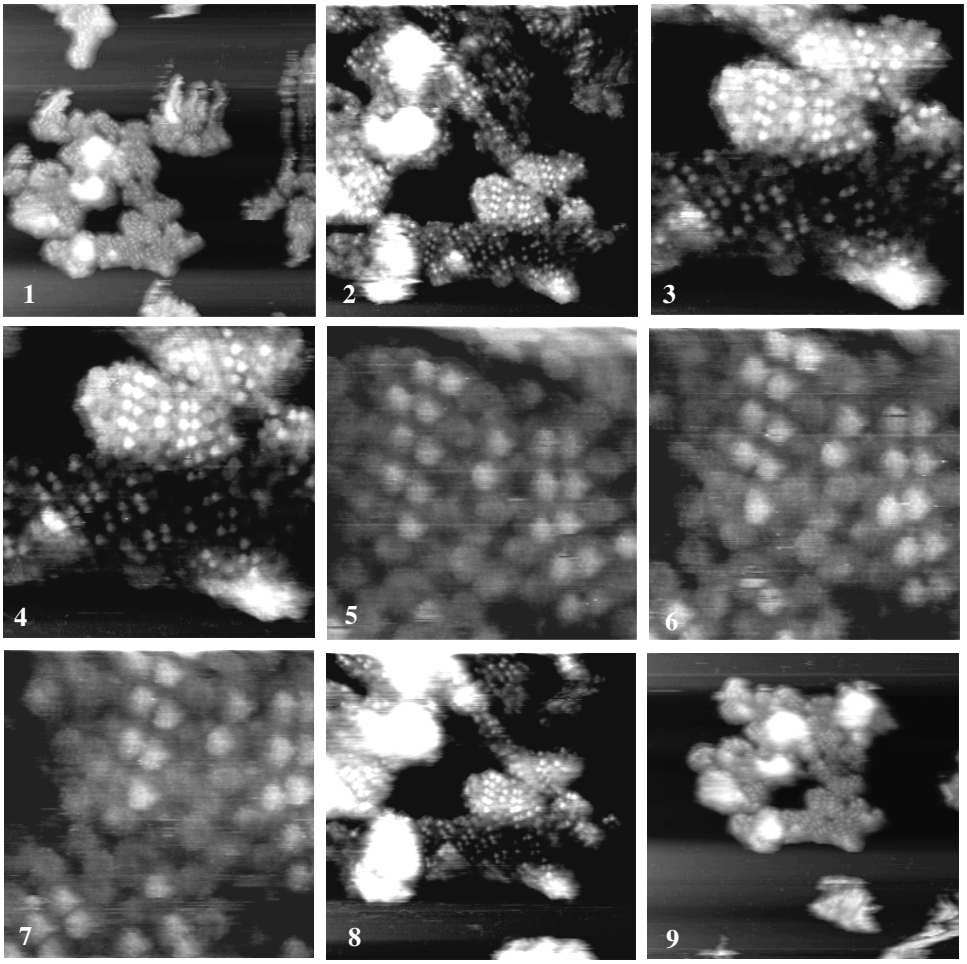

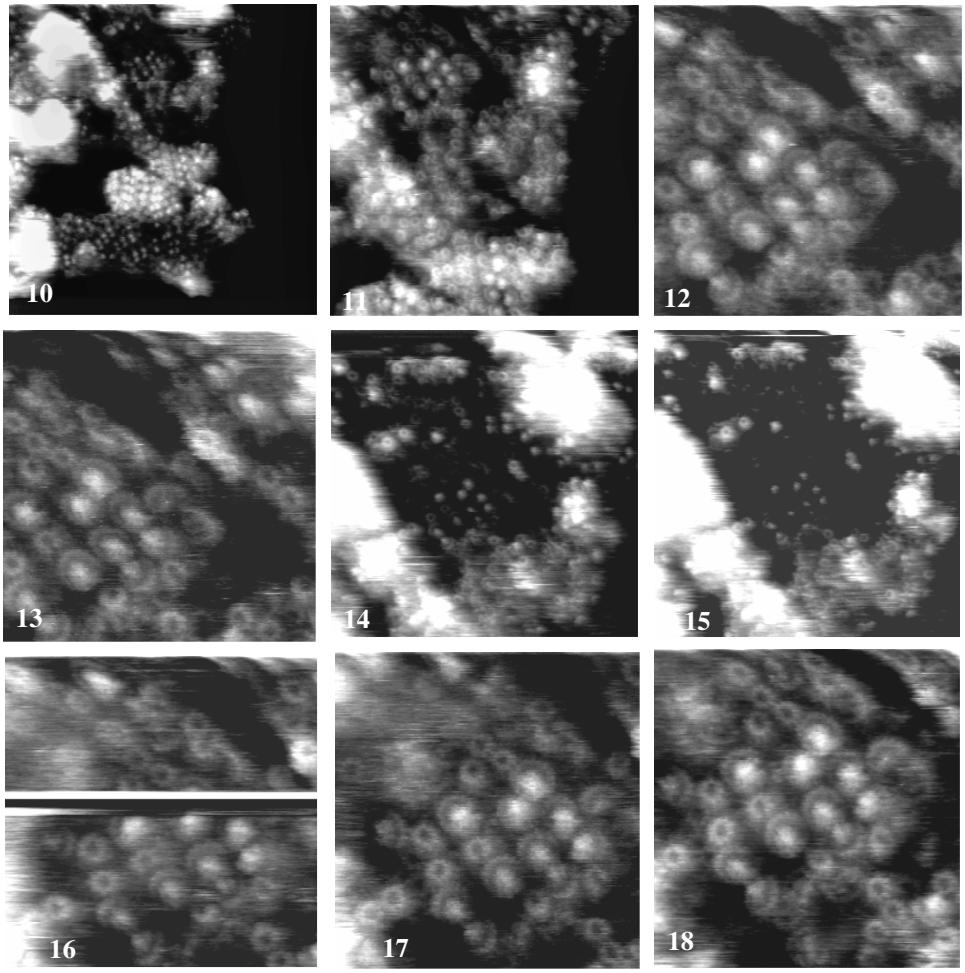

Fig. 6.2. *Set of 18 consecutive images of the same area of a photosynthetic membrane. Total time between the first and the last image shown here was ~ 18 min (~ 1 min per image). Scan sizes: 1000x1000 nm^2 (frames 1, 9), 500x500 nm^2 (frames 2, 8, 10), 250x250 nm^2 (frames 3, 4, 11, 14, 15), 100x100 nm^2 (frames 5, 6, 7, 12, 13, 16, 17, 18).*

In Fig. 6.2 it can be seen that during the first round of zooming-in into the membrane (frames 1 - 7) the resolution was not high enough to resolve clearly the ring-like shapes of LH1 and LH2 complexes, and only protruding RC H-subunits were the most apparent features in the images (white blobs in all first 7 images). During further zooming-out (frames 8 and 9) and the second round of zooming-in in to the same membrane (frames 10 - 13) the shape of the scanning tip was apparently changed and it became much sharper, as much more fine details of the membrane surface, such as LH2 rings, LH1 rings surrounding RC's, and even LH ring subunits, could be resolved (frames 11 - 13). In the third round of zooming-

out (frames 14, 15) and zooming-in (frames 16 - 18) the resolution remained remarkably high and could be maintained long enough to record several images of the same membrane area. We would like to stress that in the given example all other scanning parameters were kept unchanged during imaging. Thus, all the changes in the resolution we demonstrated in Fig. 6.2 were caused purely by the uncontrollable modification of the tip shape.

The question arises if we can increase the yield of high-resolution topographs and ensure better reproducibility in AFM imaging of membrane proteins, in particular. One obvious way is to change AFM tips, as they become blunt and do not produce high-resolution data any longer. However, this way might be thought to be not very effective in the sense of its relative high cost. One can also try to use silicon tips, instead of silicon nitride tips, which are usually much sharper than standard silicon nitride tips and are believed to have a less "sticky" surface, thus decreasing the chance of the tip contamination. But, the problem with silicon tips is that, in general, all silicon cantilevers have properties which are very different in comparison with standard and widely used silicon nitride cantilevers, namely silicon tips are much stiffer and have much higher resonance frequencies. This suggests additional difficulties when using silicon tips for imaging. To our best knowledge, nowadays most of the research teams performing high-resolution AFM imaging on biological samples use silicon nitride tips. This fact of course does not exclude the possibility of further investigation of silicon tips for the purpose of their application in high-resolution imaging of biological samples in liquids. Finally, single-walled carbon nanotubes have exceptional characteristics such as very small radius (1-2 nm), high aspect ratio and increased mechanical robustness which make them perfect candidates to be tried to improve reproducibility and reliability of high-resolution AFM topographs. A project devoted to the fabrication of single-walled carbon nanotubes is currently in progress in our group (Vera, 2004).

Damping of the free amplitude

The second factor which has a great impact on the yield of high-resolution images of membrane proteins using tapping mode AFM was the amount of the damping of the free tapping amplitude during scanning. This phenomenon can be shortly formulated as follows: the less free amplitude is damped, the less energy is transferred by the tip to the surface and the sample damage is minimized, which is directly related to the resolution which can be potentially achieved. Furthermore, the low amplitude damping and the tip shape (discussed in the previous sub-section) are very closely related, as can be demonstrated in Fig. 6.3.

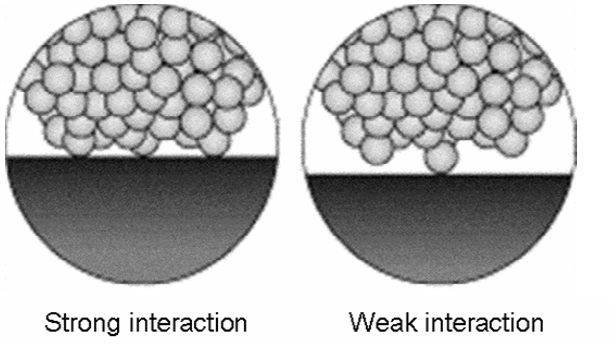

Fig. 6.3. *Schematic drawing of the contact area of the AFM tip and the surface during imaging. The resolution apparently depends on the strength of the interactions between the tip and the surface.*

Obviously, weak interactions (very soft tapping, i.e. low damping) increase the chance to scan the surface with the very apex of the tip, thus increasing the resolution tremendously (Fig. 6.3, right). In contrast, when the damping is high, the interactions between the tip and the surface become stronger, this increases the contact surface area between the tip and the sample with inevitable loss of small protrusions on the tip apex and consequently of the resolution (Fig. 6.3, left).

Interestingly, for contact mode AFM it was shown that the interactions between the tip and the sample can be electrostatically balanced by varying the ionic strength of the recording buffer (Muller et al 1999b). In this way, the "macro-tip" could be rested on a "cushion" of a repulsive force between the probe and the surface, while only the "micro-tip", the small protrusion on the "macro-tip", underwent attraction towards the surface and in this way ensured the high-resolution imaging. As for the tapping mode AFM, it was shown that the resolution of the topographs acquired in tapping mode did not depend on the concentration of monovalent ions in the solution (Möller et al 1999). Most probably, in tapping mode the amount of damping in the system plays a role of a "balance", when only the "micro-tip" touches the surface at low damping, to draw an analogy with the ionic strength of the solution serving as a balance in contact mode. Practically, the best results could be obtained by us when the damping of the free amplitude was ~ 5-10%.

To conclude, successful high resolution imaging of membrane proteins in tapping mode in liquid depends on a subtle interplay between the scanning tip sharpness and the amount of the energy which is transferred to the system by the tip. Careful control of the free amplitude damping is very important, since in many cases it positively affects the tip shape and eventually resolution.

Summary

Understanding biomembranes is one of the most important and topical research areas in biology. At present, the photosynthetic membrane of purple bacteria is one of the best studied and characterized biomembranes and is an ideal system to examine new aspects in membrane biology such as membrane supramolecular organization, biogenesis, assembly, and coupling of photosystems to secondary electron transfer complexes.

The main goal of this thesis was to investigate the supramolecular architecture of a photosynthetic membrane from *Rhodobacter sphaeroides* purple bacteria cells. This is extremely timely, since we now know all of the structures of photosynthetic pigment-protein LH and RC complexes, ATP-synthase and bacterial cytochrome bc_1 complexes. We employed tapping mode AFM imaging in liquid in order to obtain and analyze high-resolution topographs of photosynthetic membrane proteins in their native lipid bilayer environment. In **Chapter 1** an introduction is given in general features and functional properties of biomembranes and membrane proteins. Function, composition and supramolecular organization of a photosynthetic membrane from purple bacteria are discussed. An introduction to the basic principles of AFM, the powerful tool for study of biological processes, is given.

Chapter 2 reports AFM investigation of structural and physical properties of the peripheral light-harvesting complex LH2 from *Rhodobacter sphaeroides* both in the reconstituted 2D-crystals and in native membranes containing only LH2 complexes. We have shown that regardless of the type of crystalline packing and environment (fully native or within the 2D-crystal), the LH2 complex behaved as an essentially rigid structure with conserved circular shape and invariable ring size. AFM topographs of LH2-only native membranes indicated similar (crystalline-like) spatial organization of the LH2 complexes in the 2D-crystals and detergent treated native membranes. The mechanism of the influence of the detergent molecules and sample deposition onto the mica substrate on the arrangement of the LH2 complexes in the native membranes observed by us was proposed.

AFM study of 2D-crystals and native membranes containing a mutant lacking the reaction center complex, which normally sits within the LH1 ring providing a barrier to substantial changes in shape, is presented in **Chapter 3**. This approach has revealed the inherent flexibility and lack of structural coherence of this complex in a reconstituted lipid bilayer at room temperature. Circular, elliptical and even polygonal ring shapes as well as arcs and open rings have been observed for LH1; in contrast, no such variations in structure were observed for the peripheral LH2 complex under the same conditions. The basis for these

differences between LH1 and LH2 is suggested to be the H-bonding patterns that stabilize binding of the bacteriochlorophylls to the LH polypeptides. The demonstration of a flexible and even breakable LH1 ring architecture provides a rationale for the passage of quinol from the RC to the quinone pool prior to reduction of the cytochrome bc_1 complex.

In order to investigate the functionally crucial organisation of LH and RC complexes, native photosynthetic membranes from the wild-type purple bacterium *Rhodobacter sphaeroides* were imaged by AFM. High-resolution AFM topographs of a native bacterial photosynthetic membrane presented in **Chapter 4** demonstrate first view of any multi-component membrane, which shows the relative positions and associations of the photosynthetic complexes and reveals crucial new features of the organisation of the network – we found that the membrane is divided into specialised domains each with a different network organisation and wherein one type of complex predominates. Close packing of linear arrays of dimers of LH1-RC-PufX complexes, which are separated by narrow 'energy conduits' of peripheral LH2 complexes, represents the basic requirement for the efficient harvesting, transmission and trapping of light energy in this bacterium.

In **Chapter 5** results obtained by high-resolution AFM imaging on native membranes where one or more components of the wild-type photosynthetic unit have been genetically removed are reported. We demonstrated for the first time by direct AFM imaging of native membranes that, in both $LH2^+$ and $LH2^-$ membranes, PufX protein plays a significant role in organizing LH1-RC core complexes by causing their dimerization. We have shown that LH2 also had an ordering effect on the core complexes when PufX is absent from the LH1-RC core in semiaerobically grown cells. Additionally, general features of the supramolecular architecture of native membranes from semiaerobically grown cells could be resolved and compared with the native photosynthetic membrane architecture found in photosynthetically grown cells (described in Chapter 4).

In **Chapter 6** possibilities for future experiments in AFM on bacterial photosynthesis are suggested. Recommendations on the high-resolution AFM tapping mode in liquid imaging of membrane proteins are given.

Samenvatting

De studie van biomembranen is een van de belangrijkste en meest actuele onderzoeksgebieden binnen de biologie. Op dit moment is het fotosynthetisch membraan van paarse bacteriën een van de meest bestudeerde en best gekarakteriseerde biomembranen. Hierdoor vormt het een ideaal systeem om nieuwe aspecten in membraan biologie te onderzoeken, zoals de supra-moleculaire organisatie, de biogenese, het opbouw proces, en de koppeling van fotosystemen aan secundaire electron-overdracht complexen.

Het doel van dit onderzoek is het in kaart brengen van de supramoleculaire architectuur van het fotosynthetisch membraan van de paarse bacterie *Rhodobacter sphaeroides*. Het onderzoek vindt op het juiste tijdstip plaats omdat nu de structuren van alle fotosynthetische pigment-eiwit LH en RC complexen, ATP-synthase en bacterieel cytochroom bc_1 complexen bekend zijn. We hebben tapping-mode AFM in vloeistof toegepast om daarmee topografische afbeeldingen met zeer hoge resolutie te maken van fotosynthetische membraan eiwitten in de natuurlijke lipide dubbellaag omgeving. In **Hoofstuk 1** wordt een introductie gegeven over de algemene en functionele eigenschappen van biomembranen en membraan eiwitten. De functie, samenstelling en supramoleculaire organisatie van het fotosynthetisch membraan van paarse bacteriën wordt bediscussieerd. Daarnaast worden de basis principes van AFM, een krachtige techniek voor de studie van biologische processen, geïntroduceerd.

Hoofdstuk 2 behandelt het onderzoek met behulp van AFM aan de structurele en fysieke eigenschappen van het perifere light-harvesting complex LH2 van *Rhodobacter sphaeroides*, zowel in gereconstrueerde 2D-kristallen als in natuurlijke membranen die alleen LH2 complexen bevatten. We hebben aangetoond dat de LH2 complexen, onafhankelijk van het soort kristallijne pakking en omgeving (volledig natuurlijk of binnen het 2D-kristal), zich gedragen als een hoofdzakelijk starre structuur met circulaire vorm en constante ring grootte. AFM afbeeldingen van alleen LH2 bevattende natuurlijke membranen gaven een vergelijkbare (kristallijn-achtige) ruimtelijke organisatie van de LH2 complexen weer in de 2D-kristallen en de met detergent behandelde natuurlijke membranen. Een mechanisme wordt voorgesteld met betrekking tot de invloed van de detergent moleculen en de sample depositie op het mica substraat op de door ons geobserveerde organisatie van de LH2 complexen in het natuurlijke membraan.

Een AFM studie van 2D-kristallen en natuurlijke membranen afkomstig van een mutant zonder reactie centrum complex is beschreven in **Hoofdstuk 3**. Het RC is normaal gesproken binnen de LH1 ring gelokaliseerd, waardoor het een barrière vormt voor grote vormveranderingen van de ring. Deze studie aan complexen

zonder RC heeft de inherente flexibiliteit en lage structurele coherentie van dit complex in een gereconstrueerde lipide dubbellaag bij kamer temperatuur aangetoond. Circulaire, elliptische en zelfs polygonale ring vormen evenals bogen en open ringen zijn voor LH1 waargenomen; zulke variaties in de structuur werden niet waargenomen in LH2 onder dezelfde condities. Als basis voor deze verschillen tussen LH1 en LH2 wordt het verschil in H-bindings patronen, die de binding tussen de bacteriochlorophyll moleculen en de LH polypeptides stabiliseren, gesuggereerd. De demonstratie van een flexibele en zelfs breekbare LH1 ring architectuur vormt een mogelijke basis voor de passage van quinol van het RC naar het quinone reservoir voorafgaand aan de reductie van het cytochroom bc_1 complex.

Om de functioneel cruciale organisatie van LH en RC complexen te bestuderen, zijn de natuurlijke fotosynthetische membranen van het wild-type paarse bacterie *Rhodobacter sphaeriodes* afgebeeld met AFM. Hoge resolutie AFM afbeeldingen van een natuurlijk fotosynthetisch membraan, zoals gepresenteerd in **Hoofdstuk 4**, geven een eerste blik op een multi-component membraan in het algemeen. De afbeeldingen laten de relatieve posities en associaties van de fotosynthetische complexen zien en onthullen cruciale nieuwe kenmerken van de organisatie van het netwerk – we vonden dat het membraan is opgedeeld in gespecialiseerde domeinen, elk met een andere netwerkorganisatie en waarin één type complex overheerst. Een dichte pakking van lineaire reeksen van dimeren van LH1-RC-PufX complexen die van elkaar zijn gescheiden door smalle 'energie geleiders' van perifere LH2 complexen, vormt de basis voorwaarde voor efficiënte licht absorptie, energie geleiding, gevolgd door de vastlegging van de energie in de bacterie.

In **Hoofdstuk 5** worden resultaten getoond van hoge resolutie AFM op natuurlijke membranen waarin een of meer componenten van de fotosynthetische unit genetisch zijn verwijderd. We demonstreren voor het eerst, door AFM afbeeldingen te maken op natuurlijke membranen, dat in zowel $LH2^+$ als in $LH2^-$ membranen het PufX eiwit een belangrijke rol speelt in de organisatie van de LH1-RC core complexen door het veroorzaken van de dimerisatie van deze complexen. We laten zien dat LH2 ook een ordenend effect heeft op de core complexen als PufX afwezig is in the LH1-RC core in semi-aerobisch gekweekte cellen. Tevens konden algemene kenmerken van de supramoleculaire architectuur van natuurlijke membranen van semi-aerobisch gekweekte cellen in kaart worden gebracht en vergeleken met de natuurlijke fotosynthetische membraan architectuur waargenomen in fotosynthetisch gekweekte cellen (beschreven in Hoofstuk 4).

In **Hoofdstuk 6** worden mogelijkheden voor toekomstige experimenten met AFM op bacteriële fotosynthese behandeld. Tevens worden aanbevelingen gedaan voor

het afbeelden met hoge resolutie tapping-mode AFM in vloeistof van membraan eiwitten.

Abbreviations

AFM	atomic force microscope
ATP	adenosine triphosphate
Bchls	bacteriochlorophylls
CMC	critical micelle concentration
DDM	detergent *n*-dodecyl-β-D-maltoside
DOPC	lipid dioleoyl-phosphatidylcholine
EM	electron microscope
His	histidine
H-bond	hydrogen bond
ICM	intracytoplasmic membrane
LD	linear dichroism
LDAO	detergent lauryldimethylamine N-oxide
LH	light-harvesting
LH1	light-harvesting complex 1
LH2	light-harvesting complex 2
LH3	light-harvesting complex 3
LhaA	light harvesting apparatus assembly protein
NMR	nuclear magnetic resonance
OD	optical density
ORF	open reading frame
OTG	detergent n-octyl-β-D-thioglucopyranoside
PGC	photosynthetic gene cluster
Phe	phenylalanine
PSU	photosynthetic unit
Q	quinone
Q_B	quinone-binding site
RC	reaction center
RT	room temerature
SDS	detergent sodium dodecylsulfate
SDS-PAGE	SDS polyacrylamide gel electrophoresis
Trp	tryptophan
Tyr	tyrosine
UPB	upper pigmented band
WT	wild type
β-OG	detergent octyl-β-D-glucopyranoside

References

1. Aagaard, J., and W. R. Siström. 1972. Control of synthesis of reaction centre bacteriochlorophyll in photosynthetic bacteria. *Photochem. Photobiol.* 15:209-225.
2. Abrahams, J., A. Leslie, R. Lutter, and J. Walker. 1994. Structure at 2.8 Å resolution of F_1-ATPase from bovine heart mitochondria. *Nature.* 370:621-628.
3. Abramson, J., I. Smirnova, V. Kasho, G. Verner, H. R. Kaback, S. Iwata. 2003. Structure and Mechanism of the Lactose Permease of *Escherichia coli. Science.* 301:610-615.
4. Allen, J. P., G. Feher, T. O. Yeates, H. Komiya, and D. C. Rees. 1987. Structure of the reaction center from *Rhodobacter sphaeroides* R26: The protein subunits. *Proc. Natl. Acad. Sci. USA.* 84:6162-6166.
5. Argaman, M., R. Golan, N. H. Thomson, and H. G. Hansma. 1997. Phase imaging of moving DNA molecules replicated in the atomic force microscope. *Nucleic Acids Res.* 25:4379-4384.
6. Bahatyrova, S., R. N. Frese, K. O. van der Werf, C. Otto, C. N. Hunter, and J. D. Olsen. 2004a. Flexibility and size heterogeneity of the LH1 light harvesting complex revealed by atomic force microscopy: functional significance for bacterial photosynthesis. *J. Biol. Chem.* 279:21327-21333.
7. Bahatyrova, S., R. N. Frese, C. A. Siebert, J. D. Olsen, K. O. Van der Werf, R. Van Grondelle, R. A. Niederman, P. A. Bullough, C. Otto, and C. N. Hunter. 2004b. The native architecture of a photosynthetic membrane. *Nature.* 430:1058-1062.
8. Barz, W. P., and D. Oesterhelt. 1994. Photosynthetic deficiency of a PufX deletion mutant of *Rhodobacter sphaeroides* is suppressed by point mutations in the light-harvesting complex genes *pufB* or *pufA*. *Biochemistry*. 33:9741-9752.
9. Barz, W. P., F. Francia, G. Venturoli, B. A. Melandri, A. Verméglio, and D. Oesterhelt. 1995a. Role of the PufX protein in photosynthetic growth of *Rhodobacter sphaeroides*. 1. PufX is required for efficient light-driven electron transfer and photophosphorylation under anaerobic conditions. *Biochemistry*. 34:15235-15247.
10. Barz, W. P., A. Verméglio, F. Francia, G. Venturoli, B. A. Melandri, and D. Oesterhelt. 1995b. Role of the PufX protein in photosynthetic growth of *Rhodobacter sphaeroides*. 2. PufX is required for efficient ubiquinone/ubiquinol exchange between the reaction center Q_B site and the cytochrome bc_1 complex. *Biochemistry*. 34:15248-15258.
11. Beekman, L. M., L, M. P. Beekman, F. van Mourik, M. R. Jones, H. M. Visser, C. N. Hunter, and R. van Grondelle.1994. Trapping kinetics in mutants of the photosynthetic purple bacterium *Rhodobacter sphaeroides*: influence of the charge separation rate and consequences for the rate-limiting step in the light-harvesting process. *Biochemistry.* 33:3143-3147.
12. Bennink, M. L., D. N. Nikova, K. O. van der Werf, and J. Greve. 2003. Dynamic imaging of single DNA–protein interactions using atomic force microscopy. *Analit. Chem. Acta*. 479:3-15.
13. Berry, E. A., L.-S. Huang, L. K. Saechao, N. G. Pon, M. Valkova-Valchanova, and F. Daldal. 2004. X-ray structure of *Rhodobacter capsulatus* cytochrome bc_1: Comparison with its mitochondrial and chloroplast counterparts. *Photosynth. Res.* 81:251-275.
14. Blankenship, R. E. 2002. In *Molecular Mechanisms of Photosynthesis*, 61–82, Blackwell Science Ltd., Oxford.
15. Boekema, E. J., J. F. van Breemen, H. van Roon, and J. P. Dekker. 2000. Arrangement of photosystem II supercomplexes in crystalline macrodomains within the thylakoid membrane of green plant chloroplasts. *J. Mol. Biol.* 301:1123-1133.
16. Breyton, C., W. Haase, T. A. Rapoport, W. Kühlbrandt, and I. Collinson. 2002. Three-dimensional structure of the bacterial protein-translocation complex SecYEG. *Nature.* 418:662-665.

17. Chang, C. H., D. Tiede, J. Tang, U. Smith, J. Norris, and M. Schiffer. 1986. Structure of *Rhodopseudomonas sphaeroides* R-26 reaction center. *FEBS Lett.* 205:82-86.
18. Chang, M. C., L. Meyer, and P. A. Loach. 1990. Isolation and characterization of a structural subunit from the core light-harvesting complex of *Rhodobacter sphaeroides* 2.4.1 and *puc*705-BA. *Photochem Photobiol.* 52:873–881.
19. Cogdell, R. J., P. K. Fyfe, S. J. Barret, S. M. Prince, A. A. Freer, N. W. Isaacs, P. McGlynn, and C. N. Hunter. 1996. The purple bacterial photosynthetic unit. *Photosynth. Res.* 48:55-63.
20. Conroy, M. J., W. H. J. Westerhuis, P. S. Parkes-Loach, C. N. Hunter, and M. P. Williamson. 2000. The solution structure of *Rhodobacter sphaeroides* LH1β reveals two helical domains separated by a more flexible region: structural consequences for the Lh1 complex. *J. Mol. Biol*. 298:83-94.
21. Czajkowsky, D. M., S. Sheng, and Z. Shao. 1998. Staphylococcal α-hemolysin can form hexamers in phospholipid bilayers. *J. Mol. Biol.* 276:325-330.
22. Davis, C. M., P. L. Bustamante, J. B. Todd, P. S. Parkes-Loach, P. McGlynn, J. D. Olsen, L. McMaster, C. N. Hunter, and P. A. Loach. 1997. Evaluation of structure-function relationships in core light-harvesting complex of photosynthetic bacteria by reconstitution with mutant polypeptides. *Biochemistry.* 36:3671-3679.
23. Deinum, G., S. Otte, A. Gardiner, T. Aartsma, R. J. Cogdell, and J. Amesz. 1991. Antenna organization of *Rhodopseudomonas viridis* in relation to the redox state of the primary electron donor. *Biochim. Biophys. Acta*. 1060:125-131.
24. Deisenhofer, J., O. Epp, K. Miki, R. Huber, and H. Michel. 1985. Structure of the protein subunits in the photosynthetic reaction centre of *Rhodopseudomonas viridis* at 3 Å resolution. *Nature*. 318:618-624.
25. Engel, A., and D. J. Müller. 2000. Observing single biomolecules at work with the atomic force microscope. *Nature Struct. Biol.* 7:715-718.
26. Ermler, U., G. Fritzsch, S. Buchagan, and H. Michel. 1994. Structure of the photosynthetic center from Rhodobacter sphaeroides at 2.65 Å resolution: cofactors and protein-cofactor interactions. *Structure.* 2:925-936.
27. Farchaus, J., and D. Oesterhelt. 1989. A *Rhodobacter sphaeroides puf* L, M, and X deletion mutant and its complementation in trans with a 5.3 kb *puf* operon shuttle fragment. *EMBO J.* 8:47–54.
28. Farchaus, J. W., W. P. Barz, H. Grünberg, and D. Oesterhelt. 1992. Studies on the expression of the *pufX* polypeptide and its requirement for photoheterotrophic growth in *Rhodobacter sphaeroides. EMBO J.* 11:2779-2788.
29. Feniouk, B. A., D.A. Cherepanov, N. E. Voskoboynikova, A. Y. Mulkidjanian, and W. Junge. 2002. Chromatophore vesicles of *Rhodobacter capsulatus* contain on average one F_OF_1-ATP synthase each. *Biophys. J.* 82:1115-1122.
30. Fleming, G. R., and R. van Grondelle. 1997. Femtosecond spectroscopy of photosynthetic light-harvesting systems. *Curr. Opin. Struct. Biol.* 7:738-748.
31. Fotiadis, D., L. Hasler, D. J. Müller, H. Stahlberg, J. Kistler, and A. Engel. 2000. Surface tongue-and groove contours on lens MIP facilitate cell-to cell adherence. *J. Mol. Biol.* 300:779-789.
32. Fotiadis, D., P. Qian, A. Philippsen, P. A. Bullough, A. Engel, and C. N. Hunter. 2004. Structural analysis of the reaction center light-harvesting complex 1 photosynthetic core complex of *Rhodospirillum rubrum* using atomic force microscopy. *J. Biol. Chem.* 279:2063-2068.
33. Francia, F., J. Wang, G. Venturoli, B. A. Melandri, W. P. Barz, and D. Oesterhelt. 1999. The reaction center-LH1 antenna complex of *Rhodobacter sphaeroides* contains one PufX molecule which is involved in dimerization of this complex. *Biochemistry*. 38:6834-6845.
34. Frese, R. N., J. D. Olsen, R. Branvall, W. H. J. Westerhuis, C. N. Hunter, R. van Grondelle. 2000. The long-range supraorganization of the bacterial photosynthetic unit: A key role for PufX. *Proc. Natl. Acad. Sci. USA.* 97:5197-5202.

35. Fritzsch, G., J. Koepke, R. Diem, A. Kuglstatter and L. Baciou. 2002. Charge separation induces conformational changes in the photosynthetic reaction centre of purple bacteria. *Biol. Crystallogr., Acta Crystallogr. Sect. D*. 58:1660-1663.
36. Germeroth, L., F. Lottspeich, B. Robert, and H. Michel. 1993. Unexpected similarities of the B800-850 light-harvesting complex from *Rhodospirillum molischianum* to the B870 light-harvesting complexes from other purple photosynthetic bacteria. *Biochemistry.* 32:5615-5621.
37. Gibson, L. C., P. McGlynn, M. Chaudhri, and C. N. Hunter. 1992. A putative anaerobic coproporphyrinogen III oxidase in *Rhodobacter sphaeroides*. II. Analysis of a region of the genome encoding *hem*F and the *puc* operon. *Mol. Microbiol*. 21:3171–3186.
38. Gonçalves, R. P., J. Busselez, D. Lévy, J. Seguin, and S. Scheuring. 2004. Membrane insertion of *Rhodopseudomonas acidophila* light harvesting complex 2 investigated by high resolution AFM. *J. Struct. Biol*. In press.
39. Hartigan, N., H. A. Tharia, F. Sweeney, A. M. Lawless, and M. Z. Papiz. 2002. The 7.5-Å electron density and spectroscopic properties of a novel low-light B800 LH2 from *Rhodopseudomonas palustris. Biophys. J*. 82:963-977.
40. Hasler, L., J. B. Heymann, A. Engel, J. Kistler, and T. Walz, 1998. 2D crystallization of membrane proteins: rationales and examples. *J. Struct. Biol*. 121:162-171.
41. Hess, S., M. Chachisvilis, K. Timpmann, M. R. Jones, G. J. S. Fowler, C. N. Hunter, and V. Sundstrom. 1995. Temporally and spectrally resolved subpicosecond energy transfer within the peripheral antenna complex (LH2) and from LH2 to the core antenna complex in photosynthetic purple bacteria. *Proc. Natl. Acad. Sci. USA*. 92:12333-12337.
42. Hirai, T., J. A. W. Heymann, D. Shi, R. Sarker, P. C. Maloney, and S. Subramaniam. 2002. Three-dimensional structure of a bacterial oxalate transporter. Nature Struct. Biol. 9:597-600.
43. Hong, X., Y.-X. Weng, and M. Li. 2004. Determination of the topological shape of integral membrane protein light-harvesting complex LH2 from photosynthetic bacteria in the detergent solution by small-angle X-ray scattering. *Biophys. J.* 86:1082-1088.
44. Hu, X., T. Ritz, A. Damjanovich, and F. Autenrieth. 2002. Photosynthetic apparatus of purple bacteria. *Quat. Rev. Biophys.* 35:1-62.
45. Huang, Y., M. J. Lemieux, J. Song, M. Auer, D. N. Wang. 2003. Structure and mechanism of the glycerol-3-phosphate transporter from *Escherichia coli. Science.* 301:616-620.
46. Hunter, C. N., H. J. M. Kramer, and R. van Grondelle. 1985. Linear dichroism and fluorescence emission of antenna complexes during photosynthetic unit assembly in *Rhodopseudomonas sphaeroides*. *Biochim. Biophys. Acta.* 807:44-51.
47. Hunter, C. N., J. D. Pennoyer, J. N. Sturgis, D. Farrelly, and R. A**.** Niederman. 1988. Oligomerization states and associations of light-harvesting pigment-protein complexes of *Rhodobacter sphaeroides* as analyzed by lithium dodecyl sulfate-polyacrylamide gel electrophoresis. *Biochemistry*. 27:3459-3467.
48. Ikeda-Yamasaki, I., T. Odahara, K. Mitsuoka, Y. Fujiyoshi, and K. Murata. 1998. Projection map of the reaction center-light harvesting 1 complex from *Rhodopseudomonas viridis* at 10 Å resolution. *FEBS Lett.* 425:505–508.
49. Jamieson, S. J., P. Wang, P. Qian, J. Y. Kirkland, M. J. Conroy, C. N. Hunter, and P. A. Bullough. 2002. Projection structure of the photosynthetic reaction centre-antenna complex of *Rhodospirillum rubrum* at 8.5 Å resolution. *EMBO J.* 21:3927-3935.
50. Jones, M. R., G. J. S. Fowler, L. C. D. Gibson, G. G. Grief, J. D. Olsen, W. Crielaard, and C. N. Hunter. 1992. Mutants of *Rhodobacter sphaeroides* lacking one or more pigment-protein complexes and complementation with reaction center, LH1, and LH2 genes. *Mol. Microbiol*. 6:1173-1184.
51. Jungas, C., J. L. Ranck, J. L. Rigaud, P. Joliot, and A. Verméglio. 1999. Supramolecular organization of the photosynthetic apparatus of *Rhodobacter sphaeroides. EMBO J.* 18:534-542.

52. Karrasch, S., P. A. Bullough, and R. Ghosh. 1995. The 8.5 Å projection map of the light-harvesting complex 1 from *Rhodospirillum rubrum* reveals a ring composed of 16 subunits. *EMBO J*. 14:631-638.
53. Kassies, R., K.O. van der Werf, A. Lenferink, C. N. Hunter, J. D. Olsen, V. Subramaniam, C. Otto. 2004. Combined AFM and confocal fluorescence microscope for applications in bio-nanotechnology. *Journal of Microscopy*. In press.
54. Katona, G., U. Andreasson, E. M. Landau, L. E. Andreasson, and R. Neutze. 2003. Lipidic cubic phase crystal structure of the photosynthetic reaction centre from *Rhodobacter sphaeroides* at 2.35 Å resolution. *J. Mol. Biol.* 331:681-692.
55. Ketelaars, M., A. M. van Oijen, M. Matsushita, J. Köhler, J. Schmidt, and T. J. Aartsma. 2001. Spectroscopy on the B850 band of individual light-harvesting 2 complexes of *Rhodopseudomonas acidophila* I. Experiments and Monte Carlo simulations. *Biophys. J*. 80:1591-1603.
56. Ketelaars, M., C. Hofmann, J. Kohler, T. D. Howard, R. J. Cogdell, J. Schmidt, T. J. Aartsma. 2002. Spectroscopy on individual light-harvesting 1 complexes of *Rhodopseudomonas acidophila*. *Biophys J.* 83:1701-1715.
57. Kiley, P. J., and S. Kaplan. 1988. Molecular genetics of photosynthetic membrane biosynthesis in *Rhodobacter sphaeroides*. *Microbiol. Rev*. 52:50–69.
58. Koepke, J., X. Hu, C. Münke, K. Schulten, and H. Michel. 1996. The crystal structure of the light-harvesting complex 2 (B800-850) from *Rhodospirillum molischianum*. *Structure*. 4:581-597.
59. Lilburn, T. G., and J. T. Beatty. 1992. Suppressor mutants of the photosynthetically incompetent PufX deletion mutant *Rhodobacter capsulatus* DRC6 (pTL2). *FEMS Microbiol. Lett*. 100:155–160.
60. Lilburn, T. G., C. E. Haith, S. Prince, and J. T. Beatty. 1992. Pleiotropic effects of *pufX* gene deletion on the structure and function of the photosynthetic apparatus of *Rhodobacter capsulatus. Biochim. Biophys. Acta.* 110:160-170.
61. Lilburn, T. G., R. C. Prince, and J. T. Beatty. 1995. Mutation of the Ser2 codon of the light-harvesting B870α polypeptide of *Rhodobacter capsulatus* partially suppresses the *Puf*X phenotype. *J Bacteriol*. 177:4593–4600.
62. Lodish, H., A. Berk, S. L. Zipursky, P. Matsudaira, D. Baltimore, and J. E. Darnell. 2000. Molecular cell biology. 4th edition. *W. H. Freeman and company, New-York.*
63. McDermott, G., S. Prince, A. Freer, A. Hawthornthwaite-Lawless, M. Papizm R. Cogdell, and N. Isaacs. 1995. Crystal structure of an integral membrane light-harvesting complex from photosynthetic bacteria. *Nature*. 374:517-521.
64. McGlynn, P., C. N. Hunter, and M. R. Jones. 1994. The *Rhodobacter sphaeroides* PufX protein is not required for photosynthetic competence in the absence of a light-harvesting system. FEBS Lett. 349:349-353.
65. McGlynn, P., W. H. Westerhuis, M. R. Jones, and C. N. Hunter. 1996. Consequences for the organization of reaction center-light harvesting antenna 1 (LH1) core complexes of *Rhodobacter sphaeroides* arising from the deletion of amino acid residues from the C terminus of the LH1 polypeptide. *J. Biol. Chem.* 271:3285-3292.
66. McLuskey, K., S. Prince, R. J. Cogdell, and N. Isaacs. 2001. The crystallographic structure of the B800-820 LH3 light-harvesting complex from the purple bacterium *Rhodopseudomonas acidophila* strain 7050. *Biochemistry.* 40:8783-8789.
67. Miller, J. F, S. B. Hinchigeri, P. S. Parkes-Loach, P. M. Callahan, J. R. Sprinkle, J. R. Riccobono, and P. A. Loach. 1987. Isolation and characterization of a subunit form of the light-harvesting complex of *Rhodospirillum rubrum*. *Biochemistry.* 26:5055–5062.
68. Möller, C., M. Allen, V. Elings, A. Engel, and D. J. Müller. 1999. Tapping-mode atomic force microscopy produces faithful high-resolution images of protein surfaces. *Biophys. J*. 77:1150-1158.
69. Monger, T., and W. W. Parson. 1977. Singlet-triplet fusion in *Rhodopseudomonas sphaeroides*. *Biochim. Biophys. Acta.* 460:393-407.

70. Montoya, G., M. Cyrklaff, and I. Sinning. 1995. Two-dimensional crystallization and preliminary structure analysis of light-harvesting 2 (B800-850) complex from the purple bacterium *Rhodovulum sulfidophilum*. *J. Mol. Biol*. 250:1-10.
71. Müller, D. J., G. Büldt, and A. Engel. 1995a. Force-induced conformational change of bacteriorhodopsin. *J. Mol. Biol.* 249:239-243.
72. Müller, D. J., F. A. Schabert, G. Büldt, and A. Engel. 1995b. Imaging purple membranes in aqueous solutions at subnanometer resolution by atomic force microscopy. *Biophys. J.* 68:1681-1686.
73. Müller, D. J., W. Baumeister, and A. Engel. 1996. Conformational change of the haxagonally packed intermediate layer of *Deinococcus radiodurans* imaged by atomic force microscopy. *J. Bacteriol*. 178:3025-3030.
74. Müller, D. J., W. Baumeister, and A. Engel. 1999a. Controlled unzipping of a bacterial surface layer with atomic force microscopy. *Proc. Natl. Acad. Sci. USA*. 96:13170-13174.
75. Müller, D. J., D. Fotiadis, S. Scheuring, S. A. Müller, and A. Engel. 1999b. Electrostatically balanced subnanometer imaging of biological specimens by atomic force microscope. *Biophys. J*. 76:1101-1111.
76. Müller, D. J., A. Engel, U. Matthey, T. Meier, P. Dimroth, K. Suda. 2003. Observing membrane protein diffusion at subnanometer resolution. *J. Mol. Biol.* 327:925-930.
77. Nagarajan, V., and W. Parson. 1997. Excitation energy transfer between the B850 and B875 antenna complexes of *Rhodobacter sphaeroides*. *Biochemistry*. 36:2300-2306.
78. Naylor, G. W., H. A. Addlesee, L. C. D. Gibson, and C. N. Hunter. 1999. The photosynthesis gene cluster of *Rhodobacter sphaeroides*. *Photosynth. Res*. 62:121-139.
79. Niederman, R. A., D. E. Mallon, and J. J. Langan. 1976. Membranes of Rhodopseudomonas sphaeroides IV. Assembly of chromatophores in low-aeration cell suspensions. *Biochim. Biophys. Acta*. 440:429-447.
80. Niederman, R. A., D. E. Mallon, and L. C. Parks. 1979. Membranes of *Rhodopseudomonas sphaeroides*. VI. Isolation of a fraction enriched in newly synthesized bacteriochlorophyll α-protein complexes. *Biochim. Biophys. Acta.* 555:210-220.
81. Nikova, D. N., L. H. Pope, M. L. Bennink, K. A. van Leijenhorst-Groener, K. O. van der Werf, and J. Greve. 2004. Unexpected binding motifs for subnucleosomal particles revealed by atomic force microscopy. *Biophys. J*. 87:4135-4145.
82. Noji, H., R. Yasuda, M. Yoshida, and K. Kinosita. 1997. Direct observation of the rotation of F_1-ATPase. *Nature.* 386:299–302.
83. Noort, S. J. T. van, K. O. van der Werf, A. P. M. Eker, C. Wyman, B. G. de Grooth, N. F. van Hulst, and J. Greve. 1998. Direct visualization of dynamic protein-DNA interactions with a dedicated atomic force microscope. *Biophys. J.* 74:2840-2849.
84. Olsen, J. D., G. D. Sockalingum, B. Robert, and C.N. Hunter. 1994. Modification of a hydrogen bond to a bacteriochlorophyll a molecule in the light-harvesting 1 antenna of *Rhodobacter sphaeroides*. *Proc. Natl. Acad. Sci. USA*. 91:7124-7128.
85. Olsen, J. D., J. N. Sturgis, W. H. J. Westerhuis, G. J. S. Fowler, C. N. Hunter, and B. Robert. 1997. Site-directed modification of the ligands to the bacteriochlorophylls of the light-harvesting LH1 and LH2 complexes of *Rhodobacter sphaeroides. Biochemistry.* 36:12625-12632.
86. Ostafin, A. E., N. S. Ponomarenko, J. A. Popova, M. Jäger, E. J. Bylina, J. R. Norris. 2003. Characterization of expressed pigmented core light harvesting complex (LH1) in a reaction center deficient mutant of *Blastochloris viridis***.** *Photosynth. Res.* 77:53-68.
87. Pablo, P. J. de, J. Colchero, J. Gomez-Herrero,and A. M. Baro. 1998. Jumping mode scanning force microscopy. *Appl. Phys. Lett*. 73:3300-3302.
88. Papiz, M. Z., S. M. Prince, A. M. Hawthornthwaite-Lawless, G. McDermott, A. A. Freer, N. W. Isaacs, and R. J. Cogdell. 1996. A model for the photosynthetic apparatus of purple bacteria. *Trends Plant Sci*. 1:198-206.
89. Papiz, M. Z., S. M. Prince, T. Howard, R. J. Cogdell, and N. W. Isaacs. 2003. The structure and thermal motion of the B800-850 LH2 complex from *Rhodopseudomonas acidophila* at

2.0 Å resolution and 100K: new structural features and functionally relevant motions. *J. Mol. Biol.* 326:1523-1538.

90. Parkes-Loach, P. S., C. J. Law, P. A. Recchia, J. Kehoe, S. Nehrlich, J. Chen, and P. A. Loach. 2001. Role of the core region of the PufX protein in inhibition of reconstitution of the core light-harvesting complexes of *Rhodobacter sphaeroides* and *Rhodobacter capsulatus*. *Biochemistry.* 40:5593-5601.
91. Pugh, R.J., P. McGlynn, M. R. Jones, C. N. Hunter. 1998. The LH1-RC core complex of *Rhodobacter sphaeroides*: interaction between components, time-dependent assembly, and topology of the PufX protein. *Biochim. Biophys. Acta.* 1366:301-316.
92. Pullerits, T., and V. Sundström. 1996. Photosynthetic light-harvesting pigment-protein complexes: toward understanding how and why. *Acc. Chem. Res.* 29:381-389.
93. Recchia, P. A., C. M. Davis, T. G. Lilburn, J. T. Beatty, P. S. Parkes-Loach, C. N. Hunter, and P. A. Loach. 1998. Isolation of the PufX protein from *Rhodobacter capsulatus* and *Rhodobacter sphaeroides*: evidence for its interaction with the alpha-polypeptide of the core light-harvesting complex. *Biochemistry.* 37:11055-11063.
94. Rigaud. J.L., M. Chami, O. Lambert, D. Lévy, J.-L. Ranck. 2000. Use of detergents in two-dimensional crystallization of membrane proteins. *Biochim Biophys. Acta*. 1508:112-128.
95. Roszak, A. W., T. D. Howard, J. Southall, A. T. Gardiner, C. J. Law, N. W. Isaacs, and R. J. Cogdell. 2003. Crystal structure of the RC-LH1 core complex from *Rhodopseudomonas palustris*. *Science.* 302:1969-1972.
96. Schabert, F. A., and A. Engel. 1994. Reproducible acquisition of *Escherichia coli* porin surface topographs by atomic force microscopy. *Biophys. J.* 67:2394-2403.
97. Schabert, F. A., C. Henn, and A. Engel. 1995. Native *Escherichia coli* OmpF porin surfaces probed by atomic force microscopy. *Science.* 268:92-94.
98. Scheuring, S., D. J. Müller, P. Ringler, J. B. Heymann, and A. Engel. 1999. Imaging streptavidin 2D crystals on biotinylated lipid monolayers at high resolution with the atomic force microscopy. *J. Microsc.* 193:28-35.
99. Scheuring, S., F. Reiss-Husson, A. Engel, J.-L. Rigaud, and J. L. Ranck. 2001. High-resolution AFM topographs of the *Rubrivivax gelatinosus* light harvesting complex 2. *EMBO J.* 20:3029–3035.
100. Scheuring, S., J. Seguin, S. Marco, D. Lévy, C. Breyton, B. Robert, and J.-L. Rigaud. 2003a. AFM characterization of tilt and intrinsic flexibility of *Rhodobacter sphaeroides* light harvesting complex 2 (LH2). *J. Mol. Biol.* 325:569-580.
101. Scheuring, S., J. Seguin, S. Marco, D. Lévy, B. Robert, and J.-L. Rigaud. 2003b. Nanodissection and high-resolution imaging of the *Rhodopseudomonas viridis* photosynthetic core complex in native membranes by AFM. *Proc. Natl. Acad. Sci. USA.* 100:1690-1693.
102. Scheuring, S., F. Francia, J. Busselez, B. A. Melandri, J.-L. Rigaud, and D. Lévy. 2004a. Structural role of PufX in the dimerization of the photosynthetic core-complex of *Rhodobacter sphaeroides*. *J Biol. Chem.* 279:3620-3626.
103. Scheuring, S., J. N. Sturgis, V. Prima, A. Bernadac, D. Lévy, and J.-L. Rigaud. 2004b. Watching the photosynthetic apparatus in native membranes. *Proc. Natl. Acad. Sci. USA*. 101:11293-11297.
104. Scheuring, S., J.-L. Rigaud, and J. N. Sturgis. 2004c. Variable LH2 stoichiometry and core clustering in native membranes of *Rhodospirillum photometricum*. *EMBO J.* 23:4127 – 4133.
105. Siebert, C. A., P. Qian, D. Fotiadis, A. Engel, C. N. Hunter, and P. A. Bullough. 2004. Molecular architecture of photosynthetic membranes in *Rhodobacter sphaeroides*: the role of PufX. *EMBO J.* 23:690-700.
106. Simon, R., U. Priefer, and A. Pühler. 1983. A broad host range mobilization system for *in vivo* genetic engineering: transposon mutagenesis in Gram-negative bacteria. *Bio/Technology*. 1:37–45.

107. Singer, S. J., and G. L. Nicolson. 1972. The fluid mosaic model of the structure of cell membranes. *Science*. 175:720-731.
108. Stahlberg H., D J. Müller, K. Suda, D. Fotiadis, A Engel, T. Meier, U. Matthey, and P. Dimroth. 2001. Bacterial Na^+-ATP synthase has an undecameric rotor. *EMBO reports*. 2:229-233.
109. Stamouli, A., S. Kafi, D. C. G. Klein, T. H. Oosterkamp, J. W. M. Frenken, R. J. Cogdell, and T. J. Aartsma. 2003. The ring structure and organization of light harvesting 2 complexes in a reconstituted lipid bilayer, resolved by atomic force microscopy. *Biophys. J.* 84:2483 - 2491.
110. Sturgis, J. N., and R. A. Niederman. 1996. The effect of different levels of the B800-850 light-harvesting complex on intracytoplasmic membrane development in *Rhodobacter sphaeroides*. *Archives of Microbiology.* 165:235-242.
111. Sturgis, J. N., J. D. Olsen, B. Robert, and C. N. Hunter. 1997. Functions of conserved tryptophan residues of the core light-harvesting complex of *Rhodobacter sphaeroides. Biochemistry.* 36:2772-2778.
112. Tadros, M. H., R. Frank, B. Dörge, N. Gad'on, J. Y. Takemoto, and G. Drews. 1987. Orientation of the B800-850, B870, and reaction center polypeptides on the cytoplasmic and periplasmic surfaces of *Rhodobacter capsulatus* membranes. *Biochemistry*. 26:7680-7687.
113. Todd, J. B., P. S. Parkes-Loach, J. F. Leykam, and P. A. Loach. 1998. In vitro reconstitution of the core and peripheral light-harvesting complexes of *Rhodospirillum molischianum* from separately isolated components. *Biochemistry.* 37:17458-17468.
114. Vera, I. J. M. 2004. Fabrication of carbon nanotube atomic force microscopy probes by catalytic chemical vapor deposition. *M. Sc. Project report*.
115. Verméglio, A., and P. Joliot. 1999. The photosynthetic apparatus of *Rhodobacter sphaeroides*. *Trends Microbiol*. 7:435-440.
116. Visscher, K. J., H. Bergström, V. Sundström, C. N. Hunter, and R. van Grondelle. 1989. Temperature-dependence of energy-transfer from the long wavelength antenna BChl-896 to the reaction centre in *Rhodospirillum rubrum*, *Rhodobacter sphaeroides* (WT and M21 mutant) from 77 to 177K, studied by picosecond absorption spectroscopy. *Photosynth. Res.* 22:211-217.
117. Vos, M. H., R. J. van Dorssen, J. Amesz, R. van Grondelle, and C. N. Hunter. 1988. The organisation of the photosynthetic apparatus of *Rhodobacter sphaeroides*: studies of antenna mutants using singlet-singlet quenching. *Biochim. Biophys. Acta.* 933:132-140.
118. Walz, T., and R. Ghosh. 1997. Two-dimensional crystallization of the light-harvesting 1-reaction center photounit from *Rhodospirillum rubrum*. *J. Mol. Biol*. 265:107-111.
119. Walz, T., S. J. Jamieson, C. M. Bowers, P. A. Bullough, and C. N. Hunter. 1998. Projection structures of three photosynthetic complexes from *Rhodobacter sphaeroides*: LH2 at 6 Å, LH1 and RC-LH1 at 25 Å. *J. Mol. Biol.* 282: 833-845.
120. Werf, K.O. van der, C. A. J. Putman, B. G. de Grooth, F. B. Segerink, E. H. Schipper, N. F. van Hulst, and J. Greve. 1993. Compact stand-alone atomic force microscope. *Rev. Sci. Instrum.* 64:2892-2897.
121. Werf, K. O. van der, C. A. J. Putman, B. G. de Grooth, and J. Greve. 1994. Adhesion force imaging in air and liquid by adhesion mode atomic force microscopy. *Appl. Phys. Lett*. 65:1195-1197.
122. Westerhuis, W. H. J., M. Vos, R. van Grondelle, J. Amesz, and R. A. Niederman. 1998. Altered organization of light-harvesting complexes in phospholipid-enriched *Rhodobacter sphaeroides* chromatophores as determined by fluorescence yield and singlet-singlet annihilation measurements. *Biochim. Biophys. Acta*. 1366:317-329.
123. Westerhuis, W. H. J., C. N. Hunter, R. van Grondelle, and R. A. Niederman. 1999. Modeling of oligomeric-state dependent spectral heterogeneity in the B875 light-harvesting complex of *Rhodobacter sphaeroides* by numerical simulation. *J. Phys. Chem. B.* 103:7733–7742.

124. Westerhuis, W. H. J., J. N. Sturgis, E. C. Ratcliffe, C. N. Hunter, and R. A. Niederman. 2002. Isolation, size estimates and spectral heterogeneity of an oligomeric series of light-harvesting 1 complexes from *Rhodobacter sphaeroides*. *Biochemistry.* 41:8698-8707.
125. Young, C. S., R. C. Reyes, and J. T. Beatty. 1998. Genetic complementation and kinetic analyses of *Rhodobacter capsulatus ORF1696* mutants indicate that the ORF1696 protein enhances assembly of the light-harvesting 1 complex. *J. Bacter*. 180:1759-1765.
126. Young, C. S., and J. T. Beatty. 1998. Topological model of the *Rhodobacter capsulatus* light-harvesting complex I assembly protein LhaA (previously known as ORF1696). *J. Bacteriol*.180:4742-4745.

Acknowledgements

Everything is good in its season, and it is time now to thank all the people, my colleagues and friends, who were one way or another involved in my Ph.D. research in the Biophysical Engineering Group. I am deeply grateful to all of you, as only with your help and support I could successfully reach this final stage of my doctoral study. In particular, I would like to express my sincere appreciation to:

Professor Jan Greve, for giving me an opportunity to join the BPE group.

Dr. Cees Otto, my supervisor, for his tactful approach, guidance and motivating discussions in the course of four years.

Professor Vinod Subramaniam, for guiding me in the final stage of my Ph.D. research and useful remarks.

The colleagues and experts in the photosynthesis research field from the University of Sheffield, Professor Neil Hunter, Dr. John Olsen, Professor Per Bullough, Dr. Alistair Siebert and Dr. Jaimey Tucker, for the fruitful collaboration. Thank you all for sharing your vast knowledge on bacterial photosynthesis in all its aspects and for providing me with diverse biological samples for AFM measurements. I am especially thankful to John Olsen, for being my teacher and advisor in all possible biological and biochemical questions, for all his expertise and willingness to share it, for his endless enthusiasm and encouragement.

Professor Rienk van Grondelle and Dr. Raoul Frese from the Vrije Universiteit, Amsterdam, for the successful collaboration. Many discussions with Raoul Frese stimulated my interest and extended my knowledge on the bacterial photosynthesis considerably, I appreciate that a lot. It was nice to work as a team and to perform AFM experiments together ("clicker/operator") and to share all the flights and falls of AFM workaday routine.

Kees van der Werf, for the created by him AFM set-up which was proved to be an excellent tool for the achievement of the goals of my research, for introducing me into the AFM field and for the technical support during the whole project.

Dr. Martin Bennink, for the software support and constructive discussions.

Mark Smithers from the CMA lab, MESA+ institute, for the help with SEM imaging.

Dessy Nikova, for sharing her experimental knowledge on AFM imaging, true willingness to help, friendliness and cheerfulness.

Roel Kassies, for fruitful discussions on the project we were both involved, for his understanding, encouragement and for a friendly working atmosphere.

Natallia Uzunbajakava, for her good advices, suggestions and moral support.

Alexei Kharine, for the help in various aspects of life.

Ine Segers-Nolten, Kirsten van Leijenhorst-Groener, Roy Kolkman, Anthony de Vries, Johan van Hespen, Aufried Lenferink, Henk-Jan van Manen, Alexander Serov, Serguei Kruglik, Evgueni Krioukov, Yuri Aksenov, Andrei Dergachev, Anna Petuhova, for their friendly help.

Sylvia Winters, for her professionalism, energy and cheerfulness.

Valeri Souchkov, for knowing the answers to all the questions, from how to cook "borsch" to how the synchrophasotron works☺. Thanks for being there for me in bad and good times!

Finally, I would like to express my heartfelt gratitude to my family for their sincere love, faith and endless support.

Publications

Publications in peer-reviewed journals:

1. Bahatyrova, S., Frese, R.N., Siebert, C.A., Olsen, J.D., Werf, K.O. van der, van Grondelle, R., Niederman, R.A., Bullough, P.A., Otto, C. & Hunter, C.N. 2004. The native architecture of a photosynthetic membrane. *Nature*. 430:1058-1052.
2. Bahatyrova, S., Frese, R.N., Werf, K.O. van der, Otto, C., Hunter, C.N. & Olsen, J.D. 2004. Flexibility and size heterogeneity of the LH1 light harvesting complex revealed by atomic force microscopy. *J. Biol. Chem*. 279:21327-21333.
3. Frese, R.N., Olsen, J.D., Bahatyrova, S., de Wit, C.D., Siebert, C.A., Hunter, C.N., Otto, C. & van Grondelle, R. Protein packing in a photosynthetic membrane. *To be submitted to EMBO J.*

Conference abstracts:

1. Bahatyrova, S., Frese, R.N., Werf, K.O. van der, Olsen, J.D., Hunter, C.N., Subramaniam, V., & Otto, C. (2004). High-resolution atomic force microscope imaging of photosynthetic 2D-crystals and native membranes, pp. 35. In: *Programme and Abstracts Book, ALW/FOM/VvBBMT-Meeting on Molecular and Cellular Biophysics, Lunteren.*
2. Bahatyrova, S., Frese, R.N., Werf, K.O. van der, Hunter, C.N., Olsen, J.D., & Otto, C. (2004). Flexibility and size heterogeneity of the LH1 light-harvesting complex: high-resolution atomic force microscope study, pp. 138-139. In: *Proceedings of the Dutch Annual Conference on BioMedical Engineering*, Papendal.
3. Olsen, J.D., Bahatyrova, S., Hunter, C.N., & Otto, C. (2004). Highly variable morphology of the light-harvesting 1 complex imaged by atomic force microscopy, pp. 105. In: *Proceedings of the 13th International Congress on Photosynthesis,* Montreal.
4. Frese, R.N., Bahatyrova, S., Siebert, C.A., Niederman, R., Olsen, J.D., Grondelle, R. van, Otto, C., Hunter, C.N. (2004). The organization of native bacterial photosynthetic membranes probed with AFM and polarized light spectroscopy, pp. 84. In: *Proceedings of the 13th International Congress on Photosynthesis,* Montreal.
5. Bahatyrova, S., Frese, R.N., Werf, K.O. van der, Bennink, M.L., Olsen, J.D., Hunter, C.N., & Otto, C. (2003). Atomic Force Microscope Study of Rhodobacter Sphaeroides Light-Harvesting Complexes LH1 and LH2: variability in the crystal morphology, pp. 40. In: *Programme and Abstracts Book, ALW/FOM/VvBBMT-Meeting on Molecular and Cellular Biophysics, Lunteren.*
6. Bahatyrova, S., Frese, R.N., Werf, K.O. van der, Hunter, C.N., Olsen, J.D., & Otto, C. (2003). Comparison of light-harvesting complexes LH1 and LH2 2D-crystals: atomic force microscope study, pp. 66-68. In: *Proceedings of the Dutch Annual Conference on BioMedical Engineering*, Papendal.
7. Bahatyrova, S., Kassies, R., Hunter, C.N., Grondelle, R. van, Greve, J., & Otto, C. (2002). High-resolution AFM imaging of two-dimensional crystals of light-harvesting complexes LH2, pp. 9-10. In: *Proceedings of the Dutch Annual Conference on BioMedical Engineering*, Papendal.
8. Bahatyrova, S., Kassies, R., Hunter, C.N., Grondelle, R. van, Greve, J., & Otto, C. (2001). Imaging Aggregates of Isolated Light-Harvesting Complexes LH2 with the Atomic Force Microscope, pp. 93. In: *9th European Conference on the Spectroscopy of Biological Molecules, Book of Abstracts*, Prague.
9. Bahatyrova, S., Kassies, R., Hunter, C.N., Grondelle, R. van, Greve, J., & Otto, C. (2001). Imaging aggregates of isolated light-harvesting complexes LH2 with the atomic force microscope, pp. 12-13. In: *Proceedings of the Dutch Annual Conference on BioMedical Engineering*, Papendal.